

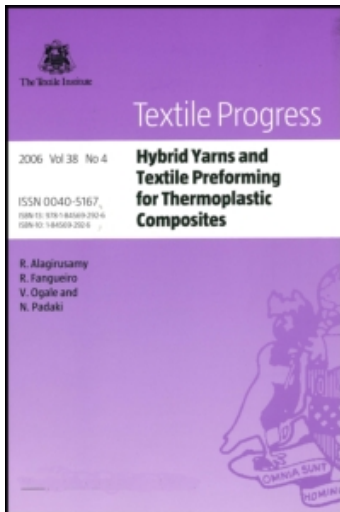
This article was downloaded by: [Clemson University]

On: 4 September 2009

Access details: Access Details: [subscription number 784173612]

Publisher Taylor & Francis

Informa Ltd Registered in England and Wales Registered Number: 1072954 Registered office: Mortimer House, 37-41 Mortimer Street, London W1T 3JH, UK



## Textile Progress

Publication details, including instructions for authors and subscription information:

<http://www.informaworld.com/smpp/title~content=t778164492>

### Physical principles of electrospinning (Electrospinning as a nano-scale technology of the twenty-first century)

D. Lukáš <sup>a</sup>; A. Sarkar <sup>a</sup>; L. Martinová <sup>a</sup>; K. Vodsed'álková <sup>a</sup>; D. Lubasová <sup>a</sup>; J. Chaloupek <sup>a</sup>; P. Pokorný <sup>a</sup>; P. Mikeš <sup>a</sup>; J. Chvojka <sup>a</sup>; M. Komárek <sup>a</sup>

<sup>a</sup> Department of Nonwovens, Faculty of Textile Engineering, Technical University of Liberec, Liberec, Czech Republic

Online Publication Date: 01 June 2009

**To cite this Article** Lukáš, D., Sarkar, A., Martinová, L., Vodsed'álková, K., Lubasová, D., Chaloupek, J., Pokorný, P., Mikeš, P., Chvojka, J. and Komárek, M.(2009)'Physical principles of electrospinning (Electrospinning as a nano-scale technology of the twenty-first century)',*Textile Progress*,41:2,59 — 140

**To link to this Article:** DOI: 10.1080/00405160902904641

**URL:** <http://dx.doi.org/10.1080/00405160902904641>

## PLEASE SCROLL DOWN FOR ARTICLE

Full terms and conditions of use: <http://www.informaworld.com/terms-and-conditions-of-access.pdf>

This article may be used for research, teaching and private study purposes. Any substantial or systematic reproduction, re-distribution, re-selling, loan or sub-licensing, systematic supply or distribution in any form to anyone is expressly forbidden.

The publisher does not give any warranty express or implied or make any representation that the contents will be complete or accurate or up to date. The accuracy of any instructions, formulae and drug doses should be independently verified with primary sources. The publisher shall not be liable for any loss, actions, claims, proceedings, demand or costs or damages whatsoever or howsoever caused arising directly or indirectly in connection with or arising out of the use of this material.

## Physical principles of electrospinning (Electrospinning as a nano-scale technology of the twenty-first century)

D. Lukáš\*, A. Sarkar, L. Martinová, K. Vodsed'álková, D. Lubasová,  
J. Chaloupek, P. Pokorný, P. Mikeš, J. Chvojka and M. Komárek

*Department of Nonwovens, Faculty of Textile Engineering, Technical University of Liberec, Studentská 2, Liberec 461 17, Czech Republic*

(Received 3 March 2009; final version received 7 April 2009)

The history of electrospinning is briefly introduced at the beginning of the article. The fundaments of the process are then analysed physically to be translated into a successful technology. Self-organisation of fluid in electrospinning is perceived as a consequence of various instabilities, based on electrohydrodynamics and, thus, highlighted as a key factor, theorising the subject successfully to elevate it to a highly productive technology to manufacture nano-scale materials. The main physical principle of the self-organisation is appearance of unstable tiny capillary waves on liquid surfaces, either on a free liquid surface or on that confined in a capillary, which is influenced by external fields. The jet path is described, as well as its possible control, by special collectors and spinning electrodes. Two electrospinning variants, i.e. melt and core–shell electrospinning, are discussed in detail. Two scarcely referred exceptional features of electrospinning, electric wind and accompanying irradiations, are introduced in in-depth detail. Lastly, care is taken over the quality of polymeric solutions for electrospinning from the standpoint of Hansen solubility parameters and entanglements among polymeric chains.

**Keywords:** electrospinning; electrospinning variants; nanofibres; liquid jet; self-organisation; dielectric diffusion; radiation; polymer solution

### 1. Introduction

This work aims to introduce textile technologists and researchers to the technological, as well as physical, analyses of the extremely attractive field of electrospinning. Care has been taken to include as many references as possible for a well-organised treatise on the fundamentals of the subject, encompassing most of the aspects that are yet unavailable. However, for understanding some of the basic aspects, one might refer to the monographs of Filatov et al. [1], Ramakrishna et al. [2], Reneker and Fong [3] and Reneker and Yarin [4]. The list of references attached to this contribution, nevertheless, does not claim to be a comprehensive one, since researchers throughout the world have been studying the subject extensively for the last two decades.

Structurally, electrospun polymeric jet almost resembles a tree, as shown in Figure 1. It has remarkable manifold external morphology, with its ‘roots’ evolving from a charged, extremely thin surface layer, called Debye’s layer, of the polymer solution that serves as one of the electrodes, connected to a high voltage source. Tracing the jet further downstream, one finds a stable part of the jet that looks like a tree stem. Noticeably, the following whipping zone/bending instability of the jet looks out like branches of the tree with lives of

---

\*Corresponding author. Email: david.lukas@tul.cz

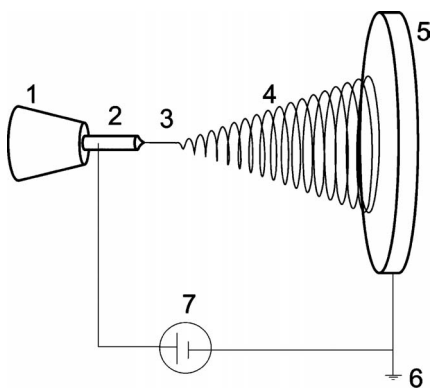


Figure 1. Schematic diagram of an electrospinning set-up: (1) syringe and metering pump, (2) needle/capillary serving as the electrode, (3) stable part of the jet, (4) whipping/coiling zone, (5) collector, (6) ground and (7) high voltage supply,

the form of jet coil cascades and jet-branching. Eventually, the nanofibres collected on the other electrode, so-called collector, may literally be thought of as the ‘fruits’ of the entire process.

Physically, the phenomenon of electrospinning is a consequence of a tug of war between electrostatic and capillary forces. The first of them speaks of charged liquid bodies that disintegrate due to long range repulsive Coulombic forces between ions of the same signs, while the last one causes liquid particles to flock together to minimise the liquid surface area and surface energy, resulting from short distance inter-molecular interactions at quantum level. Liquid bodies disintegrate in two possible ways depending on their internal molecular structure. Simple liquids, having small molecules, spray in clouds of small charged droplets with a tendency to break down further until one single elementary charge remains trapped in each of them, as claimed by Grigor'ev and Shir'aeva [5]. Liquids with higher viscosity, particularly polymer solutions and polymer melts with sufficiently entangled macromolecules, disintegrate in long tiny liquid columns while moving from one electrode to the other. The internal pressure of electric nature, caused by an enormous concentration of charged particles of similar nature, forces them to be stretched longitudinally. This stretching tendency, along with jet inertia and rheology, results in a wild lateral jet motion and enormous elongation leading to quick decrease of the jet radius, typically down to several hundreds or tens of nanometres. Narrowing down of the jet diameter results in an increased curvature of the jet segments that brings about an associated phenomenon that effectively drives the solvent out from the jet.

To admit without any exaggeration, the process has potential to revolutionise spinning technology. It resembles biological procedures in some ways, wherein bio-nanofibres like cellulose and collagen are created by self-organisation. Unlike a typical classic non-woven technology that has a line for production of carded needle-punched non-wovens, the devices and equipments in the electrospinning process are free of complex passive or rotating components. Various physical phenomena, as has been mentioned above, as well as detailed below, play the role of these traditional components when fibre is spun under external electric field. So, the magnificence of mechanical engineering is substituted indirectly by external fields in helping in diverse physical self-organisation. Hence, a better understanding of its intrinsic physical fundamentals is needed for further technological developments, and so, this review is largely devoted to the physical insight in an attempt to enlighten the marvellous phenomenon of electrically driven polymeric jets.

Electrospinning technology can be divided into two branches. Previously, it was based on less productive needle/capillary spinners with production rates in the order of unit grams per hour. Recently, technologies that are based on highly productive jet creation from free liquid surfaces by self-organisation have been developed. These effective methods may be classified as needless electrospinning. These technologies to produce polymeric nanofibrous materials are of primary interest for various disciplines, like medicine, biology, chemical, textile and material engineering, where nanoporous materials are employed as filters, scaffolds for tissue engineering, protective clothing, drug delivery systems, substrates for catalysis, etc.

The present paper is organised as follows:

Section 2 ('Historical overview') describes unusual dramatic development in understanding of the phenomenon of electrospinning from both theoretical and technological points of view. It will be shown that the earliest observation of electrohydrodynamic-related phenomena dates back to the end of the sixteenth century. Also, the initial pioneering or innovative works, which subsequently resulted in electrospinning, surprisingly, took place at the same end of the nineteenth centenary. Electrospinning theory emerged from works of Rayleigh, Taylor and Landau in the realm of electrohydrodynamics. These original ideas were refreshed and further developed after the 1970s, accompanied by needs, achievements and expectation of Hi-Tech sectors of industry and market.

Section 3 ('Theoretical evolution of electrospinning') starts with electrostatics, electric bi-layer and surface tension to take the reader to the world of fundamental areas of physics that critically affect electrospinning. This section continues with the description of specific phenomena as electric pressure and disintegration of liquid bodies under the action of Coulombic forces. Sub-section 3.6 is primarily devoted to the engineering and basic physical principles of needless electrospinning that elevates this technology to industrial level. The section concludes with a generalised model, unifying electrospinning with all other electrohydrodynamic phenomena, from the point of view of dielectric diffusion.

Section 4 ('Liquid jet in an electric field') starts with the Rayleigh instability, which is the most significant factor that hinders an otherwise smooth spinning process. The instability is also a theoretical key to electrospinning from free liquid surface, since both belong to the phenomena of self-organisation of a fluid due to the mechanism of the fastest forming instability. The succeeding part of the section describes an allometric relation, according to which an electrified jet is elongated initially in a stable mode. Bending instability of the jet is, then, simply introduced as the consequence of the Earnshaw's theorem. The section concludes with a thermodynamic approach to describe one of the most fascinating features of electrospinning that enables the jet to oust small solvent molecules almost instantaneously. The phenomenon is explained using Thomson-Kelvin law.

Section 5 ('Special collectors') deals with a recent effort to modify electrospinning set-ups to create various patterning and productivity enhancement. The section divided into three sub-parts is devoted to static collectors, dynamic collectors and spinning electrodes along with a theoretical description of a electrostatic field in the vicinity of a charged grid.

In Section 6 ('Electrospinning variants'), the first part of the section focuses on solvent-free methods of electrospinning. Text includes references to the most significant works, describing developments in the construction of apparatuses, scientific approaches and different methods of mathematical modelling in melt-electrospinning. The last part of the section concentrates on core-shell electrospinning that is a sophisticated route to

producing composite functionalised nanofibres with almost strictly organised core–shell structure. ‘Exceptional features of electrospinning’ (Section 7), like electric wind and various kinds of radiations accompanying jet creation and nanofibre formation, are considered vital too. Electrostatic wind can heavily influence the jet path and formation of nanofibre layers. Radiations accompanying electrospinning span from St. Elmo’s fire over soft Roentgen beams to radioactive radiation caused by trapping daughter nuclei of Radon decay.

Section 8 (‘Polymeric solutions for electrospinning’) deals with the effect of polymer solutions with different properties that significantly influence both initiation of electrospinning and morphology of nanofibres. The aim of this part is to define key parameters of a polymer solution, which are responsible for electrospinning and formation of nanofibre sheet without defects in the reproducible quality. Repeatedly, it has been found that properties of solvents have a dominant effect on the spinning process. The structure of the polymer has an impact on its solubility. Chain entanglement is one of the many parameters that can significantly influence fibre formation during polymer electrospinning. Berry number, the dimensionless product of the intrinsic viscosity and concentration,  $[\eta]c$ , is discussed. The Hansen solubility parameters are used for predicting polymer solubility. This approach can help to optimise a solvent or a mixture of solvents.

## 2. Historical overview

Investigation of physical phenomena, connected to electrospinning, can be traced back to 1600, when William Gilbert (\*1544 +1603), the English physician and natural philosopher, wrote his principal work ‘*De Magnete, Magneticisque Corporibus, et de Magno Magnete Tellure*’, published in the year 1600. In his work, Gilbert gave a full account of his research on magnetic bodies and electrical attractions, as presented by Gwinn [6]. Gilbert was the first person to discover that a spherical drop of water on a dry surface was drawn up in a conical shape, when a piece of rubbed amber was brought within its proximity, as shown in Figure 2. In fact, such shape deformation of liquid bodies in an external electrostatic field governs the modern electrospinning technology. Gilbert’s experiment was carried out with

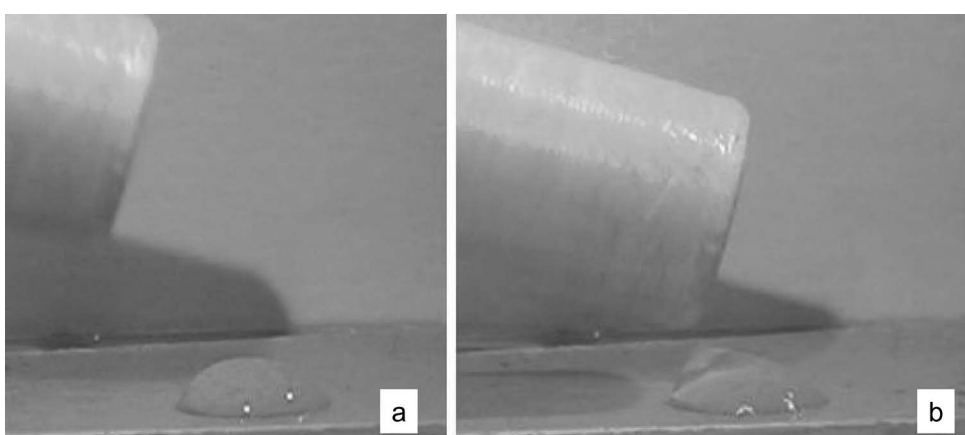


Figure 2. A spherical drop: (a) of water on a flat solid surface is drawn up in a conical shape, (b) when a charged PVC rod is brought within a suitable distance from it.

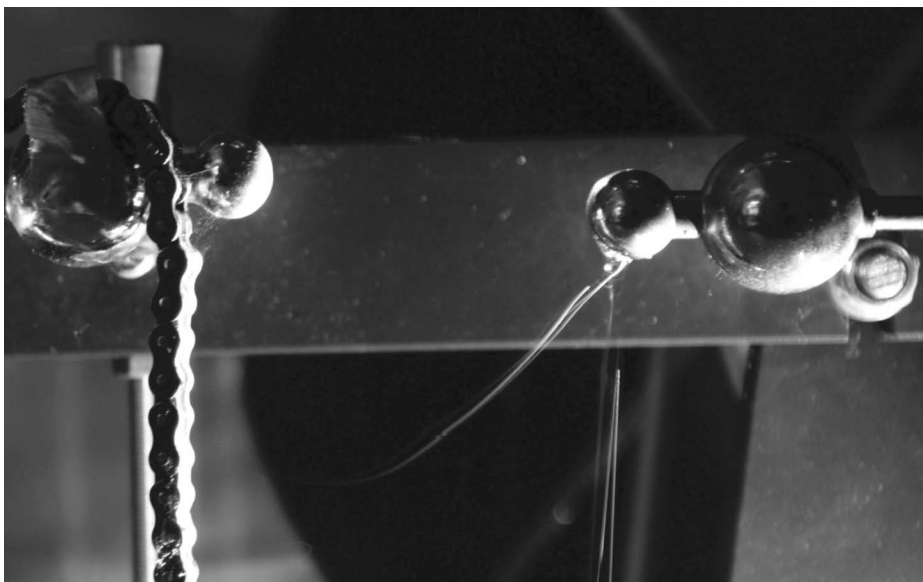


Figure 3. Morton's invention: the composite liquid, i.e. polymeric solution, realises a discharge between positive and negative conductors, interconnected with a high voltage machine, in the form of electrospinning jets. Nanofibres are collected on a metallic chain on the left, serving as a collector, hanging on the negative conductor.

a plastic pen, charged electrostatically with a textile piece. The charged pen is then able to attract tiny ripped pieces of paper, instead of water droplets. Another closely related work to electrospinning was done in 1749, when Nollet [7] demonstrated how a water jet disintegrated when it was charged. However, as Gilbert and Nollet did not have a sufficiently high voltage source to study the droplet motions in stronger electrostatic fields, mankind had to wait nearly another 300 years until Morton commercially patented his work [8].

Electrospinning as a physical phenomenon, and also as an application to spin tiny fibres was probably first suggested by Morton [8] in his patent submitted in 1900. In his noteworthy work, Morton employed suitable sources of high tension of static electricity, such as a Holtz' static machine, induction coils of large size, or Tesla and Thomson machines to create fibrous masses by electrospinning. As shown in Figure 3, Morton's apparatus was composed of a glass vessel with tubular bottom through which a 'composite fluid' flowed out in the form of droplets. These droplets touched a metallic sphere at the end of a conductor, connected to a positive terminal of a high voltage source/machine. The composite liquid realised discharge between positive and negative terminals of conductors in the form of electrospinning jets, while fibres were collected on a metallic chain, hanging from the negatively charged conductor. The macromolecular theory to handle polymers did not surface in Morton's times, hence he worked with fluids referred to as 'composite fluids'. These fluids used by him are described as liquid glue, collodion, and a solution of pure rubber and sulphuric ether. Interestingly, Morton's idea was much ahead of his time, since he used needle as well as needless forms of electrospinning to spin fibres.

The principle of modern needle electrospinning originated through Zeleny's work [9], who designed a needle/capillary apparatus (Figure 4) for studying electrical discharges from liquid points. His pioneering work, however, is rarely mentioned in modern literatures in the present context of the section. Zeleny was primarily interested in discharge phenomena from

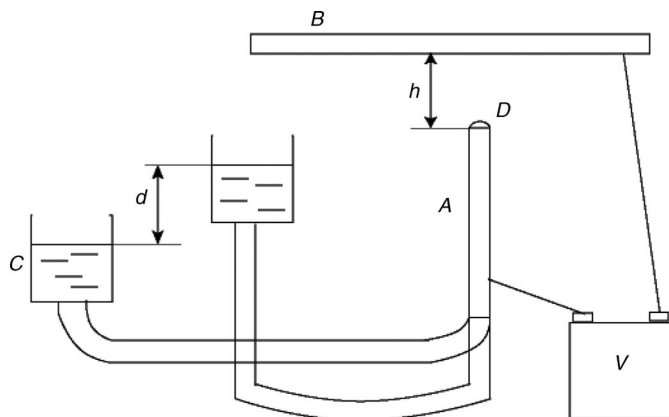


Figure 4. Zeleny's needle/point apparatus on which Taylor founded his theory: (A), (B), (C) and (V) are the capillary of length 'L', collector, container providing the hydrostatic pressure and the power supply, respectively.

metallic points, like tiny cylindrical electrodes. Through his experimental works, Zeleny found that current emanating from metallic points permanently increased the threshold potential at which the discharge was initiated. So, he chose an alternative method to save his laborious work to renew metallic surfaces by using liquid points by presenting a narrow glass or metallic capillary, supplied with acidified water, from a container. Using the apparatus, Zeleny was even able to measure electrostatic intensities at the tips of those capillaries. The set of his critical field strength values is used in Section 3. He was also aware of the creation of very fine fibre-like liquid jets in his apparatus [10] but, unfortunately, it did not attract his further attention. His apparatus (Figure 4) is, nevertheless, used as a basic electrospinner and with some mere cosmetic changes, employed by most research workers to date.

Formhals is commonly recognised as the father of present day electrospinning technology through his patent [11]. His invention speaks about methods and/or set-ups to produce artificial threads of fibres, using electric field, and their collection in spools for use in common textile technology as weaving and knitting, as shown in Figure 5. However, his

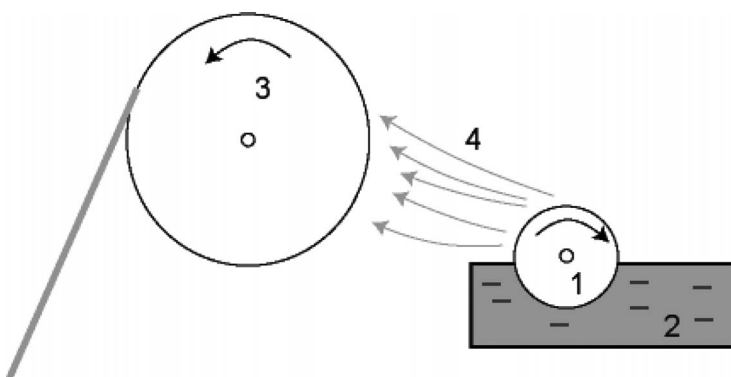


Figure 5. Formhals' apparatus for producing artificial threads of fibres through electrospinning and collection of those threads in spools: a slender serrated wheel (1) rotates in a pool (2) filled with a polymeric solution. Nanofibres (4) are trapped in piles by another slender wheel (3) that serves as a collector. A yarn, composed of nanofibres, is continuously removed and collected from the rotating collector.

patent does not concern the phenomenon of electrospinning in its essence, and Formhals even admitted, 'It is already known to make use of the action of an electrical field on liquids which contain solid materials dissolved in them with a view to forming threads for the production of silk-like spun fibres'. Probably, he referred to Morton's work.

All the above-mentioned works and patents did not result in industrially manufactured fibrous materials, and unfortunately further development and application of the said principle for electrospinning took quite a considerable period from the time of its origin. Neither Morton's and Zeleny's nor Formhals' work reached industrial application in spite of the fact that their inventions had high commercial potential. The probable reasons for that might be lack of appropriate equipments that should have enabled the researchers to discover the 'nanodimension' of electrospun fibres, since the first prototype electron microscope came into existence in 1931. The other reason could be the absence of industrial initiative and interest to manufacture electrospun materials until 1980s of the former century. Briefly speaking, the fields of tissue engineering, electronics, ultrafiltration, etc., that use such nanomaterials, developed only in recent times. Progress in scientific understanding sometimes takes a long time before being reflected to a society's development at large.

The novel idea of electrospinning, however, continued to develop through Norton's [12] work, who rather dealt with a melt polymer spinning. In his patent, Norton used an airblast to assist fibre formation. A decisive breakthrough in the development and application of electrospinning took place in USSR through Rosenblum and Petrianov-Sokolov. Their effort led to the first known industrial facility for producing fibrous materials by the method for military gas masks, that were constructed in the city of Tver' in 1939, as referred to in Filatov [13].

An American company, Donaldson, develops nanofibre products and nanofibre filter media for applications, where sub-micron fibre diameters, high filtration efficiency, high surface area and other unique material properties are useful. Donaldson Co., Inc., in 1981 introduced the first commercial products containing electrospun nanofibres in the United States. Donaldson has been using its patented and patent-pending nanofibre filter media in Ultra-Web<sup>®</sup> filters for dust collection, Spider-Web<sup>®</sup> filters for gas turbine air filtration and Donaldson Endurance<sup>TM</sup> air filters for heavy-duty engines.

Presently, the unique electrospinning technology, producing nanofibres at commercial scale, is Nanospider<sup>TM</sup>. It is developed by Czech company Elmarco, Liberec, which enables industrial production of non-woven textiles made up of fibres from 200 to 500 nm in diameter. Such materials are widely utilised in many fields, e.g. filtration, healthcare, building construction, automotive industries, industry, cosmetics and many others. Nanospider<sup>TM</sup>, needless electrospinning technology, was first patented by Jirsak et al. [14] of the Technical University of Liberec. Elmarco produced the pilot manufacturing line for nanofibre production in 2004, and in 2006 offered the first models for industrial production. Recent models of Nanospiders<sup>TM</sup> have production rates up to 30 m/min with the fabric width bigger than 1 m.

The earliest theoretical work related to electrospinning phenomena was done by Rayleigh [15], who calculated the limiting charge at which an isolated drop of certain radius became unstable. Basic theoretical analysis in the area of electrospraying and electrospinning was made by Taylor [16], following Zeleny's works [9, 10] to formulate instability criteria of spherical drops of liquid (both for charged and uncharged spheroids) when subjected to an external electrostatic field. He observed that elongated spheroids quickly developed an apparently conical end due to electrical forces, and liquid spray appeared from vertex of the cone. Through a detailed analysis, Taylor [17] obtained the characteristic value of the cone's semi-vertical vertical angle,  $\alpha$ , as 49.3°, as shown in Figure 5. This

achievement enabled him to formulate the expression for predicting the critical potential and voltage at which jets or drops appeared from the liquid point of the modified Zeleny apparatus [16] at zero hydrostatic pressure. It is noteworthy that Taylor found the practical interest of the subject of his research in the area of meteorology and did not relate his effort to fibre spinning at all. He was convinced that the studied phenomenon had strong relevance to the production and character of thunderstorm rains.

Some other American meteorologists were attracted by the disintegration of water drops in an electric field too. For instance, Matthews [18] studied mass loss and distortion of freely falling water drops in an electric field. Results of his experimental work were used by Taylor to prove his theoretical prediction of instability of uncharged liquid spheroids in external electrostatic fields.

Theoretical background of electrohydrodynamics was presented by Landau. He co-authored with Lifshitz, between 1938 and 1960, to bring out a series of volumes under the heading of 'Course of Theoretical Physics', covering a lot of branches of physics. The volume of 'Electrodynamics of Continuous Media' by Landau and Lifshitz [19] covers the theories of electromagnetic fields in matter, and that of macroscopic electric and magnetic properties of matter. Some of the sections of the book are actually based on original research performed by the authors. The authors dealt with the critical charge density, induced on a surface of conductive liquid for the development of unstable surface waves [19]. The particular problem turned out to be a foundation for the development of a generalised theoretical modelling of electrospinning, extending from a capillary to a needleless spinner.

Research in electrospinning has received a great deal of attention recently, especially after Doshi and Reneker [20], Srinivasan and Reneker [21] and Reneker and Chun [22], spun various kinds of polymers to characterise their properties. Some other contemporaneous works in this area were focussed on the role of polymer chain entanglements on fibre formation during electrospinning of polymer solutions in good solvents, e.g. Shenoy et al. [23], and on enhancement of productivity and efficiency of the technology through experiments and modelling of multiple jets, e.g. Theron et al. [24].

### 3. Theoretical evolution of electrospinning

In general, electrospinning may be thought to be a member of a larger group of physical phenomena, classified as electrohydrodynamics. This important group of electrical appearances concerns the nature of ion distribution in a solution, caused by the influence of electric field, generated by organised groups of charges, to give a wide range of solution behaviour, such as electrophoresis, electroosmosis, electrocapillarity and electrodiffusion, as recorded by Bak and Kauman [25]. This section will briefly describe how the theory of electrohydrodynamics has been evolving since the initial pioneering experimental observations. To start with, it is convenient to introduce an overview of the basic principles of electrostatics and capillarity to enable deeper understanding of physical principles of electrospinning.

#### 3.1 Basics of electrostatics

Historically, the basic law of electrostatics is the Coulomb law, describing a force  $\vec{F}$  by which a charge  $q_2$  acts on a charge  $q_1$  on a distance  $\vec{r}$  in a space with electric permittivity,  $\epsilon$ :

$$\vec{F} = \frac{1}{4\pi\epsilon} \frac{q_1 q_2}{r^2} \frac{\vec{r}}{|\vec{r}|}. \quad (3.1)$$

Coulomb force per unitary charge is called field strength or field intensity, and is commonly denoted as  $\vec{E}$ :

$$\vec{E} = \frac{\vec{F}}{q_1}. \quad (3.2)$$

For electrostatic field, it holds the superposition principle. For charges  $q_1$  and  $q_2$  that generate electrostatic fields with intensities  $\vec{E}_1$  and  $\vec{E}_2$ , respectively, the resultant/joint field  $\vec{E}$  is determined by the following sum:

$$\vec{E} = \vec{E}_1 + \vec{E}_2. \quad (3.3)$$

The space dependence of intensity generated by a point charge,  $\vec{E} \approx 1/r^2$ , together with the superposition principle, leads to an alternative formulation of Coulomb law that is called Gauss theorem of electrostatics. According to this theorem, the scalar product of intensity,  $\vec{E}$ , with a surface area element  $d\vec{s}$ , integrated along a closed surface  $S$ , is equal to a charge,  $q$ , trapped inside the close surface by permittivity,  $\epsilon$ . The surface area element  $d\vec{s}$  is considered here as a vector normal to the surface element:

$$\oint_S \vec{E} d\vec{s} = \frac{q}{\epsilon}. \quad (3.4)$$

Gauss's principle in electrostatics describes electrostatic field property from a macroscopic point of view. It has also a microscopic variant, given by

$$\vec{\nabla} \cdot \vec{E} = \frac{\rho}{\epsilon}, \quad (3.5)$$

where  $\vec{\nabla} \cdot \vec{E}$  is the divergence of vector  $\vec{E}$ , and  $\vec{\nabla}$  is called 'nabla' or Hamilton operator, having in the Cartesian coordinate system a meaning of the symbolic vector  $\vec{\nabla} = (\partial/\partial x, \partial/\partial y, \partial/\partial z)$ . Instead of the macroscopic net charge  $q$  in Gauss theorem (3.4), there appeared a microscopic parameter,  $\rho$ , the charge density, in Equation (3.5). This equation is also known as the first Maxwell law.

Another consequence of Coulomb law is the fact that electrostatic field is the conservative one and, hence, there exists a potential  $\varphi$  that unequivocally determines the field intensity by means of the following relation:

$$\vec{E} = -\vec{\nabla} \varphi. \quad (3.6)$$

The substitution from Relation (3.6) into Equation (3.5) provides us with the so-called Poisson Equation,

$$\Delta \varphi = -\frac{\rho}{\epsilon}, \quad (3.7)$$

in which  $\Delta$ , known as the Laplace operator, denotes the scalar product of two Hamilton operators,  $\Delta = \vec{\nabla} \cdot \vec{\nabla}$ . Thus, it has the shape of  $\Delta = \partial^2/\partial x^2 + \partial^2/\partial y^2 + \partial^2/\partial z^2$ . A particular case of the Poisson Equation is the Laplace Equation,  $\Delta \varphi = 0$ , that holds for the areas of a space without any net charge, i.e. where  $\rho(x) = 0$ .

### 3.2 Surface tension and electric bi-layer

Electrospun nanofibres are not the only ‘nanoscale objects’ in electrospinning. Surfaces of physical bodies, including liquids and polymeric solution, within a depth of several tens or units of nanometres, embody properties quite differently from those in the bulk. Even without any external electrostatic field, a liquid surface exhibits surface tension that is the consequence of short range inter-molecular forces and, hence, this phenomenon itself is bound to a liquid surface layer, whose thickness is comparable with the reach/range of inter-molecular forces. If, moreover, on surface of a liquid, under an external electrostatic field, charges tend to distribute in a way to shield the field in the bulk, then an ‘electric bi-layer’ is formed.

#### 3.2.1 Surface tension

Electrospinning is commonly described as a tug of war between electric and capillary forces. So, a brief introduction to the nature of capillary phenomena is meaningful. The phenomenon of surface tension will be explained for the sake of brevity, using a lattice model at zero temperature limits. Details about this simple approach to surface tension can be found in Lukas et al. [26].

A regular cubic lattice of cells in a three-dimensional space may be imagined as in Figure 6. Each cell may be considered to be occupied by one of the two species of fluids, out of which one is assigned with a value 1 and depicted as white, the second kind is allocated a value 2 and black colour. There are various interaction energies between various pairs of cells. These interactions represent short range molecular interactions and hence they appear in-between neighbouring cells only. Only cells with a common wall are counted as neighbours. As a rule, particles of the same nature attract each other more than different ones. So, interaction energies  $E$  between neighbouring cells of the same kind of fluids have to be modelled smaller, e.g.  $E(1, 1) = 1$  e.u. and  $E(2, 2) = 2$  e.u., than the interaction

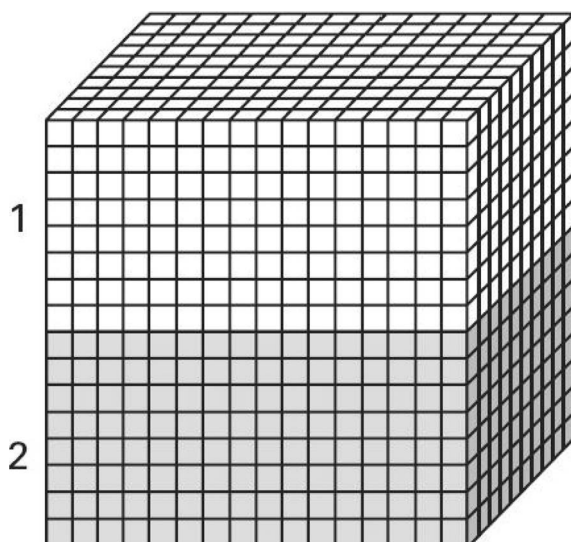


Figure 6. Lattice model of a binary mixture of fluids: at the zero temperature limit, fluids separate completely, since the system minimises its total energy. There is an extra energy bonded to the interface between liquids, whose surface density is called surface energy.

energy  $E$  between neighbours of a different nature, e.g.  $E(1, 2) = E(2, 1) = 3$  e.u. The energy is expressed here in arbitrary energy units, e.u. The lattice model of this binary mixture of fluids tends naturally to minimise its total/free energy. At the zero temperature limit, the fluids separate completely, since the system minimises its total energy, as shown in Figure 6. Unlike bulks of both fluids, there is an extra energy belonging to the interface between them, since in bulks the interaction energy per a bond is equal either to 1 e.u. or 2 e.u., while cells on the interface create at least one bond in which energy content is higher and equal to 3 e.u. The effect of the increment of total energy due to interaction energy between different species of fluid particles is associated with the interface in a depth comparable with the order of short range inter-molecular forces and, hence, the phenomena of surface energy belongs to a superficial layer with thickness in nanometre scale. The same effect appears at each boundary independent of physical state of the material.

Creation of a new area  $A$  of a rectangular interface of a width  $w$  needs some force  $F$  acting on a side of the length  $w$ . The work,  $W$ , done by the displacement of the side  $w$  through a distance  $l$  is  $W = Fl$ . This work has to be equal to the surface energy,  $W_A$ , of an elementary area of interface having an area of  $A = wl$ . Surface energy,  $W_A$ , according to its aforementioned definition, is equal to  $W_A \equiv W/A = F/w \equiv \gamma$ . The equation also defines surface tension  $\gamma$  as force acting on a unit length of the triplet line. If one divides an ideally spherical liquid droplet of radius  $r$  into two mirror parts, cutting it along its equator, the linear force  $\gamma$  of surface tension acts along the perimeter given by  $o = 2\pi r$ , which creates a total capillary force,  $F_c = 2\pi r\gamma$  that attracts and tends to attach the hemispheres together. This force causes a capillary/Laplace pressure  $p_c = F/\pi r^2 = 2\gamma/r$  if the droplet is again constructed from its two parts.

Two generalised relationships for the above-cited brief introduction to capillary phenomena will be used further. The first of them is the expression for capillary force, given by

$$F_c = o\gamma \cos \theta, \quad (3.8)$$

where  $\theta$  represents the contact angle between the vector, representing the surface tension and the plain of perimeter.

The other well-known Laplace–Young formula represents the generalised capillary pressure  $p_c$  caused by an arbitrarily curved liquid surface as a multiple of the surface tension and a sum of two principal curvatures  $K_1$  and  $K_2$ :

$$p_c = \gamma(K_1 + K_2). \quad (3.9)$$

In the case of sphere of radius  $R$ , both principal curvatures  $K_1$  and  $K_2$  are of the same value and are equal to  $1/R$ , i.e.  $K_1 + K_2 = 2/R$ , in agreement with the previously derived formula for capillary pressure,  $p_c = 2\gamma/r$ . More information about surface tension and capillary pressure are given in Adamson and Gast [27] and Shchukin et al. [28].

### 3.2.2 Electric bi-layer

Electric bi-layer is another object with nanodimension in electrospinning. Referring to the second part of Figure 7, one may consider a plane surface of polymer solution, containing ions both in polymer macromolecules and their solvent. Let the ion valence be considered as one for simplification, and  $e$  denote the elementary electric charge. In electrospinning, electric potential,  $\varphi_o$ , at the liquid/polymer solution surface is generated by the electrostatic

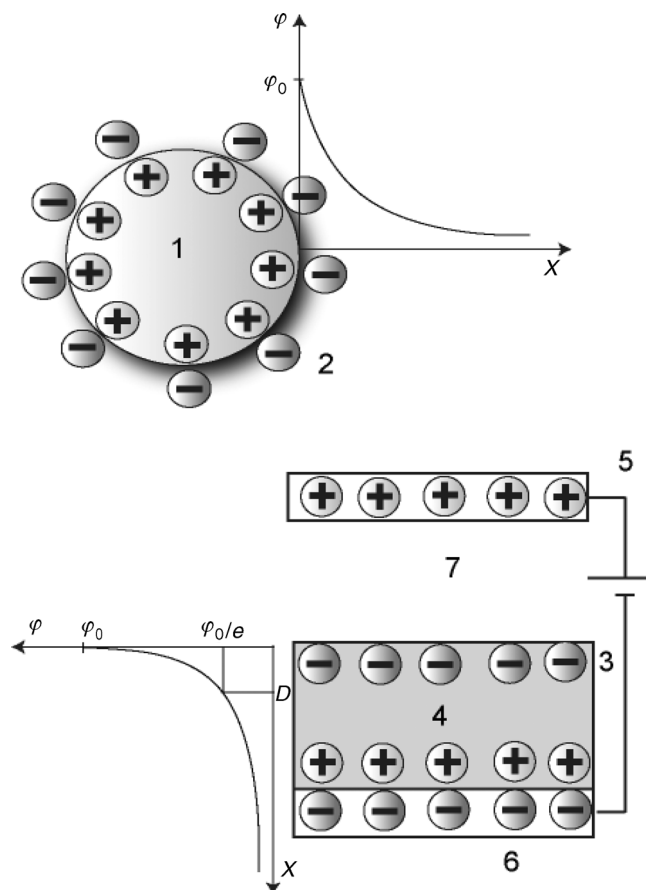


Figure 7. A charged colloid particle (1) in an electrolyte: a positively charged colloid particle is surrounded by a cloud of negative ions (2). Similarly, electrostatic potential  $\varphi$ , close to polymer solution surface in electrospinner is quenched with increasing distance,  $x$ , from the particle surface, as sketched in the lower figure part. A cloud of ions (3) in a polymer solution (4) is induced by an electrostatic field between a collector (5) and an electrode (6). The thickness of the ionic atmosphere in the vicinity of the solution surface is called the ‘Debye’s length’,  $D$ .

field in between two electrodes. One of the electrodes is in touch with the polymer solution and the other, the collector, is kept at a faraway distance from the free surface of the polymeric solution. The space between the free surface of the polymer and the collector, so-called fibre spinning zone, is filled by air or any other medium, e.g. air. An electrospinner, from the point of view of ion distribution, resembles the situation in the vicinity of a charged colloid particle. The similitude is indicated in Figure 7, where the collector plays the role of organised groups of charges on colloid particles. The only difference between colloid particle and electrospinner is the gap coined by the space between the collector and liquid surface. The electric potential,  $\varphi$ , having the value,  $\varphi_0$ , at the solution surface decreases with the depth in the solution as quenched by the ion distribution in the solution surface layer, i.e. as quenched by induced charges that shield the electric field towards the bulk of the solution. For the sake of simplification, relative parallel placement of both the collector

and the solution surface will be considered henceforth. The parallel configuration gives rise to simple symmetric equipotential surfaces that are parallel to them too. So, the electrostatic potential  $\varphi(x)$  can be considered as the function of the only variable  $x$ , which is the distance measured along the axis, perpendicular to the collector and solution surfaces, with its origin located at the solution surface, pointing to the polymer solution bulk.

To derive  $\varphi-x$  relationship, one has to start with a rule that governs the distribution of ions acted upon by the external electrostatic field as well as the field generated by ions themselves. The probability,  $p(x)$ , of finding an ion at a particular depth,  $x$ , in the solution depends on its energy,  $e\varphi(x)$ , through the Boltzmann distribution  $\exp(-e\varphi(x)/k_B T)$ , vide Kittel and Kroemer [29], where  $k_B$  is the Boltzmann constant, and  $T$  being the absolute temperature in Kelvin. The electrolyte for this moment comprises two kinds of ions of opposite charge  $+e$  and  $-e$ . Their volumetric concentrations are  $n^+(x) = n_0 \exp(-e\varphi(x)/k_B T)$  and  $n^-(x) = n_0 \exp(+e\varphi(x)/k_B T)$ , where  $n_0$  is the concentration of charges, when the solution is not affected by any external electrostatic field. The concentration  $n_0$  is universal for both the ions as the solution is electroneutral as a whole. The charge distribution is also governed by the one-dimensional Maxwell's first law of electrostatics, generally expressed in the form of the Poisson Equation with the potential gradient  $d\varphi(x)/dx$  having the non-zero component along the  $x$ -axis only. Mathematically, the particular shape of Equation (3.7) for this case becomes

$$\frac{d^2\varphi(x)}{dx^2} = -\frac{\rho(x)}{\varepsilon}, \quad (3.10)$$

where

$$\rho(x) = en^+(x) - en^-(x) = n_0 e \left[ \exp\left(\frac{-e\varphi(x)}{k_B T}\right) - \exp\left(\frac{+e\varphi(x)}{k_B T}\right) \right]. \quad (3.11)$$

Symbol  $\rho(x)$  is the density of net charge, and  $\varepsilon$  is the solution susceptibility. Equation (3.10) has been solved previously by Gouy [30] and Chapman [31] for a complex charge density, as described by Equation (3.11). This non-linear differential equation is called the Poisson–Boltzmann Equation. The charge density  $\rho(x)$  distribution is generally linearised to ease further analysis by assuming  $e\varphi(x)/(kT) \ll 1$ . The linearisation, based on the first two terms of the following series  $\exp x \cong 1 + x + \dots$  and  $\exp(-x) \cong 1 - x + \dots$ , leads to the simplified charge density  $\rho(x) = n_0 e [(1 - e\varphi(x)/k_B T) - (1 + e\varphi(x)/k_B T)] = -2n_0 e\varphi(x)/k_B T$ . By substituting this linearised charge density in Equation (3.10), the one-dimensional linearised form of the Poisson–Boltzmann Equation, known as Debye and Huckel [32] Equation, is obtained:

$$\frac{d^2\varphi(x)}{dx^2} = -\frac{2n_0 e^2 \varphi}{\varepsilon_0 k_B T}. \quad (3.12)$$

The linearisation leads to the physically acceptable solution  $\varphi(x) = \varphi_0 \exp(-\sqrt{n_0 e^2 / (\varepsilon_0 k_B T)} x) = \varphi_0 \exp(-x/D)$ . More details about this approach can be found in Feynman et al.'s lectures on physics [33]. The quantity

$$D = \sqrt{\frac{\varepsilon_0 k_B T}{2n_0 e^2}} \quad (3.13)$$

is associated with the thickness of the ionic atmosphere in the vicinity of the solution surface and is called ‘Debye’s length’, as shown in Figure 7. When the depth in the bulk of the liquid from the surface increases by  $D$ , the potential decreases with a rate of  $1/e$ , where  $e$  is now the base of natural logarithm. Consequently, inside conductive bodies with high ion or free charge concentration, the potential is constant and field intensity is zero. More general solution of the one-dimensional Poisson–Boltzmann Equation (3.13) for 2:1 and 1:2 electrolytes as  $\text{K}_2\text{SO}_4$  and  $\text{CaCl}_2$  was brought about by Andrietti et al. [34].

With respect to electrospinning, one can underline that Debye’s length is the thickness of the ion cloud in the vicinity of the liquid surface. As this thickness in conductive liquids is generally not more than several units or tens of nanometres and it decreases with the ion concentration,  $n_0$ , the external electrostatic field is able to influence directly only the molecules or their parts that are close to the liquid surface. It is convenient to underline at this juncture that during electrospinning the electrostatic field preferably grasps the surface layer of the liquid, where net charge density is enormously high. The surface husk of the liquid is transmitted into an electrospinning jet that is supposed to be highly charged too.

### 3.3 Electric pressure

Electric pressure is another basic concept in electrospinning besides surface tension and electric bi-layer. Its analysis will start with the derivation of the field strength at the surface of a charged conductive liquid, as given by Smith [35].

Two points,  $A$  and  $B$ , in the vicinity of the surface of a charged conductive liquid drop, may be considered. The first of them is taken outside the drop, while the last one inside the liquid. Field strengths  $\vec{E}_1$  and  $\vec{E}_2$  might, then, be considered as the contributions to the total field strength  $\vec{E}$ , i.e. to the total electrostatic intensity,  $\vec{E} = \vec{E}_1 + \vec{E}_2$ . Particularly,  $\vec{E}_1$  is the contribution to the total field strength from charges that reside on surface element of drop, denoted by  $\delta S$ , and  $\vec{E}_2$  is the field strength contribution of charges from the rest of the liquid and from all other charges in space. For more details, Figure 8 may be consulted.

It is worth mentioning that the orientation of the total field strength,  $\vec{E}$ , has to be perpendicular to the surface of the conductor, and the same is presupposed for electrostatic intensities,  $\vec{E}_1$  and  $\vec{E}_2$ , since the charge distribution is considered to be in equilibrium. To be more concrete, it is obvious that any tangential component of field strength  $\vec{E}_2$  with respect to the liquid surface should violate the equilibrium, since then the charge will move along the liquid surface and the system cannot be considered as a one in equilibrium. For the same reason,  $\vec{E}$  has to be zero in the liquid bulk; otherwise, a charge there should move too. Thus, the induced charge on the liquid drop, causing the field strength value  $\vec{E}_1$ , shields the external field inside the drop, as has been shown in the article about the electric bi-layer. So, the analysis may be carried out with the values of field strengths instead of their vector nature.

As inside the conductive liquid, the total electric field,  $E(B)$  strength, is zero, two equations can be constructed for the total field strength at the points  $A$  and  $B$ . At point  $B$ , the following relation holds true:

$$E(B) = E_2(B) - E_1(B) = 0, \quad (3.14)$$

and at the point  $A$ , holds

$$E(A) = E_1(A) + E_2(A). \quad (3.15)$$

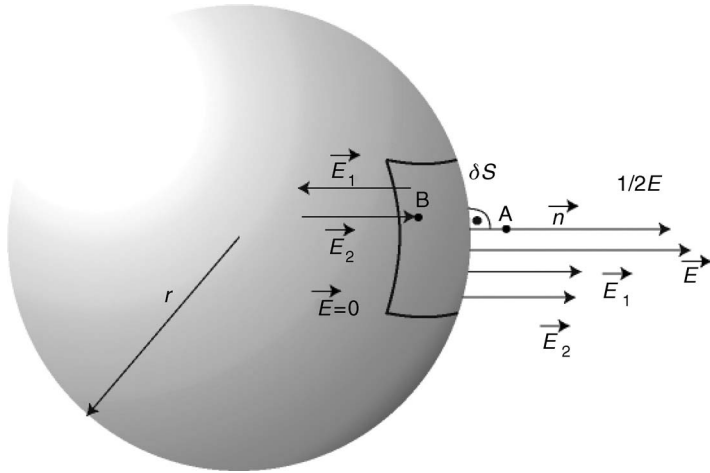


Figure 8. A charged, perfectly conductive drop has a normal  $\vec{n}$  perpendicular to an elementary area,  $\delta S$ , of its surface. The total field strength,  $\vec{E}$ , in the vicinity of the drop's surface is the sum of strengths  $\vec{E}_1$  and  $\vec{E}_2$ . Particularly,  $E_1$  is the contribution to the total field strength, created by charges on a surface element,  $\delta S$ , and  $E_2$  is the contribution from all resting charges on the sphere and from other charges in space. Point A is just outside the droplet, while point B is inside it.

Because of the infinitesimally small distance between points A and B, the absolute values of  $E_1$  and  $E_2$  at these points may virtually be considered unchanged. On the other hand, since  $E_1$  is generated by the surface charge and  $E_2$  by the charge in the rest of the liquid sphere and elsewhere in the space, the mutual orientation of these electric intensities varies at points A and B, as has been expressed by Equations (3.14) and (3.15). The direct consequence of these equations is given as follows:

$$E_1 = E_2 = \frac{1}{2}E. \quad (3.16)$$

Application of Gauss theorem of electrostatics, introduced as Equation (3.4), in the vicinity of the surface element,  $\delta S$ , results in the following relation, as depicted in Figure 8:

$$E\delta S = \frac{\sigma\delta S}{\epsilon}. \quad (3.17)$$

The quantity  $p_e$ , the surface electric pressure, which is the force per unit area at the spherical droplet surface, is given by  $p_e = \delta F/\delta S$ , where the force,  $\delta F$ , is the product of the charge  $q = \sigma\delta S$  at the surface element,  $\delta S$ , and the field strength,  $E_2$ . Hence, it holds

$$p_e = \frac{\sigma\delta S E_2}{\delta S}. \quad (3.18)$$

From Equations (3.16), (3.17) and (3.18), the following relation for electrostatic pressure is obtained:

$$p_e = \frac{1}{2}\epsilon E^2. \quad (3.19)$$

The onset of electrospinning appears under the condition that electric pressure  $p_e$  exceeds the capillary pressure,  $p_c$ , i.e.  $p_e \geq p_c$ . This condition for the electrospinning onset will be commonly used further on in the text.

### 3.4 Disintegration of liquid bodies

Disintegration of charged liquid conductive bodies to nanoscale matter can be illustrated through a single droplet. The related experimental physics, directly connected to disintegration of water drops under electric field, originated through Zeleny's [10], Doyle et al.'s [36], and Berg and George's [37] works. The stability analysis of charged liquid bodies, as carried out by Rayleigh [15], will be presented here in a simplified version to show the limiting charge,  $q$ , for spherical droplet disintegration.

Suppose that the charged droplet, embedded in a space without any other external charges, is a perfect sphere with radius  $r$ . The liquid sphere has uniform surface charge density,  $\sigma$ , and is considered as conductive. Thus, for the whole sphere, having radius  $r$ , the following relation is obtained directly from the Gauss theorem of electrostatics:

$$E4\pi r^2 = \frac{Q}{\varepsilon}, \quad (3.20)$$

where  $Q = \sigma \delta S$  is the total net charge on the liquid sphere. From Equation (3.20) immediately follows the relation,  $E = Q/4\pi \varepsilon r^2$ . According to the statement at the end of the following article, the spherical droplet dissociates under the condition  $p_e \geq p_c$ , where  $p_c$  is the capillary pressure,  $2\gamma/r$ , in a spherical droplet,  $\gamma$  being the surface tension of the liquid–gas interface. From the inequality,  $p_e \geq p_c$ , and from Equations (3.19) and (3.20) follows static disintegration criterion:

$$Q^2 \geq 64\pi^2 \varepsilon \gamma r^3. \quad (3.21)$$

The more advanced theoretical foundations for analysing the dynamic stability of charged droplets were developed by Rayleigh [15]. Rayleigh has shown in the work that capillary wave instability on the droplet surface is responsible for this phenomenon. He derived the following condition for the onset of destabilisation of a perfectly conductive spherical droplet  $Q^2 \geq (n + 2)4\pi \gamma r^3$  in CGSe units. This condition in SI units is written as

$$Q^2 \geq (n + 2)4\pi \gamma r^3(4\pi \varepsilon). \quad (3.22)$$

The integer,  $n$ , belongs to various vibration modes of the liquid droplet. The zero mode,  $n = 0$ , corresponds to radial oscillations that are unacceptable for incompressible fluids. The first mode,  $n = 1$ , represents the reciprocating translational droplet motion. Hence, the smallest possible mode number is  $n = 2$ . For this mode, the Inequality (3.21) is identical to Inequality (3.22). On the other hand, if the Inequality (3.22) permits higher values of  $n$ , then the mode with the highest  $n$  is chosen, since it represents the fastest forming instability. Details about fastest forming instabilities in electrospinning are discussed in the more simple concept of planar one-dimensional surface waves in sub-section 3.6. The droplet instability can be observed visually as the ejection of a fine jet of highly dispersed daughter droplets whose charge/mass ratios are higher than for the original droplet, as mentioned in Grigor'ev [38].

Freely charged liquid droplets are, in principle, unstable, since they elongate to reach the shape of spheroids with the major and minor axes as  $a$  and  $b$ , respectively, as was shown by Taylor [16]. As the ratio  $a/b$  increases, the critical value of  $Q$  decreases, since on the highly curved spheroid apices the charge density is significantly greater than on the surface of original spherical droplet. Thus, electric pressure  $p_e$  grows in these places more rapidly than the capillary one,  $p_c$ .

Consequently, it may be stated that charged spheroids are always unstable and therefore, disintegration proceeds inexorably, as has been mentioned earlier in the introductory part of this sub-section. It was found that the instability led to creation of daughter droplets that were approximately 10 times smaller than the original one. Daughter droplets and their offspring obey the same phenomenon too. Hence, such a cascade of droplet disintegrations leads finally to nanoparticles, i.e. nanodroplets. Analogous, but a complex self-similar process leads to the creation of nanofibres from macroscopic liquid jets in the area of electrospinning. Accordingly, condition in Equation (3.22) represents qualitative explanation of procedures that lead to the creation of still tinier objects made by charged liquid bodies.

### 3.5 Contemporaneous theories of electrospinning onset

Experimental as well as theoretical results on water droplet disintegration under the action of electrical forces can be extended to a description of electrospinning onset. Already, Rayleigh evidently knew that jets develop out of the unstable ends of ellipsoidal drops for greater values of surface charge density in these areas. Experiments have shown that the elongation of the droplet ellipsoidal shape leads to a quick development of apparently conical/wedge/vertex from which appears a jet. Particularly referring to Figure 9, it may be concluded that preliminary electrostatic analysis near a wedge-shaped conductor has quite a remarkable characteristic similarity with electrospraying and electrospinning of conductive liquids, where cone-like liquid spikes appear just before jetting and spraying. This analysis was carried out by Landau and Lifshitz [19], first published in 1956, and by Taylor [16].

Landau investigated potential  $\varphi$  near the tip of a solid and slender cone with semi-vertical angle  $2\theta_0 \cong 0$ . The problem has axial symmetry along the cone axis. The Maxwell

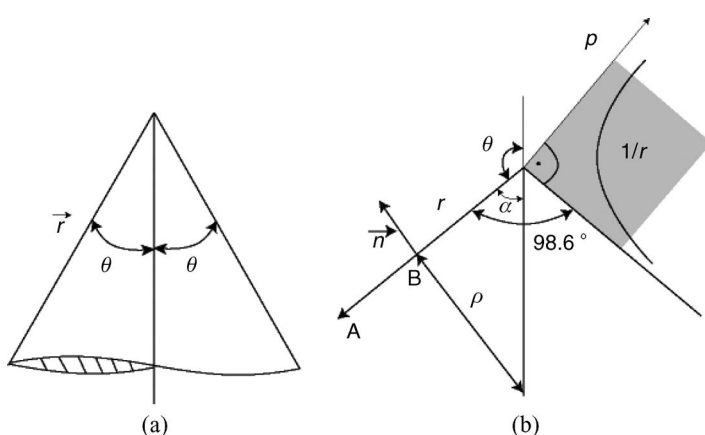


Figure 9. (a) Landau's analysis of electrostatic field near a conical body, where the field strength varies by  $r^n$  about the wedge. Variables  $(r, \theta)$  represent the polar coordinates in two dimensions. (b) Taylor's analysis of field near a liquid conical conducting surface, where field varies by  $1/\sqrt{r}$ . The characteristic value of the cone's semi-vertical vertex angle,  $\alpha$ , is  $49.3^\circ$ .

equation  $\Delta\varphi = 0$ , as stated before in the context of the above Equation (3.7), for the axially symmetric electrostatic potential  $\varphi(r, \theta)$  in spherical coordinate system  $(r, \theta, \phi)$  sounds as

$$\frac{1}{r^2} \frac{\partial}{\partial r} \left( r^2 \frac{\partial \varphi}{\partial r} \right) + \frac{1}{r^2 \sin \theta} \frac{\partial}{\partial \theta} \left( \sin \theta \frac{\partial \varphi}{\partial \theta} \right) = 0, \quad (3.23)$$

where  $r$  is the radial distance from the origin and  $\theta$  is the elevation angle, see Figure 9. Other symbols have usual meanings. It is supposed further that the origin of the coordinate system is located in the tip of the slender cone, as given in more detail by Jeans [39] about relation (3.23). Landau considered the trial solution in the vicinity of the cone tip for separating the variables,  $r$  and  $\theta$ , of the potential,  $\varphi$ , in the above equation in the form of  $\varphi(r, \theta) = R(r)S(\theta)$ , where  $R(r) = r^n$  and  $S(\theta)$  is a function of the angular variable  $\theta$  only. The potential,  $\varphi$ , has to be constant, and for convenience zero, on the cone surface. To fulfil that, one can suppose  $S(\theta)$  zero for  $\theta \rightarrow \theta_0$ . A solution trial for Equation (3.23) was then done with the following expression for  $S(\theta)$ :

$$S(\theta) = \text{Const.} \times [1 + \Psi(\theta)]. \quad (3.24)$$

Substitution of Equation (3.24) and  $R(r) = r^n$  into Equation (3.23) leads to the solution  $\Psi(\theta) = 2n \ln[\sin(\theta/2)]$ . For the potential,  $\varphi$ , to remain zero, on the conical contour, when the angle,  $\theta$ , approaches  $\theta_0$ , the expression  $1 + \Psi(\theta)$  has to diminish. This condition is satisfied when

$$n = -\frac{1}{2 \ln[\sin(\theta_0/2)]}. \quad (3.25)$$

The plot of the  $n$ - $\theta$  relationship is introduced in Figure 10. It means  $n \rightarrow 0$  with  $\theta \rightarrow 0$ . Thus, the field strength  $E$  in the vicinity of a sharp cone behaves as  $r^{n-1} \cong r^{-1}$ ,

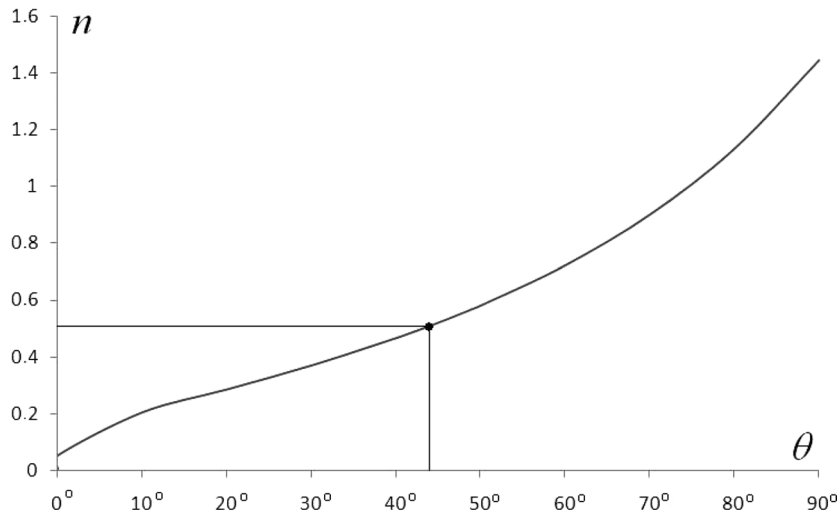


Figure 10. The plot of Landau Relation (3.25),  $n = -1/2 \ln[\sin(\theta/2)]$ . For  $n=0.5$ , the relation gives the semi-vertical angle as  $43.2^\circ$ .

since the perpendicular component of the field strength  $E_\theta$  in spherical polar coordinates reads  $E_\theta = (1/r)\partial\varphi/\partial\theta$ .

Taylor [16] solved a similar problem but with liquid cone having a semi-vertical angle  $2\theta_0$  that was non-zero. This problem attracted his attention since liquid cones were observed in his thorough experiments with soap bubbles under external electrostatic field. He considered the analogous trial solution of Equation (3.23) as Landau did,  $\varphi(r, \theta) = R(r)S(\theta)$ . Differently from Landau, Taylor, dealing with conductive liquid cones, considered a balance between the capillary  $p_c$  and electrostatic pressure  $p_e$ . The electrostatic pressure  $p_e$  has to vary along the liquid cone surface by  $1/r$  to compensate the Laplace pressure  $p_c = \gamma/(rtg\theta_0)$ . Accordingly, the electric field strength  $E$  has to vary as  $1/\sqrt{r}$  to compensate capillary effects, since the electric pressure is proportional to  $E^2$ , as given in relation (3.19). So, the function  $R(r)$  had to have the form considered by Taylor,  $R(r) = Ar^{1/2}$ , where  $A$  is a constant. Taylor also deduced the structure of  $S(\theta)$  from Equation (3.23) as a ‘fractional order Legendre Polynomial’,  $P_{1/2}(\cos\theta)$  that has been tabulated by Gray [40], so the potential is of the form:

$$\varphi = \varphi_0 + A\sqrt{r} P_{1/2}(\cos\theta). \quad (3.26)$$

For the potential to be constant along the surface of the cone, the angular part  $S(\theta)$ , i.e. the Legendre Polynomial, had to be zero on the cone surface, where  $\theta \rightarrow \theta_0$ . The fractional Legendre Polynomial vanished only at an angle of  $\theta_0=49.3^\circ$  as obvious from  $P_{1/2}(\cos\theta)$  graph in Figure 11.

On the contrary, for  $n=0.5$ , the Landau Equation (3.25) for ‘non-slender cone’ gives the semi-vertical angle  $\theta_0$  as  $43.2^\circ$ . Thus, Landau arrived at a different mathematical structure than that of Taylor with some simplified assumption, resulting in a small total variation of semi-vertical angle  $2\theta_0 \cong 12^\circ$  of the equilibrium liquid cones in external electrostatic fields. Taylor’s effort subsequently led to his name being coined with the conical shape of the fluid drops in an electric field at the critical stage just before disintegration.

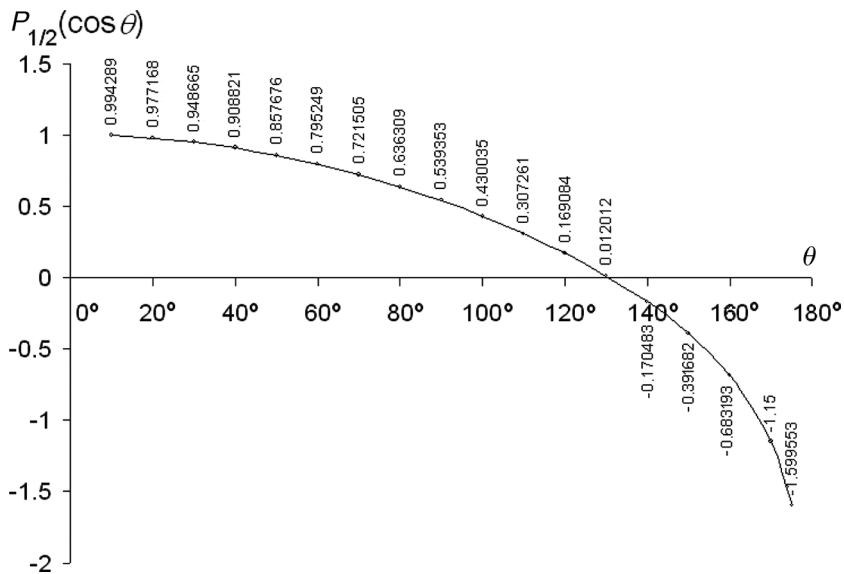


Figure 11. A plot of fractional order Legendre Polynomial  $P_{1/2}(\cos\theta)$ .

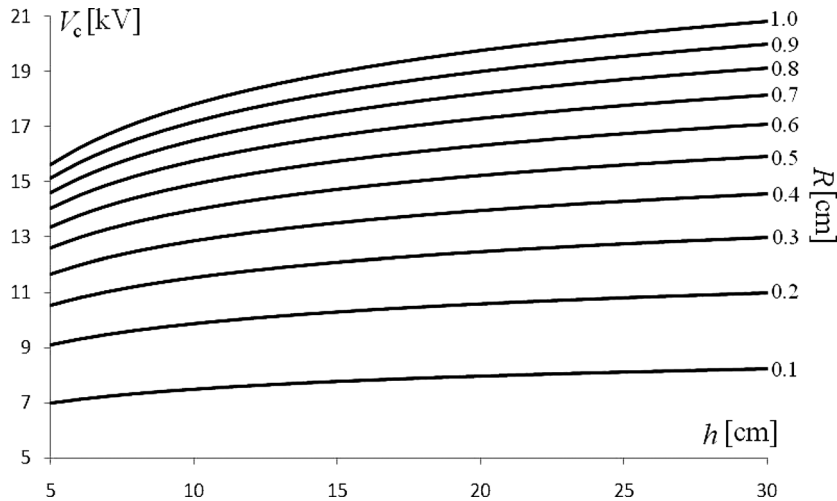


Figure 12. Critical voltages  $V_c$  for needle electrospinner and for liquid surface tension of distilled water,  $\gamma = 72 \text{ mN/m}$ . Curves represent  $V_c$  dependence on a distance,  $h$ , between the needle tip and collector for various values of needle radii,  $R$ .

Taylor [16] also determined the lowest value of voltage  $V_c$  at which a fairly conducting fluid with surface tension,  $\gamma$ , is drawn from the tube of Zeleny apparatus, see Figure 4, when the hydrostatic pressure is zero to make the top of the liquid like that of a plane mirror as

$$V_c^2 = 4 \ln\left(\frac{2h}{R}\right)(1.30\pi R\gamma)(0.09), \quad (3.27)$$

where  $h$  is the distance from the needle tip to the collector in centimetres,  $R$  denotes the needle outer radius in centimetres too, and surface tension  $\gamma$  is taken in mN/m. The factor 0.09 was inserted to predict the voltage in kilovolts. Critical voltages  $V_c$  for surface tension of distilled water,  $\gamma = 72 \text{ mN/m}$ , and various values of  $h$  and  $R$  are depicted in Figure 12.

### 3.6 Self-organisation of electrospinning jets on free liquid surfaces

It has already been underlined that self-organisation of the fluid in electrospinning is the underlying cause behind formation of the Taylor cone, the stable jet part, the whipping zone and evaporation of solvent. Now, it will be shown that the self-organising potential of electrospinning is even more powerful, since it has the power to organise individual jets on free liquid surfaces without any need to use needles/capillaries to create them. This finding is enormously attractive regarding the recent effort to elevate electrospinning technology to industrial level because it opens a chance to design simple, as well as highly productive, lines for nanofibrous layer production.

The self-organisation of jets on the free liquid surface is qualitatively illustrated in Figure 13, where a droplet of a very viscose component of epoxy resin is deposited on a bulky metallic rod of a diameter slightly greater than 1 cm. The metallic rode serves as an electrode, while a collector is placed above it. The collector is not depicted in the figure in question. The epoxy resin droplet originally has an approximately hemispherical shape when there is no electrostatic field in its vicinity, as shown in Figure 13a. The droplet

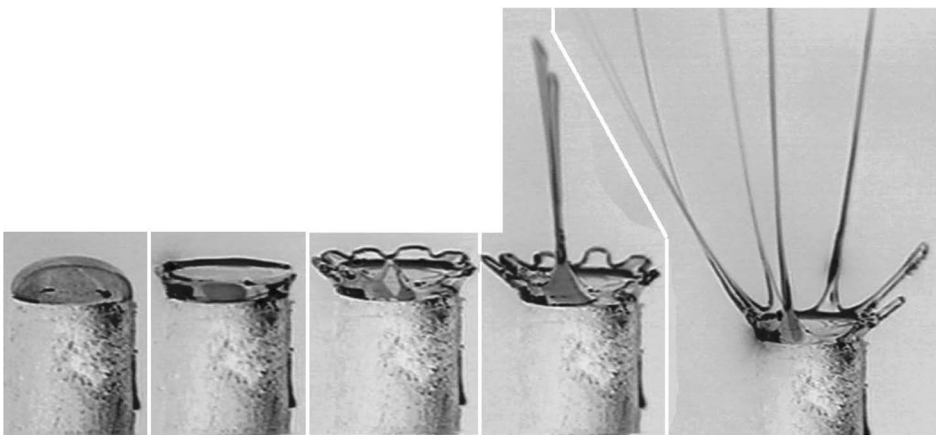


Figure 13. The self-organisation of jets on a free liquid surface is qualitatively illustrated using a motion of a droplet of a very viscous component of epoxy resin under increasing external field strength. The droplet is deposited on a bulky metallic rod of diameter slightly greater than 1 cm that serves as an electrode in an electrospinner. A collector is placed at an upper level, outside the depicted zone. At zero field strength, the viscous droplet has a hemispherical shape, as shown in the left-hand side of the figure. Above the critical field intensity value, liquid jets are self-organised, shown in the most right-hand side of the figure. (Courtesy of Sandra Torres, Technical University of Liberec.)

shape changes after the high voltage source is switched on to create an electrostatic field in the space between the electrode and the collector. The net charges induced on the droplet outer surface are of the same signs, so they mutually repel each other through electrostatic forces. The free energy of the system minimises at this stage by location of the net charges predominantly on the droplet periphery. Attractive Coulombic forces between the net charge on the droplet periphery and the collector develop a swelling droplet rim and bring about a plate-like shape of the droplet (Figure 13b). Further increment of the field strength leads to the most important feature regarding the theoretical description of the phenomenon: on the previously smooth rim, a stationary wave is organised, which is depicted in Figure 13c. If the field intensity is mounted even further, then the jets appear simultaneously from the crests of the stationary wave, as shown in Figures 13d and 13e.

Taking into account the above-mentioned observation, electrospinning, a special case of electrojetting, may really be analysed from the point of view of self-organisation of liquid jets under electric field, as detailed in Lukas et al. [41] by the mechanism of the fastest forming instability. In this analysis, it is supposed that electrohydrodynamics of a liquid surface may conveniently be analysed with the capillary waves running on an one-dimensional approximation of the fluid surface, oriented along the horizontal axis, say,  $x$ -axis, of the Cartesian system of coordinates. The wave's vertical displacement along the  $z$ -axis is described using the periodic real part of a complex quantity,  $\xi = A \exp[i(kx - \omega t)]$ , where  $k$  denotes wave number and  $\omega$  is angular frequency. The relationship between the wave number  $k$  and wavelength  $\lambda$  is,  $k = 2\pi/\lambda$ , while angular frequency  $\omega$  is related to period  $T$  as  $\omega = 2\pi/T$ .

There exist strict relationships  $\omega = f(k)$  between spatial and time-dependant parameters  $k$  and  $\omega$  of waves undergoing various force fields that are called dispersion laws. For so-called gravity waves, where the gravity field is taking into account, only the dispersion law sounds as,  $\omega^2 = gk$ , where  $g$  is gravity acceleration. This dispersion law describes heavy macroscopic waves observed usually on river, lake and sea surfaces. Since tiny

waves allow surface phenomena to occur, they are driven by surface tension in addition. Their dispersion law has a shape  $\omega^2 = gk + \gamma k^3/\rho$ , where  $\rho$  denotes liquid mass density.

The liquid in the electrospinning zone is subjected to the fields of gravitation and electricity, in addition to capillary effects, caused by surface tension and non-zero curvature of its surface. The related dispersion law of liquid surface may be given as

$$\omega^2 = (\rho g + \gamma k^2 - \varepsilon E_0^2 k) \frac{k}{\rho}. \quad (3.28)$$

For a particular liquid, the critical parameter to initiate jetting is the field strength,  $E_0$ . When  $E_0$  exceeds a critical value,  $E_c$ , the square of the angular frequency,  $\omega^2$ , becomes negative and so,  $\omega$  becomes purely imaginary. The imaginary angular frequency, defined as  $q = \text{Im}(\omega)$ , then abruptly changes the behaviour of the superficial waves that obey the following relation  $\xi = Ae^{qt} \exp(ikx)$ . According to this relationship, the wave forfeits its time dependency in its harmonic/exponential part. As a consequence, the originally running wave becomes a stationary one, as also supported by the experimental observation shown in Figure 13. On the other hand, the time dependency is moved, due to purely imaginary nature of the angular frequency, to the amplitude part of  $\xi(x, t)$ , where the term  $e^{qt}$ , having  $q > 0$ , causes the perpetual growth of the wave amplitude. The critical field strength  $E_c$  for unstable waves may be derived directly from Equation (3.28) considering that the minimum of  $\omega - k$  reaches zero value as shown in Lukas et al. [41].

$$E_c = \sqrt[4]{4\gamma\rho g/\varepsilon^2}. \quad (3.29)$$

From Equation (3.29) follows a threshold condition  $\varepsilon E_c^2/2 = \gamma/a$ , where  $a = \sqrt{\gamma/(\rho g)}$  is the capillary length, frequently used in colloid chemistry and wetting theory, vide Adamson and Gast [27]. It is noteworthy that the dynamic analysis of the electrohydrodynamic instability arrived to the condition of equal values of electric and capillary pressures in criticality. Here, electric pressure has its common form  $\varepsilon E_c^2/2$ , while capillary pressure,  $\gamma/a$ , exhibits capillary length,  $a$ , as a typical radius of curvature. It is convenient to define a dimensionless electrospinning number  $\Gamma$  as

$$\Gamma = \frac{a\varepsilon E_0^2}{2\gamma}. \quad (3.30)$$

Using this definition, electrospinning is initiated only if the electrospinning number,  $\Gamma$ , is greater than one. Its critical value reaches unity, i.e.  $\Gamma_c = 1$ .

Minimal and negative square values of the angular frequency  $\omega^2$  correspond to the maximal growth factors,  $q$ 's, inherently connected with the self-organisation caused by the mechanism of the fastest forming instability. The minimal value of  $\omega^2$  with respect to  $k$  is obtained by solving  $d\omega^2/dk = 0$ , thus obtaining two solutions  $k_1$  and  $k_2$ , that are expressed together as  $k_{1,2} = (2\varepsilon E_0^2 \pm \sqrt{(2\varepsilon E_0^2)^2 - 12\gamma\rho g})/6\gamma$ . Minimum of  $\omega^2$  occurs at that value of  $k$ , whichever is greater, for as much the smaller value of  $k$  represents local maximum of the  $\omega^2 - k$  relationship. Since the average inter-jet distance is described in terms of the wavelength,  $\lambda = 2\pi/k$ , its dependency on  $E_0$  is governed by the following relation:

$$\lambda = \frac{12\pi\gamma}{2\varepsilon E_0^2 + \sqrt{(2\varepsilon E_0^2)^2 - 12\gamma\rho g}}. \quad (3.31)$$

This can be expressed more comprehensively using the capillary length,  $a$ , and electrospinning number,  $\Gamma$ , through a dimensionless intra-jet distance  $\Lambda = \lambda/a$  as given below:

$$\Lambda = \frac{3\pi}{\Gamma + \sqrt{\Gamma^2 - 3/4}}. \quad (3.32)$$

This relationship is universal for needleless electrospinning of all conductive liquids. The critical value of the dimensionless intra-jet distance is  $\Lambda_c = 2\pi$ .

Apparently, now it seems that there exist two parallel theories explaining an onset of electrospinning: the first one for capillary spinners and the last one for electrospinning from free liquid surfaces. On the contrary, electrospinning as a phenomenon exists in its unity, independently of any theoretical tool used for its description. To show the unity of these two approaches, the critical field strength for electrospinning from free liquid surface,  $E_c$ , is first compared with  $E_c$ 's for distilled water jets from capillaries of various radii  $r$ , measured by Zeleny [9], shown in Figure 14. In his experiments, Zeleny applied no hydrostatic pressure to the liquid in the capillary, thus meeting a system of assumptions in the present case. To join the two theoretical approaches to the electrospinning onset, it is assumed for this moment

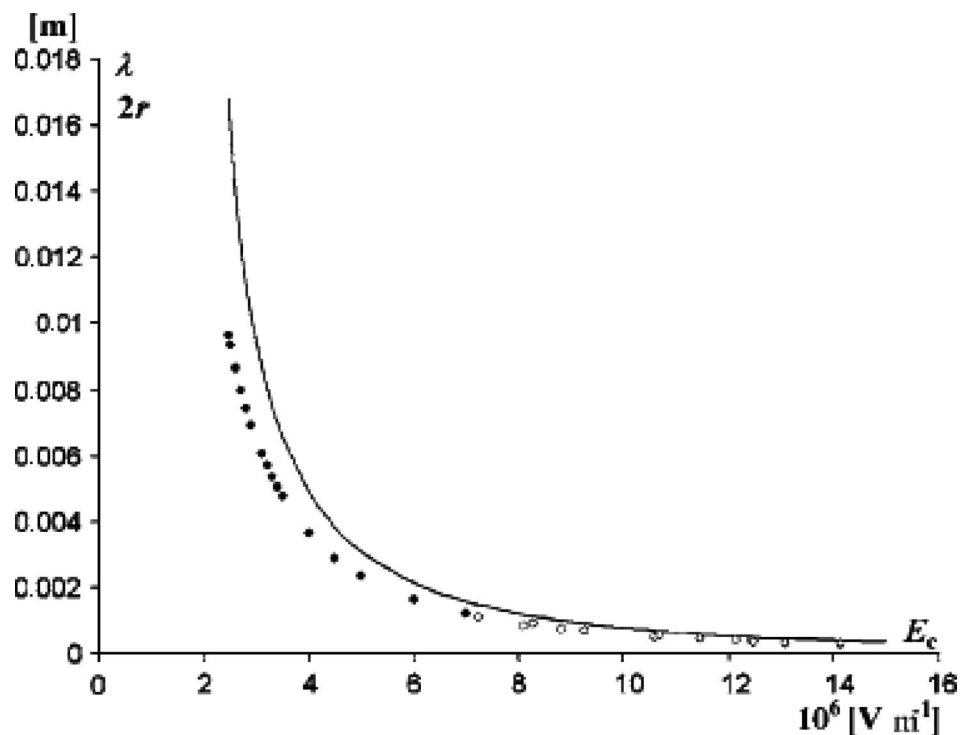


Figure 14. Dependence of the wavelength,  $\lambda$ , on the critical field strength,  $E_c$ . The  $\lambda-E_c$  relationship is plotted for distilled water with negligibly small hydrostatic pressure and ambient temperature close to 22°C. Critical field strength values, according to Zeleny's observations, are depicted as empty circles, and the ones obtained from his extrapolation formula,  $E_c\sqrt{r} = 56.9 \times 30,000 \text{ V m}^{-1/2}$  [9], are in filled-up circles. The comparison is based on the relationship  $\lambda \approx 2r$  (Lukas et al. [41]). Reprinted with permission from Lukáš D., Sarka A., Pokorný P., Journal of Applied Physics, Vol. 103, Pages 309–316, 2008. Copyright © 2008, American Institute of Physics.

that electrospinning from a needle/capillary in capillary electrospinners may occur only under the condition that the needle diameter  $2r$  is equal to the wavelength  $\lambda$  of the fastest growing wave, predicted by the theory of free liquid surface electrospinning. Critical field strengths, according to Zeleny's observations, are plotted in Figure 14 for capillary radii,  $r$ , up to  $2r = 1.086$  mm. For greater capillary radii, Zeleny's extrapolation is used according to the formula  $E\sqrt{r} = 56.9 \times 30,000 \text{ V m}^{-1/2}$  earlier introduced by Zeleny [9]. Critical field strength values, predicted by the present theory and Zeleny's experimental dataset, are quite comparable. Therefore, the theory in question and the above assumption that the critical field strength value,  $E_c$ , allows the creation of surface wave whose wavelength,  $\lambda$ , predicted using the above-mentioned Formula (3.31), is equal to the capillary diameter  $2r$ , are positively confirmed.

### 3.7 Electrospinning as an application of the physical law of dielectric diffusion

In an effort to consolidate the wave theory, presented by Lukas et al. [41], based on mostly a mathematical approach to explain electrohydrodynamics, an even more generalised and robust physical approach is adopted by Sarkar et al. [42]. Changing the standpoint in describing the system from minimisation of superficial energy, characterised by the associated wave's angular frequency, to the one considering minimisation of energy stored inside a 'condenser' by a medium of a certain permittivity seems to have the ability not only to describe the detailed behaviour of liquids in the spinning zone, but even able to unify all electrohydrodynamic phenomena, like electrospinning, electrospraying, electrocapillarity and electrophoresis. The phenomenon of dielectric diffusion was first reported by Breuer and Robinson [43] as 'When an electric field interacts with a medium of inhomogeneous dielectric constant, there is a flow of matter in the direction of increasing dielectric constant'. The stated phenomenon, however, lacked proper theoretical explanation in their report, and presently the researchers found an appropriate way to explain the phenomenon through 'minimization of energy in a capacitor' as argued in Sarkar et al. [42].

To make the considerations about dielectric diffusion concept more explicit, energy stored in a capacitor, and force acting on a dielectric body in a capacitor will be briefly described. The energy stored in a capacitor of volume  $V$ , having permittivity of  $\varepsilon$ , is given by Feynman et al. [33] as

$$U = \int \left( \frac{\varepsilon \vec{E} \vec{E}}{2} + \frac{\varepsilon c^2 \vec{B} \vec{B}}{2} \right) dV, \quad (3.33)$$

where  $c$  is the light speed and  $\vec{B}$  is the vector of magnetic intensity. The second term containing  $\vec{B}$  in Equation (3.33) describes non-equilibrium phenomena when a charge movement generates a magnetic field. The actual permittivity of a material,  $\varepsilon$ , in an electric field is a product of permittivity of vacuum,  $\varepsilon_0$ , and relative permittivity,  $\varepsilon_r$ , of the medium that indicates how the material behaves in an external electric field, i.e. ability to get polarised under an external electrostatic field. The resultant electric field intensity decreases due to higher polarisation of the more conductive medium, and as it depends non-linearly on electric field intensity, the overall energy of the system decreases eventually. Accordingly, when an electric field interacts with an inhomogeneous medium with different dielectric constants, matter with highest dielectric constant tends to fill the space between capacitor's plates. The energy stored in a capacitor in a way reflects the energy stored between the two poles of the power supply to it. Thus, ideally (neglecting internal resistance of the supply and the wire), the two plates of the capacitor have a tendency towards arriving

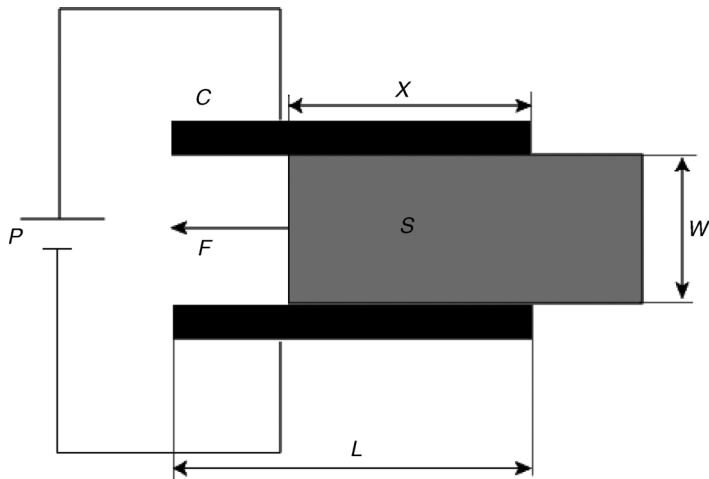


Figure 15. The force,  $F_x$ , acting on a solid dielectric slab, partially inserted in a parallel plate capacitor of width,  $W$ , tries to push the dielectric material  $S$  into the inter-plate region of the capacitor to fill it and minimise the stored energy.

equipotential condition by reducing the energy stored between them. In other words, the mass of the dielectric in the capacitor required to minimise the energy depends indirectly on its permittivity, determining its conductivity. In all practical cases, there is a potential drop across the inter-plate gap due to resistance and, therefore, a competition between the dielectrics when an inhomogeneous medium fills the charged capacitor.

According to Feynman et al. [33], the force,  $F_x$ , acting on a solid dielectric slab, partially inserted in a parallel plate capacitor (Figure 15), of width  $W$  tries to push the material into the inter-plate region of a capacitor to fill it, and is quantitatively derived using conservation of energy as

$$F_x = -\frac{\partial U}{\partial x} = -\frac{Q^2}{2} \frac{\partial}{\partial x} \left( \frac{1}{C} \right) = \frac{V^2 \varepsilon_0 W}{2} \frac{1}{d} (\kappa - 1), \quad (3.34)$$

where the symbols  $U$ ,  $Q$ ,  $C$ ,  $\varepsilon_0$  and  $\kappa$  stand for the energy stored in the condenser, the charge on the condenser, capacitance, permittivity of vacuum and dielectric constant of the material, respectively. Symbols  $W$  and  $d$  represent the width of the plates and the gap between the plates.

#### 4. Liquid jet in an electric field

Physics of jets is an extremely attractive and active field. The earliest study of jet forming and its break up was probably done by Leonardo da Vinci [44], while Nollet [45] demonstrated how a water jet disintegrates when it is charged. Very recent review work on physics of jets is written by Eggers and Villermaux [46]. The meaningful contribution to electrospinning jet behaviour is Reneker and Yarin's [4] work that is mostly focused on physical mechanisms of the jet bending, whipping, branching, splitting or on perturbation resulting in the jet break up into isolated droplets, i.e. creation of sprays or fibres in electrospinning, including non-Newtonian effects.

#### 4.1 Jet path

Three main topics are discussed in this sub-section that starts with natural tendency of each liquid jet to be detached into isolated droplets due to Rayleigh instability driven by surface tension. The next topic is devoted to ‘stable jet zone’, where the main interest is focused on a scaling law according to which jet radius decreases along the initial straight jet path. The most complex and peculiar electrospun jet behaviour is called ‘bending instability’ or ‘whipping jet zone’, where jet forms fractal like coiling and branching due to Ernshaw’s theorem, as available in Jeans [39].

##### 4.1.1 Rayleigh instability

The most significant factor that hinders a smooth spinning process of fibres from liquid jets is the Rayleigh instability, as named after Rayleigh [47]. Because of this surface tension-driven phenomenon, cylindrical jet-like liquid bodies are completely detached into isolated droplets when no precautionary measures for stabilisation are applied. Accordingly, this instability is counter-productive to engineering efforts to produce artificial fibres. It will be revealed qualitatively at the end of this sub-section that external electrostatic field also effectively protects the development of the Rayleigh instability during electrospinning.

The theoretical approach to Rayleigh instability resembles the previously mentioned electrohydrodynamic instability of free liquid surfaces introduced in sub-section 3.6, since both of them belong to the same class of self-organisation phenomena that are caused by the mechanism of the fastest forming instability. Generally, disintegration of a liquid jet of radius  $r$  occurs due to the development of wave perturbations with various wavelengths  $\lambda$  on the surface of the liquid column, where  $\lambda$  has to be greater than  $\pi r$ , according to Plateau [48]. This perturbation ultimately triggers disintegration of the cylindrical liquid jet at an avalanching rate. Several researchers have later studied this phenomenon, both theoretically and experimentally. Three such studies that were conducted by Roe [49], Tomotika [50] and Meister and Scheele [51], respectively, are cited here.

A rough analysis of the Rayleigh instability can be conducted by associating the initial shape of a jet of an incompressible liquid, i.e. a cylinder in the present case, with the final shape of a chain of spherical droplets. The volume conservation between the cylinder and the sphere is assumed, and hence holds

$$\pi r_o^2 \lambda_e = \frac{4}{3} \pi r_d^3, \quad (4.1)$$

where  $\lambda_e$  is the length of the cylinder with original radius,  $r_o$ , that is converted into one droplet of radius,  $r_d$ , as shown in Figure 16. Rearrangement of the previous relation in terms of droplet radius  $r_d$  causes it to take the following form:  $r_d = \sqrt[3]{3/4(r_o^2 \lambda_o)}$ .

The value of  $\lambda_e$ , obtainable from the volume and surface energy conservation laws, will be taken as the approximation of the Rayleigh wavelength,  $\lambda$ . The total energy of liquid bodies in spherical or cylindrical form is composed of two components. The first one is associated with the surface tension  $\gamma$ , i.e. the surface energy, while the last one is associated with the capillary pressure,  $p_c$ , i.e.  $p_c V$ . Quantities,  $S$  and  $V$  are, respectively, the surface area and the volume of the liquid bodies. The capillary pressure  $p_c$  is equal to  $2\gamma/r_d$  in a spherical droplet, while its value is  $\gamma/r_o$  in a cylinder. A liquid column will spontaneously form a droplet if its total energy is higher than the total energy of a probable subsequent

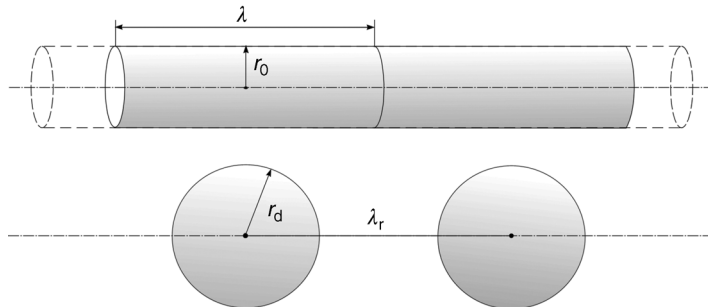


Figure 16. Rayleigh instability: a piece of liquid cylinder with the radius  $r_0$  having length  $\lambda$  is equivalent, with respect to volume, to a sphere of the radius  $r_d$ . The parameter  $\lambda_r$  is the characteristic distance between droplets into which the liquid cylinder disintegrates.

shape, the sphere. The change in energy before and after the disintegration of the liquid column clearly satisfies the relation, given as follows:

$$2\pi r_0 \lambda_e \gamma + \pi r_0 \lambda_e \gamma \geq 4\pi r_d^2 \gamma + \frac{8}{3}\pi r_d^2 \gamma, \quad (4.2)$$

where the left-hand side corresponds to the cylindrical jet, while the right-hand side describes both the surface and the volume energies of the spherical droplet. Substituting  $r_d^2$  from (4.1) into (4.2), one may obtain

$$\lambda_e \geq \frac{5^{3/4}}{3^4} r_0 \approx 1.96 \pi r_0. \quad (4.3)$$

A well-known similar inequality was first established experimentally by Plateau [48], while observing the onset of instability, marked with formation of spherical drops of oil in water mixed with alcohol from an elongated initial cylindrical shape. According to Plateau, the instability started when the cylinder length, i.e. wavelength,  $\lambda_e$ , was between  $1.99\pi r_0$  and  $2.02\pi r_0$ , quite close to the present estimation. A similar study, carried out by de Gennes et al. [52] ended up with the well-known inequality,  $\lambda_e > 2\pi r_0$ . Thus, conclusively, a drop cannot be formed when the wavelength is shorter than  $2\pi r_0$ , since the surface energy of the drop is always lower than that of the original smooth cylinder.

It is noteworthy that the exact value of the wavelength of the Rayleigh instability,  $\lambda = 2.87\pi r_0$ , cannot be derived merely on the basis of conservation of free energy. Transformation of the liquid body shape is coupled with dynamic mutation of its shape and surface area, causing changes of both surface and kinetic energies. The Rayleigh instability of liquid jets is the consequence of a temporal development and magnification of the originally tiny perturbations, also known as the capillary waves, as described by Chandrasekhar [53] and Adamson and Gast [27]. Assuming that the perturbations are harmonic surface waves, with assigned wavelength, the following relation for one-dimensional propagation of the wavy perturbation along the original cylindrical liquid column, coinciding with  $x$ -axis of cylindrical coordinate system, holds true:

$$r(x, t) = r_0 + \varepsilon \exp[i(kx - \omega t)]. \quad (4.4)$$

In the above relation, the real part of  $r$  is the radius of the liquid body as a function of space,  $x$ , and time,  $t$ ,  $r_0$  denotes original radius of a perfectly cylindrical column, and  $\varepsilon$  is the initial amplitude of the perturbation. The angular frequency of the surface wave is  $\omega$ , while  $k$  is the wave number.

Starting with the Euler Equation in cylindrical coordinates and applying appropriate boundary conditions, where a normal stress balance on the free liquid surface plays a critical role, one comes to a dispersion relation (4.5), as was shown by Chandrasekhar [53], that indicates the dependence of the angular frequency  $\omega$  on the wave number,  $k$ :

$$\omega^2 = \frac{\gamma}{\rho r_0^3} \frac{I_1(kr_0)}{I_0(kr_0)} kr_0(1 - k^2 r_0^2). \quad (4.5)$$

Liquid mass density is here denoted as  $\rho$ , while  $I_0(x)$  and  $I_1(x)$  are modified Bessel functions of the zero and first order. The relationship among dimensionless quantities,  $\omega^2 \rho r_0^3 / \gamma$  and  $kr_0$ , is depicted in Figure 17. The parameter  $kr_0$  has a critical value at 1 and, hence, the critical, previously mentioned, Plateau wavelength is  $\lambda_r = 2\pi r_0$ . Beyond this lower limit, the square of the angular frequency,  $\omega^2$ , is negative and so,  $\omega$  starts to be purely imaginary and may be denoted as  $iq$ . The negative value of  $\omega^2$  causes the imaginary part of  $\omega$ , i.e.,  $q = \text{Im}(\omega)$ , to play the role of a growing factor of the amplitude, as obvious from Equation (4.6). When  $\omega^2 < 0$ , the wave also becomes stationary, since the imaginary argument of the exponential function in Equation (4.6) loses its dependence on time, and the amplitude with positive growing factor  $q$  starts to grow instantaneously as  $\varepsilon e^{qt}$ :

$$r = r_0 + \varepsilon \exp[i(kx - iqt)] = r_0 + \varepsilon e^{qt} \exp[i(kx)]. \quad (4.6)$$

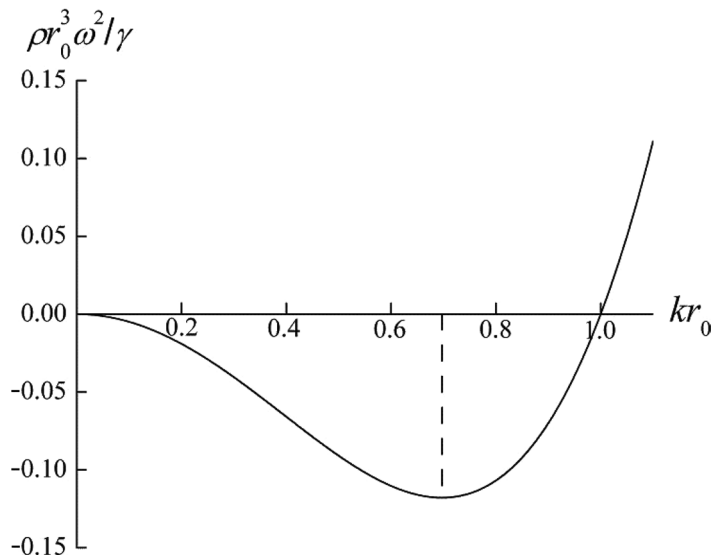


Figure 17. Dispersion law for Rayleigh instability plots dimensionless angular frequency,  $\rho \omega^2 r_0^3 / \gamma$ , against dimensionless wave number,  $kr_0$ . The fastest forming mode occurs for  $\partial \omega^2 / \partial (kr_0) = 0$ , where the wavelength  $\lambda$  reaches the value  $\lambda = 2.87\pi r_0$ .

Self-organisation, i.e. the detachment of a liquid column into equidistantly located droplets, by the mechanism of the fastest forming instability is due to the selection of the extreme value of the growing factor,  $q$ , that belongs to the minimal value of  $\omega^2$ . It is usually accepted that the resulting instability is entirely determined by the earliest state of the perturbations, for which Equation (4.5) holds. As indicated in Figure 17, the fastest forming mode occurs for  $\partial\omega^2/\partial(kr_0) = 0$ , when the wavelength is  $\lambda = 2.87\pi r_0$ . This value is called Rayleigh wavelength.

The external electrostatic field counters the development of the Rayleigh instability at least during the initial stage of the jet creation. This stage is called, by Qin et al. [54], ‘stable jet region’, since its path is quite direct. The reason for the stabilisation is the prevailing outward normal orientation of the electrostatic field strength lines with respect to the jet surface if the jet is made from conductive liquid, because one can suppose the charges are more mobile than the jet movement and so they can rearrange their positions into the equilibrium-like ones described previously in sub-section 3.3. The situation dominates especially just after the jet creation from the Taylor cone, where the electrostatic pressure,  $p_e = \epsilon E^2/2$ , acts opposite to the destructive capillary pressure. Thus, the external electric field hinders the Rayleigh instability. The stable jet region as well as its unstable part, called the whipping zone, will be detailed in the next two sub-sections.

#### 4.1.2 Stable jet zone

Qin et al. [54] introduced a robust approach for the analysis of the stable jet region, focused on the relationship between the radius  $r$  of the jet and the axial distance from the tip of the Taylor cone on the basis of allometric scaling. At this juncture, it is noteworthy that scaling and dimensional analysis were brought about by Newton, as referred by West [55], and was later developed in biology, physics of turbulence and economics, as documented by Kuikka [56]. The analysis of stable jet part involved three conservation laws of mass, net charge and energy in the jet. Conservation of mass, expressed through the continuity equation, could be referred to as

$$Q = \pi r^2 \rho v, \quad (4.7)$$

where  $Q$  symbolised the volume flow rate,  $\rho$  he liquid density and  $v$  was the axial velocity that was supposed to be constant in the whole jet cross-section, as shown in Figure 18.

Conservation of charges led to the following relation:

$$I = 2\pi r v \sigma + \kappa \pi r^2 E, \quad (4.8)$$

where  $I$  denoted the current passing through the jet, while  $\sigma$  and  $\kappa$  subsequently represented the surface charge density and bulk conductivity. Qin et al. [54] introduced a surface charge parameter,  $\alpha$  is an exponent of  $\sigma$  in Equation (4.8). This exponent was considered to be zero when no charge was on the completely non-conductive jet surface, while for all conductive jets  $\alpha = 1$ . The value of  $\alpha$  depended on factors like salt concentration in non-conductive polymer solution. Now, conductive jets only will be considered further for the sake of brevity. Equation (4.8) takes the traditional form for conductive liquids. Undoubtedly, the electrostatic intensity,  $E$ , notable in (4.8), represents the axial component of the electrostatic intensity vector that is supposed here to be non-zero, since, otherwise, the jet will not move ahead.

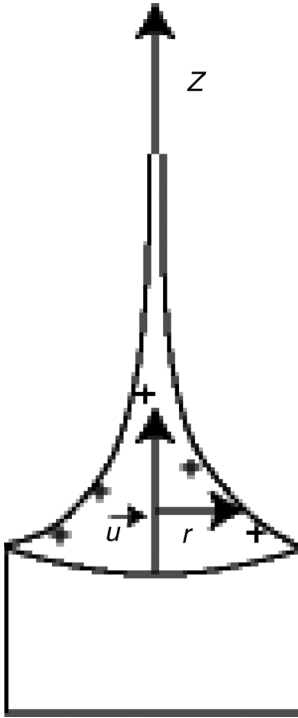


Figure 18. Stable zone of an electrospinning jet; the jet moves along the axis  $z$  with local velocity,  $\vec{u}$ . Jet radius at a level  $z$  is  $r$ .

The last conservation law, cited here, is the conservation of energy in the form of the modified Bernoulli theorem, presented commonly as

$$\vec{\nabla} \left( \frac{p}{\rho} + \frac{v^2}{2} + \varphi \right) = 0, \quad (4.9)$$

where  $\varphi$  represents potential energy per unit liquid mass. Except the kinetic energy per unit mass density,  $v^2/2$ , all the other terms in the Bernoulli Equation (4.9) are neglected in the present analysis. On the other hand, another term emerges that contains pressure  $p_E$ , generated by the axial component,  $E$ , of the electrostatic field. The pressure  $p_E$  has the form as given below:

$$p_E = \frac{2\pi r \Delta z \sigma E}{\pi r^2} = \frac{2\sigma E \Delta z}{r}, \quad (4.10)$$

where  $\Delta z$  denotes a virtual displacement along the jet axis, and so  $2\pi r \Delta z \sigma$  is the net charge on the elementary surface of the jet and hence  $2\pi r \Delta z \sigma E$  is the tangential force acting on it. All physical quantities, except material constants like  $k$  and  $\rho$ , are supposed to vary solely along the  $z$  coordinate. Accordingly, Hamilton operator  $\vec{\nabla}$ , in Equation (4.9), could be used in its one-dimensional form as  $d/dz$ . Moreover, it might be supposed that  $\sigma$  and  $E$  change along the  $z$ -axis only slowly. Consequently,  $dp_E/dz = 2\sigma E/r$  and the

modified Bernoulli Equation for the stable jet region is

$$\frac{d}{dz} \left( \frac{v^2}{2} \right) = -\frac{2\sigma E}{\rho r}. \quad (4.11)$$

The above equation is used for the dependence of the jet radius  $r$  on position  $z$  along the jet axis through ‘allometric’ relation  $r \sim z^b$ , where  $b$  is an unknown exponent, determined from the above-mentioned conservation laws, vide Equations (4.7), (4.8) and (4.11). The relation operator ‘ $\sim$ ’ stands for ‘Is proportional too’, assuming that the volume flow rate  $Q$  and the current  $I$  is unchanged along the stable jet region (i.e. neglecting evaporation and discharging). Hence, the quantity  $Q$  scales with  $r$  as  $Q \sim r^0$  and similarly, for  $I$  holds  $I \sim r^0$ . From the mass conservation, Equation (4.7) follows:

$$v \sim r^{-2} \quad (4.12)$$

and conservation of charges, i.e. Equation (4.8), gives the other two allometric relations between  $\sigma$ ,  $E$  and  $r$ :

$$\sigma \sim r \text{ and } E \sim r^{-2}. \quad (4.13)$$

Substitution from relations (4.11), (4.12) and (4.13) into the last relation in (4.13) provides the alometric relationship:

$$\frac{d}{dz} [r^{-4}(z)] \sim r^{-2}(z), \quad (4.14)$$

where  $r$  is expressed explicitly as a function of  $z$ . If  $r \sim z^b$  is used as a trial solution, then the last introduced scaling relation (4.14) can be rewritten as  $d/dz(z^{-4b}) \sim z^{-2b}$ . Differentiating the left-hand term and comparing exponents of both sides of the scaling relation, i.e.  $-4b - 1 = -2b$ , one obtains  $b = -1/2$  and the liquid jet radius,  $r$ , scales with  $z$  as

$$r \sim z^{-1/2}. \quad (4.15)$$

This scaling exponent was experimentally found for polyacrylonitrile (PAN), dissolved in *N,N*-dimethylformamide (DMF) for the stable part of the jet by Shin et al. [57].

#### 4.1.3 Bending instability

A viscoelastic electrospun polymeric jet is initiated at the tip of a Taylor cone, and at the beginning, its path is almost straight. So, this part of the jet, described in some details in the previous sub-section, is called the stable one. However, after a certain distance from the tip of the Taylor cone, the electrically driven instability sets in. The main cause for the instability is the Earnshaw’s theorem, introduced in Jeans [39], that claims: ‘A charged body placed in an electric field of force cannot rest in a stable equilibrium under the influence of the electric forces alone’.

The evidence of the Earnshaw’s theorem is rather easy. Suppose a charged body is placed in the external electrostatic field generated outside the body that is assigned a potential  $\varphi$ . Then, the energy  $w$  of each elementary charge in the body with respect to the

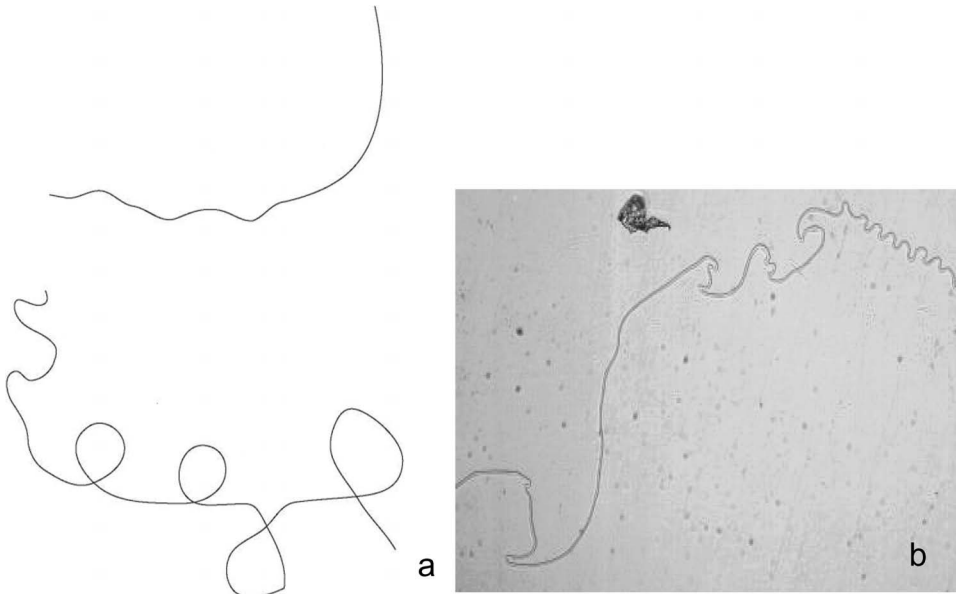


Figure 19. Loops in the unstable region of the jet, caught on a slide-glass – (a) PVA jet and (b) PEO jet.

external potential is  $w = e\varphi$  and the total energy  $W$  of the body regarding the external field is  $W = \sum_i^N e\varphi_i$ , where the summation goes through all elementary charges in the body. The potential  $\varphi$  satisfies the Laplace Equation  $\Delta\varphi = 0$  even inside the charged body, since  $\varphi$  is the external field generated by charges outside the body. Because of linearity of the Laplace operator,  $\Delta$  holds

$$\Delta W = 0. \quad (4.16)$$

It is well known that the function satisfying the Laplace Equation cannot have any local extreme including minimum, and so, any free charged body cannot reach its equilibrium position in external electrostatic field.

The electrospun jet fully confirms the conditions mentioned in the Earnshaw's Theorem, since it is charged and placed into the external electrostatic field generated by an electrode and a collector. As a result of the instability, the jet elongates dramatically, jet looping/bending appears and the jet cross-sectional radius reduces (Figure 19). The analytical description of the bending instability based on electrohydrodynamics is rather complex, and therefore, it is beyond the scope of this comprehensive description of physical principles of electrospinning. On the other hand, there exist an exhausting recent monograph by Reneker and Yarin [4] dealing, in detail, with the jet path in electrospinning, and interested readers might consult it. Therefore, the sub-section in this work will mostly be oriented towards qualitative explanation of the phenomenon.

The bending instability of a jet may be roughly considered analogous to the bending instability of a rod, when subjected to compressive forces. If a moderate load is put on the vertically straight rod, its length is reduced first, keeping its axis upright and in the original direction. There exists, however, a critical value of the load above which geometrical response of the rod to the external load dramatically changes. Instead of the

axially symmetric contraction of rod, buckling appears. Similarly dramatic is the abrupt transition between stable and whipping jet zone.

However, there are some differences between the behaviour of a contracted rod and an extended electrospun jet. Having a long cylindrical shape, the electrospun liquid jet, with its significant net charge content, experiences long range Coulomb forces among the charges. The forces tend to extend the jet in each of its regions. Prevailing Coulombic interactions here are the intrinsic ones, i.e. interactions between net charges inside the jet, since one may neglect interactions between the jet and external electrostatic field at this moment. Because of the arrangement of electrical charges along the approximately unidimensional jet, the resultant extensive Coulomb forces,  $F_c$ , acting on individual charges are highly anisotropic. Their components, along the jet axis, are due to the cylindrical jet geometry, much higher when compared to the transverse ones. Therefore, the jet starts to elongate both up and down the jet and the jet mass accelerates either ways axially with an acceleration,  $a$ . Hence, the inertial response from the jet's mass,  $m$ , immediately appears as a resisting force to Coulombic ones, since the jet acceleration obeys the Newton's first law  $F = ma$ . In spite of the mere qualitative characterisation introduced above, it is quite apprehensible that the longitudinal elongation of electrospun jet, that is present along the entire jet length, will result in a geometrical catastrophe, similar to that of compression of a rod. The jet elongation will not be axisymmetrical, since the inertial resistance in the forward and the backward directions plays a very similar role as the reactive force of the supporting base during buckling of the rod under compression. Hence, the only possible way in which the jet extends is by bending that takes a very wild form due to strength of Coulomb forces. On the contrary, liquid jets, that are solely acted upon by external forces, like gravity, can be extended without the bending. This is well instanced with a narrow stream of water that flows through a stopcock and is accelerated due to gravity. Such jet obeys Rayleigh instability but is free of any bending or whipping. One can conclude that the intrinsic Coulombic forces together with Earnshaw's Theorem, which is focused on external interactions between net jet charges and external electrostatic field, are two main reasons for the jet instability.

As the content of this sub-section is mainly qualitative, it is appropriate to accompany these considerations with several simple experiments leading to direct observation of bending instability that resembles whipping of fluid jet during electrospinning. The first experiment investigates the behaviour of 'jet' of a non-Newtonian fluid like 'Honey', met frequently in everyday life. As a stream of viscous liquid is allowed to fall by declining the spoon gradually at an altitude above a plate, the honey jet slides down and gets elongated by the gravity field. It is notable that the external gravitational forces, acting on the jet, are oriented merely downward and so the jet elongation is unilateral as opposed to previously mentioned intrinsic electrical forces in the electrospun jet that caused the jet to have bilateral extension. So, the uniform downward orientation of bulk forces is not expected to cause the bending instability of the honey stream. The situation dramatically changes in the vicinity of the plate on which the honey jet falls. The reactive/repulsive force due to the interaction with the plate and due to a non-zero elasticity of the honey column will result in its wild bending that is related closely to the phenomenon of bending instability of compression of the rod and also to the whipping of an electrospun jet because it is its unilateral counterpart.

A similar experiment can also be carried out with a thread/yarn. If a couple of decimetres of a yarn are withdrawn from its spool and thereafter straightened to be grasped with a tweezer at successive instances at various distances from its free end with an aim to shift it axially along the table surface towards its free end, then the frontal part of the yarn remains straight when the distance of the grip to the free end is relatively short. On the contrary, a

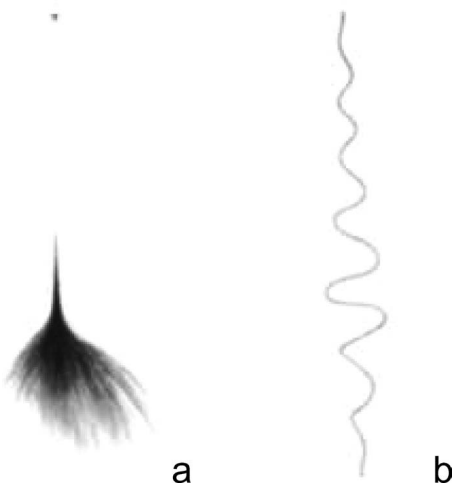


Figure 20. Instability of polyethylene-oxide jet – exposed with two various exposure times of 1 ms and 18 ns.

longer part of the thread ahead will tend to bend to create three-dimensional loops, quite similar to gyration of electrospun jets.

The experimental investigation of the bending instability of electrospun jets is quite complex at high velocities, in the order of tens of meters per second, when the bending of the jet takes place longitudinally as well as laterally. One of the techniques, developed for this research, is based on the usage of cameras with extremely high shutter speed, i.e. with an exposure time less than  $100 \mu\text{s}$ , as shown in Figure 20. Using such extremely short exposure time, it was observed that in the area of bending/whipping instability, an electrospun jet seldom splits into branches. The detailed structure of an electrospun jet was found to be quite different from apparent impressions when viewed with the naked eye. The impression is quite similar to that of a moving fan, consisting of hundreds of isolated and nearly straight elementary tiny jets.

An alternate and simple experimental way to investigate an electrospun jet path is based on an approach, called the slide-glass method, that resembles hunting for butterflies. The experimental procedure that enables us to investigate whipping jet zones by the slide-glass method uses principle of motion of a pendulum. The slide-glass is fitted horizontally, i.e. parallel to a collector, on a holder that moves back and forth in the space between an electrode and a collector. The motion of the slide-glass is driven by a pendulum mechanism as sketched in Figure 21. During the flight of the slide-glass, at an appropriate level above the electrode of an electrospinner with a polymer solution from which the jet is created, the electrospun jet is caught by it. The slide-glass is thereafter observed using a light microscope to study the jet shape. Results of these experiments are documented in Figure 21. This procedure enables one to investigate the development of the bending instability in some details.

According to the information obtained by this simple method, the development of the bending jet instability in electrospinning takes place in three stages. The first of them is smooth and sometimes a slightly curved part of a jet. This stage is followed by an abrupt development of a series of nearly harmonic waves with which the bending instability starts. The last part is marked by development of spiral loops whose radius gradually increases.

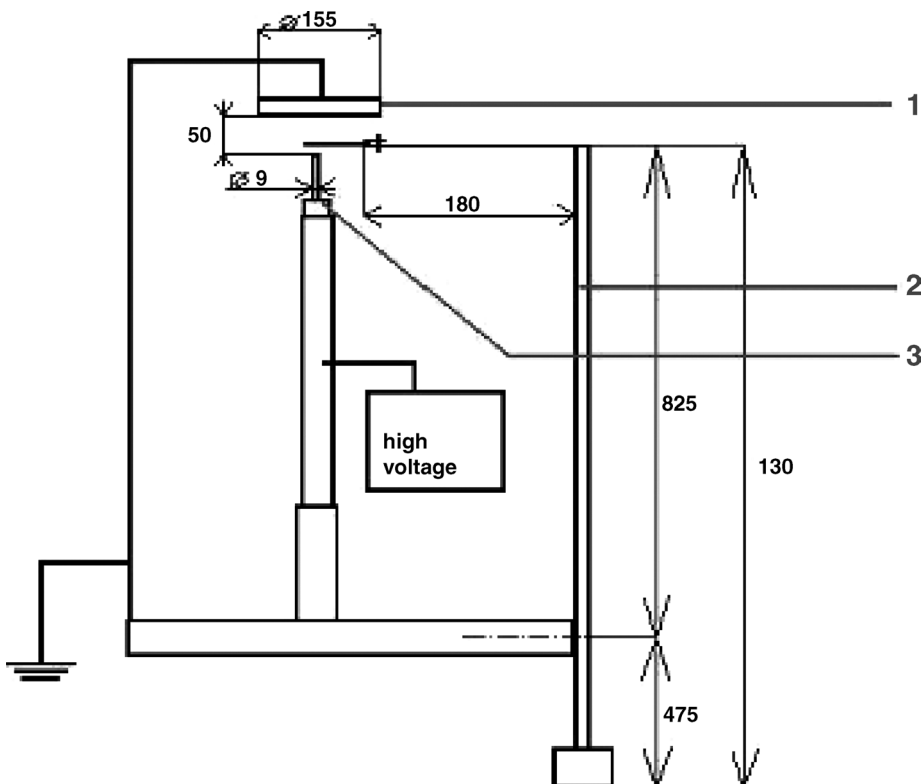


Figure 21. Schematic diagram showing the pendulum mechanism: (1) ground collector, (2) pendulum and (3) spinning electrode with a polymer.

Then, the jet instability starts to calm down. The next bending instability appears again after a period of another nearly straight jet. Smaller jet kinks are also developed on larger branches of previous loops. In other words, the jet gyration becomes fractal-like. Existence of the described jet shapes are illustrated in Figure 21.

#### 4.2 Solvent evaporation

One of the most fascinating features of electrospinning is the ability of the spun jet to oust small solvent molecules during extremely short periods of time when the jet travels from the electrode to the collector. In other words, the elongated and narrowed whipping jet operates as a significant operative dryer even at room temperature. The principle of the phenomenon leading to the evaporation of more than 80% of the solution from the jet during a fraction of a second has its explanation in the realm of thermodynamics. Particularly the phenomenon is well explained by Thomson-Kelvin law, as will be elucidated further.

One can distinguish two components of the internal/total energy  $U$  of each thermodynamic system that are particularly involved in a liquid. One of them is called the free, or Helmholtz energy,  $F$ , representing the part of the liquid energy  $U$  that can be used to do work. The other part of the liquid energy is connected with the entropy part of the total energy  $U$  that can never be obtained from the system by exploiting it at a constant temperature. This 'hidden' part of the system energy is expressed as the product of entropy

$S$  and temperature  $T$ . From the foregoing follows

$$U = F + ST. \quad (4.17)$$

Then, the differential free energy,  $dF$ , has the shape

$$dF = d(U - TS) = dU - T dS - S dT. \quad (4.18)$$

The second term on the right-hand side of Relation (4.18) can be expressed using the thermodynamic identity, as introduced by Kittel and Kroemer [29], that follows from the differential of entropy  $dS$ . Since entropy is supposed to be a function of energy  $U$ , the number of particles  $N$ , and volume  $V$ , thus  $S = S(U, N, V)$ , its differential  $dS$  has the following structure:

$$dS = \left( \frac{\partial S}{\partial U} \right)_{V,N} dU + \left( \frac{\partial S}{\partial N} \right)_{U,V} dN + \left( \frac{\partial S}{\partial V} \right)_{U,N} dV, \quad (4.19)$$

where indices  $V$ ,  $N$  and  $U$  denote constant quantities for the particular differentiation. The three particular derivatives in Equation (4.19) have well-known meanings that are

$$\left( \frac{\partial S}{\partial U} \right)_{V,N} = \frac{1}{T}, \quad \left( \frac{\partial S}{\partial N} \right)_{U,V} = -\frac{\mu}{T}, \quad \left( \frac{\partial S}{\partial V} \right)_{U,N} = \frac{p}{T}, \quad (4.20)$$

where  $\mu$  is chemical potential and  $p$  denotes pressure. Combining Equations (4.18) and (4.19), one obtains an alternative expression for the differential free energy,  $dF$ , as the consequence of the substitution for  $T dS$  in relationship (4.18):

$$dF = \mu dN - p dV - S dT. \quad (4.21)$$

Equation (4.21) is the thermodynamic relation to which behaviour of liquids with curved surfaces may be associated. The assumption of a constant temperature during processes when the surface curvature of a liquid body, a jet for instance, causes the last term on the right side of (4.21) to be considered null. The next step is to introduce into the equation in question only measurable quantities. Hence, instead of the free energy differential  $dF$ , the free energy density  $f = dF/dV$  will be considered further to obtain the following relation from (4.21):

$$f = \left( \frac{dF}{dV} \right)_T = \mu c - p, \quad (4.22)$$

where particle volume concentration  $c$  has been defined as  $c = dN/dV$ . When the liquid body's surface curvature changes, the pressure  $p$  varies according to the Laplace's law, i.e.  $p = \gamma/(r_1 + r_2)$ , while free energy density  $f$  as well as concentration  $c$  are supposed to remain unchanged. So, from the free energy density conservation one obtains

$$\mu_f c - p_f = \mu_c c - p_c. \quad (4.23)$$

Hence, the capillary pressure increment  $\Delta p = p_c - p_f$  between a curved liquid, index  $c$ , and a flat one, index  $f$ , has to be balanced by the adequate increase of chemical potential

$\Delta\mu = \mu_c - \mu_f$  that is naturally multiplied by the concentration  $c$ . Indices of  $\mu$  have the same meaning as the indices of  $p$ . The general form of Laplace/capillary pressure for a curved surface is expressed as  $p = \gamma(1/r_1 + 1/r_2)$ , where  $1/r_1$  and  $1/r_2$  are two main curvatures belonging to main radii  $r_1$  and  $r_2$ . As a nearly cylindrical liquid jet, that is related to electrospinning, has one of the radii as infinite, while the last one is equal to the jet radius  $r$ , Equation (4.23) may be written as

$$\Delta\mu = \frac{1}{c} \frac{\gamma}{r}, \quad (4.24)$$

since  $p_f$ , the capillary pressure of a flat liquid surface, is considered as zero. The last relation particularly expresses the Thomson-Kelvin law, as presented by Adamson and Gast [27]. Thomson-Kelvin law is based on the condition of thermodynamic equilibrium that is characterised by the equality of pressures, temperatures and chemical potentials in all system parts. Though apparently it may seem that the resultant relation (4.23) does not lead to any equality of chemical potentials, since it predicts the difference in chemical potentials, one may still consider the ambient air to act as an enormously huge thermodynamic reservoir where chemical potential remains nearly unchanged during jet evaporation, and so Equation (4.23) informs us about the system's tendency to reach the equilibrium by means of intense solvent evaporation.

The role of the chemical potential may be explained by considering two subsystems: a jet and its ambient environment to be at different chemical potentials. Particles flow from areas at higher chemical potential to the areas with lower chemical potential. Since all the quantities of the right-hand side of (4.23) are positive,  $\Delta\mu$  is positive too. Thus,  $\mu_c > \mu_f$  and accordingly particles of solvent will flow from the jet to the ambient air. The difference in chemical potentials increases with the jet elongation and with evaporation of the solvent from the jet/fibre, since the consequence of both these processes is the diminution of the jet radius,  $r$ . As the radius decreases, further accelerated evaporation takes place via positive feedback. Because of the polymeric nature of the jet, the solution evaporates selectively. Solvent molecules escape to the ambient air, while less mobile, heavy and entangled polymeric chains remain in the jet to form a solid fibre. In this way, electrospinning works as a very effective dryer without any need to elevate the temperature.

## 5. Special collectors

The concept of special collectors in electrospinning is very topical but unfortunately neither much explored nor frequently referred to. Probably the first modern concept working on special collectors was presented by Wannatong et al. [58], who used a rotating drum wrapped by an aluminum foil to collect electrospun fibres. Wannatong observed and described various effects of a drum movement on fibre mass properties. It was found that nanofibres grasped by a whirling drum dried faster than in common apparatuses with fixed collectors and, as supposed, they were aligned in a more isotropic manner depending on the drum's peripheral velocity. On the other hand, surprisingly, even the earliest works on electrospinning: Morton [8], Cooley [59] and Formhals [11], suggested how to use rotating wheels/reels to collect heaps of nanofibres in yarn-like structures. Recently, it is acknowledged in general that special collectors have a significant effect on morphology of resultant nanofibrous layers produced by electrospinning and so they are used to control fibre mass anisotropy, homogeneity, patterning, porosity, etc.

Application of a special collector is based on the fact that a spatial distribution of electric field has a significant effect on the jet path and, consequently, on geometrical features of the deposited electrospun layer. Even fixed grounded special collectors, consisting of conductive and non-conductive patterns, are able to invoke influential control over the local deposition of nanofibres. Inside the class of special collectors it is also very common to use one or more auxiliary electrodes. To manipulate the external electric field so as to exert some control on the electrospinning jet, the shape, position and a potential of the auxiliary electrode(s), relative to the potential of an electrospinning jet, have to be considered, suggested by Teo and Ramakrishna [60]. The effect of auxiliary electrode action on a jet path is also described in sub-section 7.1 of this work.

Special collectors can be divided into two main groups. The first of which consists of static collectors, while the last encompasses dynamic collectors, e.g. rotating collectors or collector performing any other movement. Dynamic spinning electrodes will also be discussed further within the last group. The idea of special static collectors is based on the fact that, in spite of wild whipping and gyrating electrospinning jets, nanofibres can be selectively attracted by inhomogeneous electrostatic field in the vicinity of patterned collectors. More details about this astonishing finding will be discussed in the theoretical part of this section. An alternative and more detailed approach to the division of special collectors has been introduced by Teo and Ramakrishna [60]. Their classification is based on a structure of a resultant nanofibrous layers.

### 5.1 Static collectors

In standard electrospinning set-ups, collectors are made of conductive materials, commonly metals such as aluminium or copper. Standard collectors are homogenous and so the electric field in the vicinity of them is nearly homogenous too. On the other hand, special static collectors consist of conducting and non-conducting materials that are distributed in appropriate patterns. These patterns cause electrostatic charges not to be homogeneously distributed in them. Obviously, the electric charge density is less on non-conducting and much higher on conducting areas of a pattern. The consequence of the inhomogeneous charge distribution is an uneven electrostatic field in the vicinity of the collector. So, charged jets/nanofibres are collected on the non-conducting areas with lower packing density compared to their density on conducting parts, if they are charged oppositely relative to the jet type of charge.

Figure 22 shows a specimen of a static special collector composed of conductive and non-conductive parallel strips. It was approved that nanofibres in the set-up were preferentially deposited on the conducting strips, as obvious from the same figure. Between these strips, the sparse nanofibrous collection is strongly isotropic and nearly perpendicular to the strips, as supported by polyvinylalcohol (PVA) fibres electrospun from their aqueous solution in Figure 23a. The explanation of the parallelism lies in qualitative investigation of electrostatic forces acting on a piece of an electrospun jet/nanofibre in the vicinity of the neighbouring pair of conductive strips. Suggesting that the flying nanofibre piece carries an opposite charge to the charge on both conductive strips. So, both of them attract nanofibrous elements more than non-conductive parts of the special collector and the nanofibres align preferentially on individual strips are collected on them in piles. On the other hand, elements of the jet that appear in an area just in the middle above two neighbouring strips are equally attracted by them. These two electrostatic forces will simultaneously pull the piece of a fibre/jet towards both conductive strips causing a moment of force that will lead to a change in a fibre piece orientation. These moments of force will eventually lead to a uniaxial

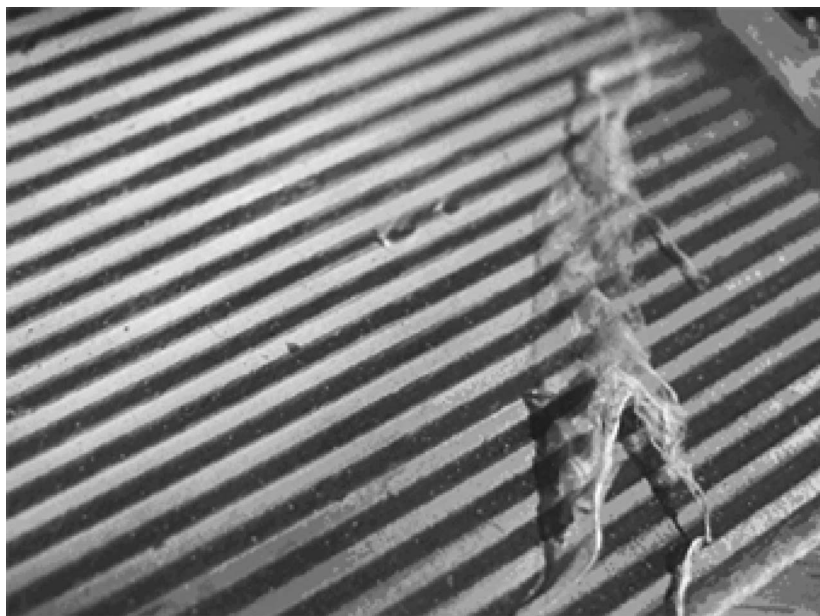


Figure 22. Special static collector consisting of Cooper strips on a laminate. Partially detached nanofibrous layer was prepared from PVA aqueous solution.

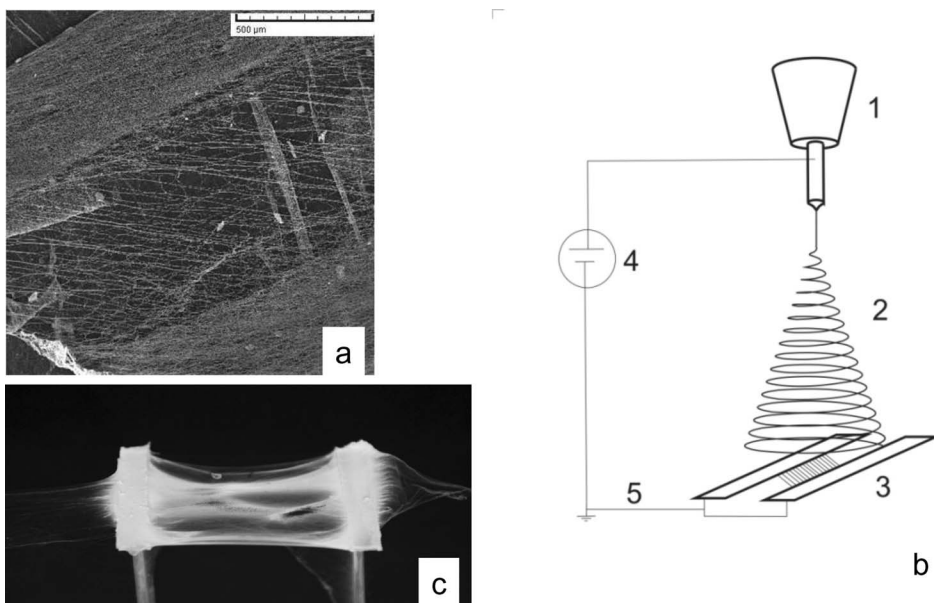


Figure 23. (a) Highly isotropic polyvinyl alcohol (PVA) nanofibrous layer collected between Cooper strips of the static special collector depicted in 22. (Courtesy of E. Kostakova, Technical University of Liberec.) (b) Schema of an apparatus consisting from a spinning electrode (1) and a high voltage source (4), where a coiled jet (2) is attracted by two charged strips serving as collector (3) that enable parallel alignment of nanofibres between the strips. Ground is denoted as (5). (c) A special collector, composed of two grounded metal stripes, collected a highly oriented nanofibrous layer. The distance between the strips is 4 cm

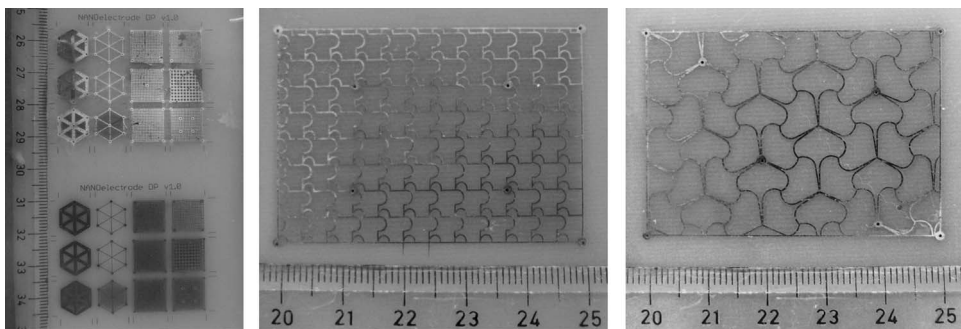


Figure 24. Three various static collectors designed as printed circuits with different shapes of conducting patterns. The attached scale is in centimetres.

alignment of a nanofibrous mass across the gap between neighbouring conductive strips, as sketched in Figure 23b. This orientation effect can be utilised for formation of oriented groups of elementary fibres to produce yarns formed by nanofibres.

More complex static-structured collectors are depicted in Figure 24. The three kinds of collectors shown there are made as flat-printed circuits without any three-dimensional elevations. The pattern thinness should be in the range of fractions of millimetre still keeping the chance for selective collection of nanofibres. This ability of nanofibres to be aligned selectively copying such fine patterns is surprising, since the field non-homogeneity spans outside the structured collector only on the distance comparable with the characteristic spacing of the pattern, as will be shown further in this section, *vide* Equation (5.5) and its commentary. Special structured collectors can also be designed as a combination of an insulator and two electrically independent groups of conductive patterns. The groups of conductors are then kept on different electrostatic potentials. One of these potentials can be chosen in such a manner that it is repulsive for the stream of impinging nanofibres/jets, and the other one as attractive. The fibrous mass, obtained on such a special collector, is a quite inhomogeneous sheet of nanofibres with empty and highly covered areas, as depicted in Figure 25.

Apart from two-dimensional special static collectors, there are also three-dimensional ones. An example of such a collector designed from a set of slender edges/lamellae is shown in Figure 26. On the top of each lamella accumulates electrostatic charge and, hence, electrospun nanofibres are deposited preferentially on the top of this kind of special, comb-like, three-dimensional collector. Various textures and spatial morphologies of nanofibrous meshes may be formed by using patterned three-dimensional collectors. For instance, several parallel combs of lamellae are able to create either voluminous nanofibrous piles, shown in Figure 27, that are potentially applicable for cultivation of living cells for tissue engineering, or these collectors can be exploited for production of pieces of yarns, as shown in Figure 28. Elementary fibres of these yarns have prevailing uniaxial orientation due to the effect, that has been described above, of nanofibrous elements orientation between two conductors, in this case lamellae, of a special structured comb-like collector.

Another kind of special porous collector could be engineered from the point of view of porosity. Porous collectors, as has been referred to by Liu and Hsieh [61], enhance diffusion and rate of evaporation of the residual solvent from the collected fibres. In a porous target, the faster solvent evaporation is due to the higher surface area that allows the solvent vapour to escape the sample, while compact collector surfaces may cause an

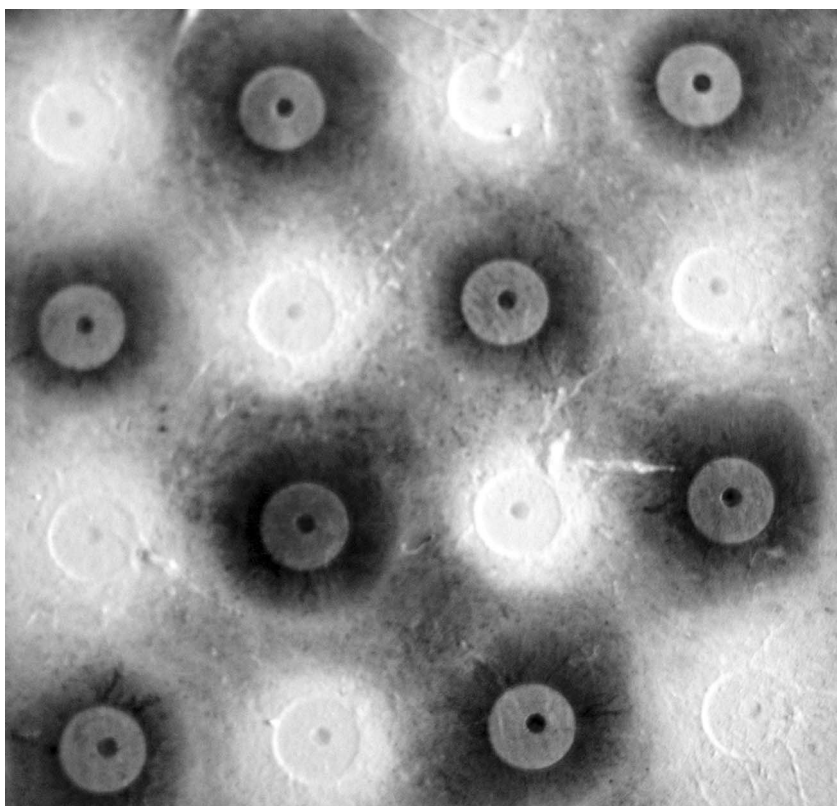


Figure 25. Special structured collector composed of combination of charged and uncharged circular patterns was covered by a white layer of PVA nanofibres.

accumulation of a solvent around the fibres due to the low solvent evaporation rate. As a consequence of wicking and diffusion of the residual solvents, the freshly collected fibres may be pulled together by capillary forces to constitute more densely packed structures. As the fibres dry faster on porous collectors, it is more likely that the residual charges remain longer on non-conductive dry collected fibres which can repulse following fibre collection.

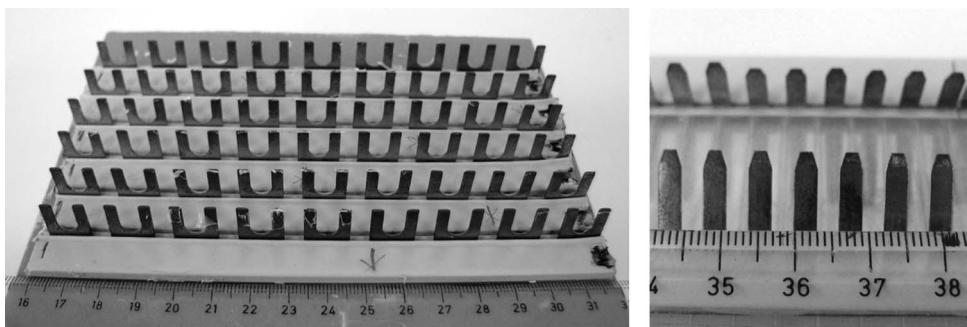


Figure 26. Two static special three-dimensional collectors composed of combs of metallic lamellae.

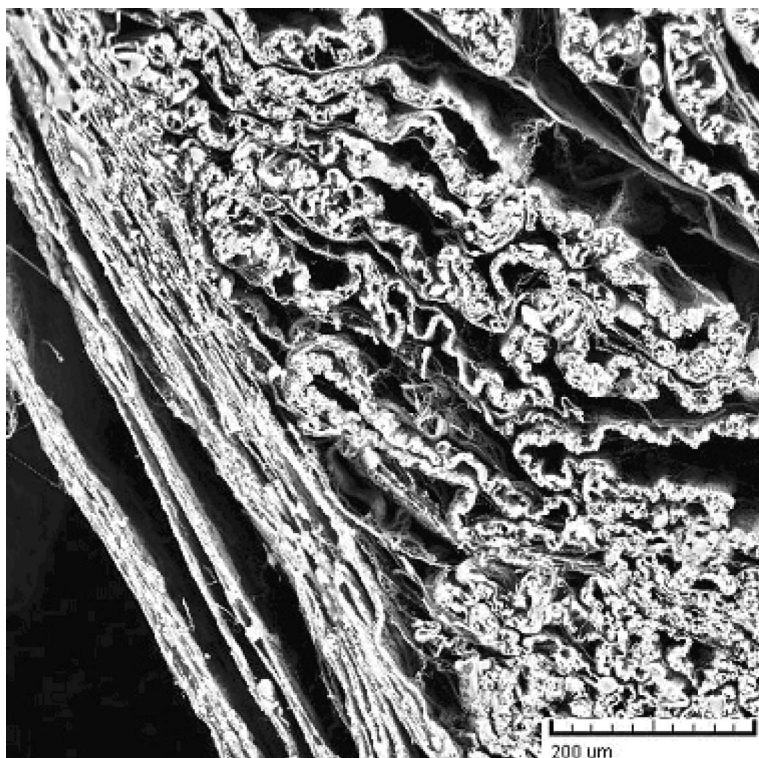


Figure 27. A cross-section of a three-dimensional voluminous nanofibrous mass, collected using a comb-like special collector depicted in the left-hand part of (26). (Courtesy of E. Kostakova, Technical University of Liberec.)

However, on a smooth surface, the residual solvents will support the residual charges to be conducted away to the collector.

### 5.2 Dynamic collectors and spinning electrodes

Next family of special collectors constitutes three-dimensional movable ones, as discussed by Sundaray et al. [62]. The special movable collector could be a drum made from homogeneous conductive material or it could be also realised as a wire drum. Rotation of the conducting collector may result in a formation of aligned fibre structures. Effect of rotating collector on fibre alignment is caused by mechanical drag force transmitted by trapped nanofibres; therefore, the fibres are parallelised depending on the speed of revolution of the drum. However, even for the conductive collector, when the deposition rate is high and the fibre mesh is thick enough, there is a high accumulation of residual charges on the fibre mass since polymer nanofibres are generally non-conductive. This collected charged fibrous layer repels next nanofibres from the collector.

When a rotating collector is used to collect aligned fibres, the movement of the yielded nanofibrous materials assists in their drying. This is useful because certain polymer solvents, such as DMF, have a high boiling point that may result in collection of very wet fibres. A rotating collector will give the solvent more time to evaporate, as highlighted by Wannatong

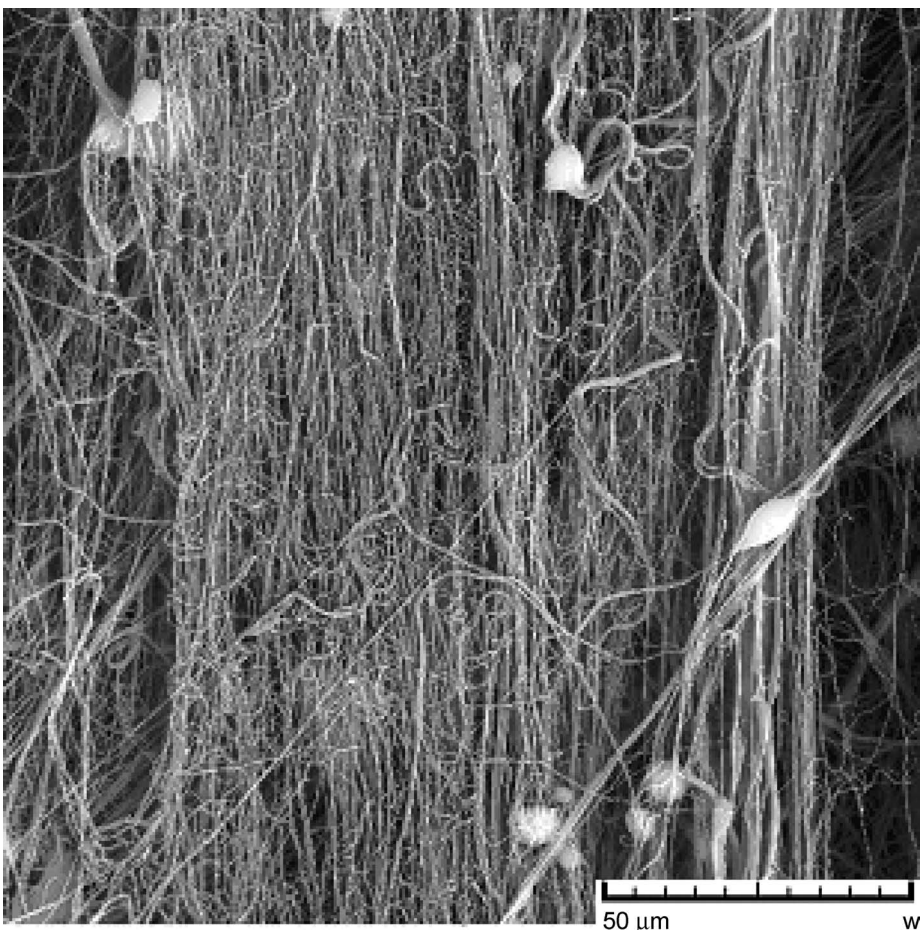


Figure 28. A detailed view of a yarn with nanofibres oriented along the yarn axis. (Courtesy of E. Kostakova, Technical University of Liberec.)

et al. [58]. More intensive evaporation improves the morphology of the fibre layers where distinct fibres are required.

The last way to create some especially arranged nanofibrous layers that is mentioned here is the utilisation of special spinning electrodes instead of simple common collectors, e.g. fixed needles or rods. For instance, the fixed metallic rod, introduced in Figure 29, has been used to prepare nanofibrous specimens depicted in Figure 25. Shape of spinning electrode affects electrostatic field-like collector shape, and hence it is possible to influence a jet path as well as the structure of the final nanofibrous layer in this way. If a special rod-like spinning electrode, depicted in Figure 30, rotates along its vertical axes, then angular velocity of the revolution regulates the diameter of the nanofibrous layer deposited on a collector. Higher angular velocities provide with bigger diameters of collected nanofibrous layers, as shown in Figure 31. Also, depending on diameter of rotation of the spinning electrode, one could say that is continual proportion.

A special spinning electrode shaped as a rotating cylinder was first introduced by Jirsak et al. [14] under the brand name of NANOSPIDER™. The cylinder slowly rotates in a pool,

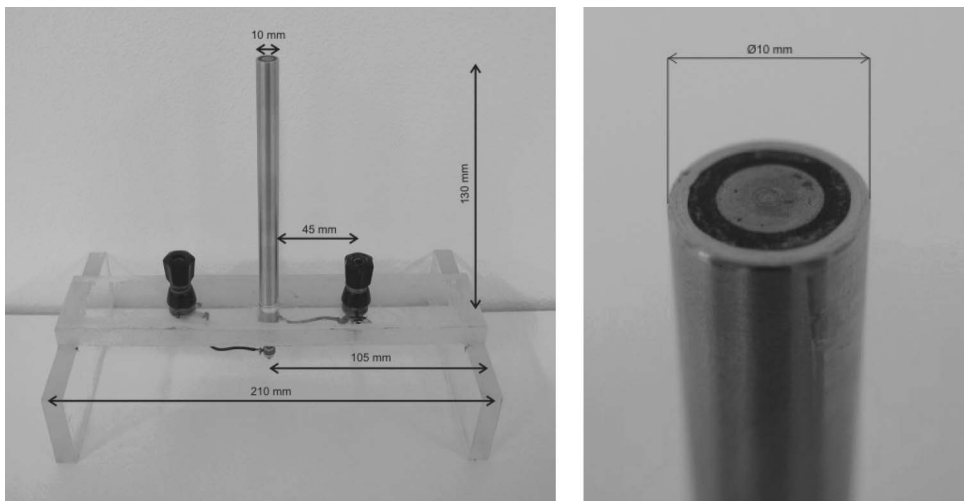


Figure 29. The rod-like spinning electrode for production nanofibrous layer and detailed top view of it.

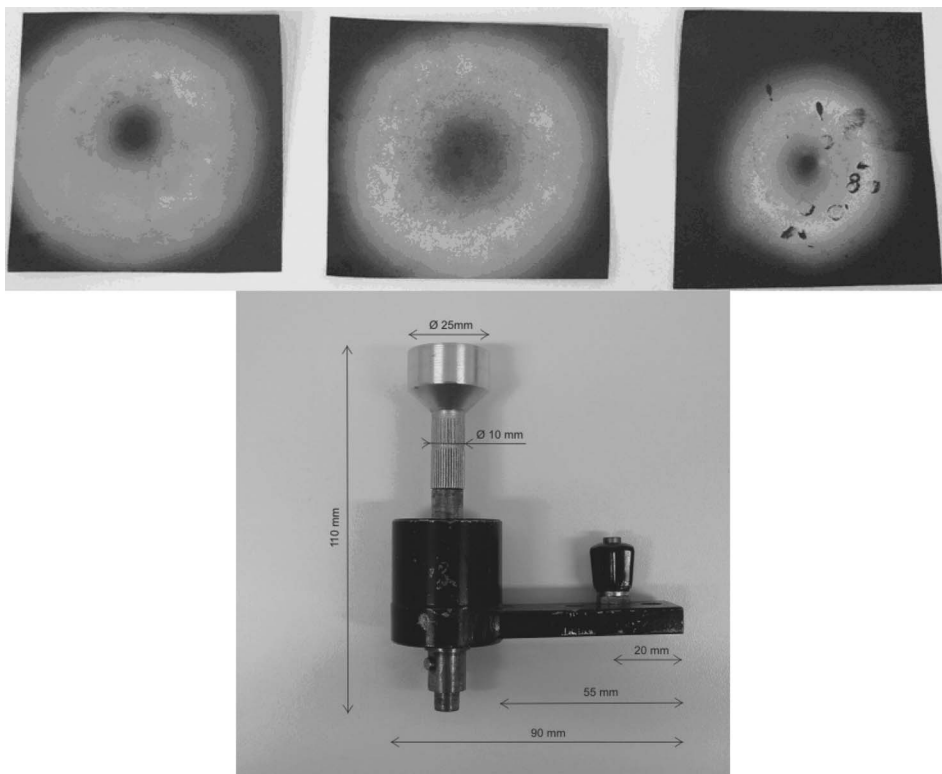


Figure 30. The rod-like spinning electrode that can rotate along its vertical axis: nanofibres are trapped by a collector in circular spots whose radii depend on the velocity of revolution, as shown in the upper part of the figure.



Figure 31. The rotating cylinder for production nanofibrous layer according to the innovative patent of Jirsak et al. [14].

filled with a polymeric solution, as depicted in Figure 31. The electrostatic field organised between the cylinder and a parallel oblong collector enables the self-organisation of jets along the upper surface of the cylinder (Figure 32) and, hence, nanofibres cover the collector in long oblong-like spot, whose length matches the length of the cylinder. If nanofibres are collected on a thin textile substrate, localised just before the collector and drawn slowly away from a spinning zone, then ‘infinite’ two-ply fabric, comprising a nanofibrous layer, are continuously produced.

### 5.3 Electrostatic field in a vicinity of a charged grid

As has been highlighted previously, special collectors are mainly designed to influence an electrostatic field in a spinning zone. Hence, it is critical to investigate electrostatic field mainly in a vicinity of structured conductive bodies. As a model, a stripped special collector will serve here as a charged regular grid of parallel wires lying in a plane having a uniform distance,  $a$ , between neighbouring wires (consult Figure 33 with indicated cross-sections of equipotential surfaces). Since the wires are placed parallel to each other, the electric field has translational symmetry along the direction parallel to the wire axes. The electrostatic potential  $\varphi$  outside the wires satisfies the Laplace Equation  $\Delta\varphi = 0$ . Considering the wires being oriented along  $y$ -axis, Laplace Equation reduces to

$$\frac{\partial^2 \varphi}{\partial x^2} + \frac{\partial^2 \varphi}{\partial z^2} = 0. \quad (5.1)$$

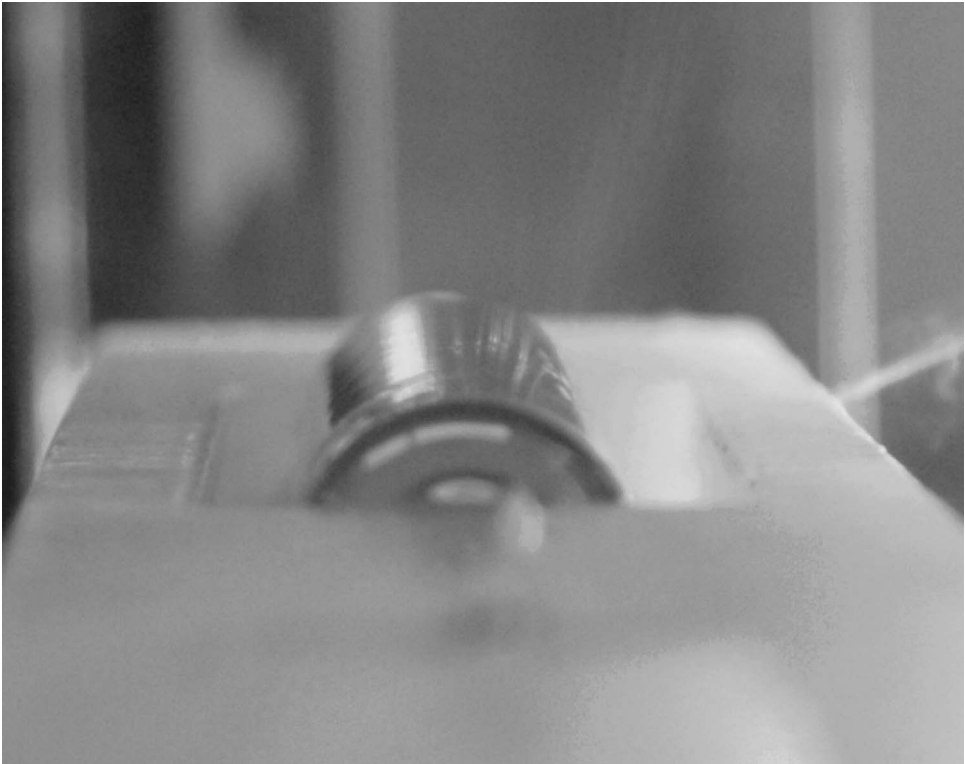


Figure 32. Side view of a special spinning electrode, applied in NANOSPIDER<sup>TM</sup>: Jets are self-organised on the upper part of surface of a long cylinder that slowly rotates in a pool filled with a polymeric solution.

Feynmann et al. [33] suggested the following trial solution of the aforementioned reduced Laplace Equation:

$$\varphi(x, z) = F_n(z) \cos kx, \quad (5.2)$$

where the wave number  $k$  is equal to  $2\pi/a$ , since the distance between neighbouring fibres plays the role of a wavelength of undulating equipotentials, and  $F_n(z)$  are originally unknown functions of  $z$ . The axes  $z$  is perpendicular to the plane of the wire grid. The

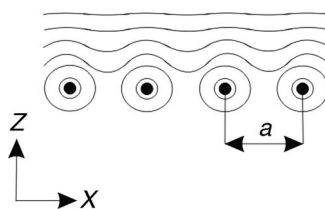


Figure 33. A grid of parallel wires: tiny wires oriented perpendicularly to the plane of the drawing are equidistantly separated along the axis  $x$ . The axis  $z$  is oriented perpendicularly to the plane of wires.

solution proposal substituted into Equation (5.1) gives

$$-\frac{4\pi^2 n^2}{a^2} F_n(z) \cos kx + \frac{d^2 F_n(z)}{dz^2} \cos kx = 0. \quad (5.3)$$

Hence, the functions  $F_n(z)$  have to fulfil the following standard differential equation:

$$\frac{d^2 F_n(z)}{dz^2} - k^2 n^2 F_n(z) = 0. \quad (5.4)$$

Solving Equation (5.4) with constant coefficients gives the solution as

$$F_n(z) = A_n \exp(-z/z_0), \quad (5.5)$$

where  $z_0 = a/(2\pi n)$  and  $A_n$  are constants. Hence, the  $n$ th Fourier component of the electrostatic field  $\varphi_n(x, z) = A_n \exp(-z/z_0) \cos(x/z_0)$  decreases exponentially with the characteristic scale length  $z_0$ . Higher is the component order  $n$ , quicker is the decrement of field with the increasing distance from the plane of the grid. Within a distance from the grid that is not greater than the characteristic pattern spacing,  $a$ , the field is nearly homogeneous because the oscillating components of the field  $\varphi_n$ , for  $n > 0$ , are negligibly small. Behind this distance remains merely the zero harmonic component of the field  $\varphi_0$ , for which  $n = 0$  and  $\varphi_0 = -E_0 z$ , where  $E_0$  is the field intensity on ‘sufficiently long’ distances from the plane of the grid.

It is supposed as well as experimentally proven, see sub-section 7.1, that polymer jets are speedily discharged during their path through their whipping zones, due to interactions of their net charges with conversely charged ambient ions. Then, nearly dried and almost neutral nanofibres strike the collector. Surprisingly, despite a massive loss of their net charge, it is possible to pattern nanofibrous layers with accuracy 0.1 mm using static special collectors and fabricate nanofibrous patterned layers. It has also to be underlined that special spinning electrodes are probably the best tools for elevating electrospinning technology to industrial levels.

## 6. Electrospinning variants

This section is devoted to the two electrospinning variants. The first one is a melt-electrospinning, where polymer melts instead of polymeric solutions are spun aiming at a lot of ecological and application benefits resulting from elision of organic solvents. The last variant is so-called ‘core–shell’ or ‘co-axial’ electrospinning, which provides bi-component fibres created from a jet embedded into another polymeric jet with a greater radius.

### 6.1 Melt-electrospinning

Over the past two decades, many published articles on electrospinning contained the claim that electrospinning is a process of jet formation from polymer solutions or from polymeric melts. Despite this commonly used affirmation, only sparse published research works were really focused on electrospinning of molten polymers. One may conclude that, as opposed to extensive research in electrospinning of polymer solutions during the last decades, the melt-electrospinning is, till date, relatively untutored. This fact is surprising since melt-electrospinning has its well-known advantages in cleaner processing, environmental safety and higher productivity with no need for solvent recycling. On the other hand, more

complicated set-ups of melt-electrospinning devices require precise control of heating for polymer melting to prevent its degradation at high temperature. There are also strict demands and restrictions on physical properties that polymers have to meet to be processed using melt-electrospinning. All of the above arguments might be taken as main disadvantages of the electrospinning variant in question.

It is noteworthy that electrospinning from a melt was first patented in the 1930s by Norton [12, 63] using an air-blast to assist fibre formation. Larrondo and Manley [64–66] were the first scientists who released a series of articles devoted merely to melt-electrospinning. In the referred three articles, they demonstrated that polymer melt could be spun using external electrostatic field of sufficient intensity. As an experimental set-up, they used an electrically heated capillary/needle and a metal plate as a collector. This set-up was widely used subsequently by the majority of other researchers in this field. The method was found to be convenient, especially for laboratory testing of various polymers for melt-electrospinning. Larrondo and Manley were qualified to produce only relatively thick fibres with diameters around  $50\text{ }\mu\text{m}$ . Higher fibre thicknesses, obtained in their experiments, were presumably caused due to the relatively high viscosity of polymer melts they used. The polymers they used had melt flow indices (MFI) from 0.5 up to 2 g per 10 min and were spun for a short drawing distance, i.e. the distance between a spinning electrode and collector, within a range of 1–3 cm. The MFI is a method of measurement and evaluation of easiness of polymer flow, standardised in ASTM D1238 and ISO 1133 standards. The electrostatic field strength interval was adjusted between 3 and  $8\text{ kV cm}^{-1}$ .

To verify the universality of physical principles in the formation of jets during electrospinning from polymeric solutions and melts, Larrondo and Manley measured the semi-vertical angles of Taylor cones, created just at the onset of jet formation. Results of their experiments showed that semi-vertical angles of Taylor cones, formed on melt surfaces, were  $50^\circ$ , which is very close to the experimental results obtained by Taylor [16], who had reported the angle to be  $49.3^\circ$ , studied on soap film and bulk water droplets. Thus, they suggested that the expression, derived by Taylor, for prediction of the critical potential differences when the jet appears in a needle electrospinner, as in Equation (3.27), can be used even for polymer melts.

Another important work on molten polymers was published by Lyons [67]. The thesis of Lyons [67], and a related article, published by Lyons, Li and Ko [68], reveal principles of electrohydrodynamic atomisation with a focus on the critical parametres, influencing melt-electrospinning, such as polymer molecular weight, tacticity of polymer and electric field strength. Experiments undertaken by Lyons et al. with different grades of polypropylene (PP) having different molecular weights and tacticities led to collection of fibres, which were subsequently classified with respect to fibre diameter, crystallinity or mechanical properties. Effects of various parameters explored in Lyons et al. [68] will be discussed in details further in the text.

Although the majority of published articles in the field of electrospinning of melts deals with the use of the PP as a fibre forming polymer, as composed by Larrondo and Manley [64–66], Lyons et al. [68], Komarek and Martinova [69], several other articles are published on similar processes for other thermoplastic polymers, such as polyethylene terephthalate, published by Ogata et al. [70], polylactic acid (PLA), as referred to in Zhou et al. [71], mixtures of polyethylene with paraffin, mentioned in Larrondo and Manley [64], or copolymers of polyethylen terephthalate with PLA or polyglycolic acid, as referred by Tureckova et al. [72].

Besides experimental works, there exist few papers with theoretical approaches to this topic. The main differences between modelling melt and solution electrospinning are

temperature and thermal changes, and also effects during the non-isothermal process in the melt variant. On the other hand, processing melts with this technology has nothing to do with modelling solvent evaporation. Modelling of the physical effects occurring in polymer melts in a strong external electrostatic field is an enormously complex task requiring strong mathematical skill. As the electrostatic fibre formation is influenced by many mutually interdependent variables, simplifications are usually utilised to exclude less important ones. Process of melt-electrospinning can be, in general, divided into three parts from the point of view of the theoretical description. The first part is the analysis of the formation of the Taylor cones. The second part describes drawing of a jet from the cone with an effort to predict jet diameters. The last part is focused on the deposition of fibres on a collector.

Theoretical works, dealing with the first part of the electrospinning process, i.e. creation of so-called Taylor cone, usually follow the original Taylor's [16] work. Larrondo and Manley [64] observed the deformation of a polymer melt droplet on the edge of a heated capillary, induced by electrostatic forces. Measurements of the molten polymer droplet shape, its dependency on the applied voltage, and careful measurements of the critical voltage values, i.e. values when the jet appears, showed good agreement with Taylor's Formula (3.27).

In another experiment, Larrondo and Manley [65] investigated a flow field inside a melt-electrospinning jet with the aid of tracer particles. Positions of the particles at various elapsed times were recorded by the motion-picture camera. Local velocities at various regions of the flow were measured and this information was used to characterise the strain rates in the different parts of the flow field. They inspected and found that the axial velocity component,  $v_z$ , in a jet fits with the following empirical expression:

$$v_z = a e^{b(z)} (1 + a_1(z)r^2), \quad (6.1)$$

while radial velocity component  $v_r$  can be expressed as

$$v_r = -a \frac{\partial b(z)}{\partial x} e^{b(z)} \left( \frac{r}{2} + a_1(z) \frac{r^3}{4} \right). \quad (6.2)$$

Symbol  $r$  denotes the radial distance from the jet axis. For a given electric field strength,  $a$  is a constant. Functions  $a_1(z)$  and  $b(z)$  depend on the axial distance  $z$  from the needle tip, and on field strength value. Details of the derivation of Equations (6.1) and (6.2) could be found in the work of Larrondo and Manley [64].

Mathematical modelling of drawing of fibre from Taylor cone in the stable jet region is described in the work published by Zhmayev et al. [73]. They modelled the stable jet region as a free surface flow of charged viscoelastic fluid in non-isothermal conditions. The model was based on thin filament approximation, applied to fully coupled momentum, continuity and energy equations. Moreover, they applied Gauss's Law and the non-isothermal constitutive model, published by Giesekus [74]. Zhmayev et al. assumed, in accordance with experimental results, that a significant degree of a jet thinning could occur even in the stable jet region. To describe this effect theoretically, they used a system of following four equations for isothermal model, introduced by Carroll and Joo [75]. This approach resembles the Qin et al.'s [54] one, mentioned in sub-section 4.1 for the modelling of solvent electrospinning jet profile. The first of the four equations is identical to the previously mentioned continuity Equation (4.7):

$$Q = \pi r^2 \rho v. \quad (6.3)$$

The next equation expresses momentum conservation and is formulated, likewise as Equation (4.9), on the basis of Bernoulli theorem [76]:

$$\rho v v' = \rho g + \frac{F'_t}{\eta r^2} + \frac{\gamma r'}{r^2} + \frac{\sigma \sigma'}{\varepsilon_0} + (\varepsilon - \varepsilon_0) E_t E'_t + \frac{2\sigma E}{r}, \quad (6.4)$$

where  $r$  is the radius of the jet,  $v$  the cross-sectional average axial fluid velocity,  $Q$  the volume flow rate,  $E$  denotes field strength, while  $E_t$  is its tangential component. Symbol  $\rho$  denotes the fluid density,  $g$  the acceleration due to gravity,  $F_t$  the tensile force in the jet found from fluid stresses,  $\gamma$  the surface tension,  $\sigma$  the surface charge density,  $\varepsilon$  and  $\varepsilon_0$  the dielectric constants of the jet and the ambient air, respectively. The primes indicate derivatives with respect to the axial direction,  $z$ . The third equation formulates charge conservation and so it is identical to Equation (4.8):

$$I = 2\pi r v \sigma + \kappa \pi r^2 E, \quad (6.5)$$

where  $E$  is the electric field,  $\kappa$  the electrical conductivity and  $I$  denotes the current. The last equation expresses the distribution of the electric field along the  $z$ -axis:

$$E(z) = E_\infty(z) - \left[ \frac{1}{\varepsilon_0} (\sigma r)' - \left( \frac{\varepsilon}{\varepsilon_0} - 1 \right) \frac{(Er^2)''}{2} \right] \ln \left( \frac{d}{r_0} \right), \quad (6.6)$$

where  $E_\infty$  is the applied external electric field,  $d$  the distance between the nozzle and the collector, and  $r_0$  is the radius of the spinneret.

Zhmayev et al. [73] simplified the law of charge conservation on the basis that low electrical conductivity of polymer melts are usually less than  $10^{-10}$  S/m; so Equation (6.5) could be simplified to the form, given as

$$I = 2\pi R v \sigma. \quad (6.7)$$

Further they assumed that radial charge conduction was instantaneous. The equilibrium value of the surface charge density at the jet inlet  $\sigma$  can be calculated as  $\sigma = \varepsilon_0 E_n(0)$ , vide Equation (3.17), where  $E_n(0)$  is the component of the field strength normal to the jet surface at the spinneret and it can be approximated with the value  $E(0)$  of the divergent field intensity around the needle of the spinneret. This assumption is actually an extreme case of so-called ‘leaky dielectric model’. The model was developed especially for slightly conducting liquids, since it postulated that unbalanced electrical charges migrate quickly towards the liquid surface. This simplification was important because it allows calculating electric current values directly. For the estimation of the real diverging field intensity values,  $E(0)$ , near the needle tip, Zhmayev et al. used the approach introduced by Mason [77]. While Equation (6.4) of momentum conservation remains unchanged, Formula (6.6) for the electric field intensity is transformed to

$$E(z) \approx E_\infty(z) - \frac{2V}{(r_0 + 2z - \frac{z^2}{d}) \ln(1 + \frac{4d}{r_0})}, \quad (6.8)$$

where  $V$  is voltage. The tangential projection of field strength to the  $z$ -axis can be expressed as  $E_t(z) = E(z)/\sqrt{1 + (r')^2}$ .

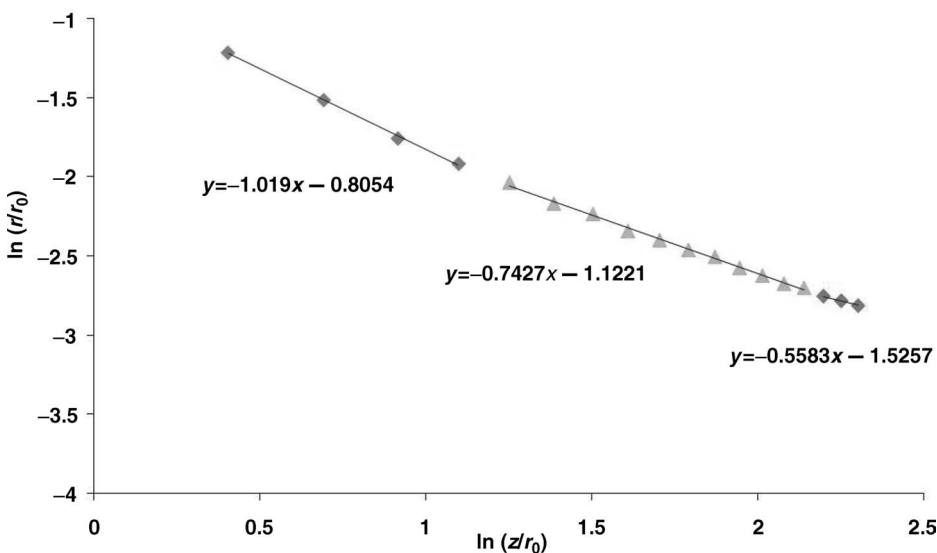


Figure 34. Precise analysis of melt-electrospinning data reported by Zhmayev et al. [73] provides the approximate relation between the radius of the jet  $r$  and the distance from the nozzle,  $r(z) \approx z^{-0.6}$ , for jet parts furthest from the nozzle. The value of the exponent varies slightly with changing temperature of the molten polymer jet.

Implementing the above-mentioned simplifications into Equations (6.5) and (6.6), the system of Equations (6.3), (6.4), (6.7) and (6.8) were obtained, and after setting boundary conditions and numerical solving, the results gave good quantitative agreement with experimental values and could predict diameters of fibres, obtained by electrospinning of molten polymer. By precise analysis of the results, reported in Zhmayev et al. [73], one may conclude that the radius of the jet,  $r$ , outside the Taylor cone depends on the distance from the nozzle,  $z$ , with approximate relation  $r(z) \approx z^{-0.6}$ , see Figure 34, while inside the cone  $r$  scales as  $r(z) \approx z^{-1}$ . Data collected by Zhmayev et al. also reveal that the value of the exponent varies slightly with the changing temperature of the molten polymer jet.

In addition to the mathematical modelling, parameters influencing the melt-electrospinning process were intensively studied by experimental tools. The molecular weight of polymer was recognised as a quite dominant parameter, determining the feasibility of electrostatically producing fibres from a melt, as reported by Lyons et al. [68]. In the same work, other parameters were also mentioned like an electric field strength, supplied melt volume, temperature, flow rate, spinneret diameter, dielectric constant, thermal conductivity and surface energy of the polymer that are the most likely to have an effect on process and morphology of collected fibres. Diameters of the collected fibres were shown to increase exponentially with increasing molecular weight of melt electrospun PP. This result was anticipated as a consequence of higher numbers of the entanglements among longer polymer chains. Factually, the molecular weight also influences the viscosity of a polymer melt. Also, the effect of tacticity in linear polymers on side chains or groups has similar kind of explanation. It was concluded that electrospinning of isotactic PP always resulted in production of fibres with lower diameters than in the case of atactic PP with very similar molecular weight.

Generally, due to high viscosities of polymer melts, the strength of electric field that is usually needed for melt-electrospinning is higher than in the case of electrospinning

from polymeric solutions. For the PP melts of different molecular weights, electric fields of 10–15 kV cm<sup>-1</sup> were capable of drawing continuous fibres, which are approximately 10 times higher than common field strength values required for solution electrospinning, as reported by Lyons et al. [68]. It was observed for different types of polymers that with increasing field strength, the mean diameter of fibres decreases.

Study on the effect of polymer volume at the tip of the capillary showed that with decreasing amount of the polymer supplied to the needle, the average diameter of collected fibres decreased significantly. It was also observed that reducing volume of the polymer resulted in smaller Taylor cone. The reduction of size of Taylor cone affects the ratio of the strength of the electric field to the transferred mass of polymer, which, consequently, leads to higher degree of drawing of melt-electrospun fibres, thus, reduction in their diameters, Lyons et al. [68].

To date, several melt-electrospinning devices have been designed, reported and/or patented, e.g. Zhou and Yoo [78] and Ogata et al. [70]. Similarly, as in the development of solution electrospinning the first experiments with its melt variant were carried out using needles/capillaries and syringes. These set-ups have their advantages in their relative simplicity and were found to be useful for verification of theoretical approaches and preparation of fibres in a laboratory scale. An exemplary set-up, using metal syringe and an electrically heated piston, as a reservoir of polymer, can be found in Larrondo and Manley's [64] article. Lyons [67] showed that glass capillary could also be used and a wire, supplying the electrical potential inside the non-conducting glass tube to prevent interaction between the high voltage field and electrically heated element, could be used. The main disadvantage of syringe set-ups is their low productivity. Difficulties with increasing number of syringes, to enhance productivity, mainly cause Coulomb interactions between the jets, and problems with uniformity of heating and polymer throughput.

An example of laboratory testing needleless melt-electrospinning set-up is depicted in Figure 35. In needleless set-ups, Taylor cones are formed on the free liquid surface, allowing

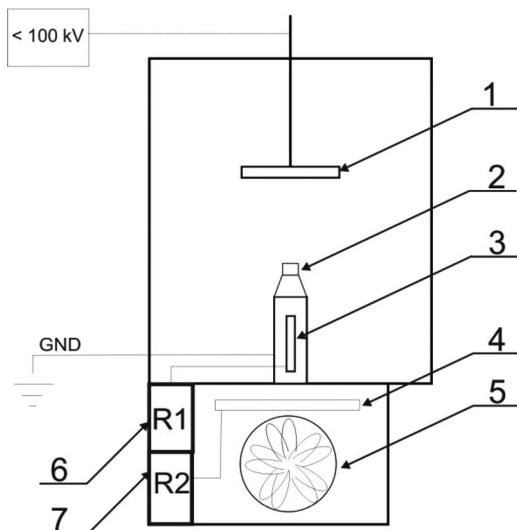


Figure 35. Laboratory needleless melt-electrospinning set-up: (1) collector, (2) heated rod-like spinning electrode, (3) cartridge heater, (4) heating of gas media, (5) ventilation blower, (6) regulator of temperature of heated electrode and (7) regulator of temperature of gas media.

multiple jets to be emitted and higher amounts of polymer to be transformed into fibres. The creation of multiple jet formation is important for industrial scale electrospinning devices. Referring to Figure 34, melt-electrospinning set-ups, unlike the solution electrospinning set-ups, usually incorporate a spinning chamber with controlled temperature of the surrounding air. The reason for this is to prevent rapid cooling of jets in the spinning region. Cooling of the jet increases its viscosity; therefore, preventing the fibre to be sufficiently drawn and elongated to a smaller diameter. Thus, the control of a temperature difference between polymer melt and the surrounding air allows governing the length of the jet region, where the fibre diameter is reduced.

## 6.2 Core–shell electrospinning

Nanofibres, produced by the electrospinning process, can be imparted with various functional attributes. These functions are determined by their complex chemical composition, or, sophisticated inner morphology. Many functionalised composite nanofibres were produced directly by electrospinning of polymer blends/mixtures or by polymer solutions with various additional chemical agents. Apart from the usage of blends, ‘core–shell electrospinning’, also called ‘co-axial electrospinning’ or ‘co-electrospinning’, is a unique sophisticated method, and an alternative route to produce composite functionalised nanofibres with almost strictly organised core–shell structure, as explained by Song et al. [79]. The shell of a nanofibre is most commonly a polymeric material, while the core can consist of other polymer of another encapsulated mass including liquids, as referred to by Bazilevsky et al. [80]. Hollow interior nanofibres are also known, as introduced by Dror et al. [81]. From the technological point of view, the fibre shell has to originate from electrospinnable fluid, while the core fluid may or may not be electrospinnable, since the physics of electrospinability is mostly governed by jet surface. According to Song et al. [79], core–shell electrospinning resembles spider silk, which represents a well-known example of compound functionalised core–shell fibres, possessing a combination of mechanical properties, not seen in any other fibre.

Like common electrospinning, its core–shell variant also occurs when electrical forces at the surface of polymer solutions overcome the surface tension, and cause an electrically charged jet to be ejected. Because of a bending instability, the jet is subsequently enormously stretched to form continuous ultrathin fibres. The necessary requirement in a wild jet motion is that its core–shell arrangement has to be preserved. Since the co-axial electrospinning has its modern history no longer than four to five years, according to Song et al. [82], relevant investigations are quite sparse.

On the other hand, the process has surprisingly deep historical roots. John F. Cooley submitted visionary patent application in the year 1899 (Cooley [59]). Referring to Figure 36a and Cooley’s patent, *A* indicates a tube made of glass or other substances, where the tube terminates at its lower end in a small nozzle that serves as a means for delivering the fluid in a free and attenuated stream into the path of convection. The tube terminates at its upper end in an enlargement or bulb *a*, which, together with the inlet-tube *b*, serves to supply the fluid to the tube *A*. In order to regulate the quantity of fluid supplied to the delivery tube *A*, the bulb, *a*, may conveniently be provided with a conical valve or plug, *c*, with a screw threaded stem, passing through a stopper, *d*, so that by raising or lowering the plug, *c*, the area of the opening, governed by said plug could be correspondingly varied. For the purpose of supplying a supplementary fluid at the outlet of the tube *A*, it is possible to surround the tube *A* with an enclosing tube *B* and make the outlet of the tube *A* conical, so that by sliding the one longitudinally on the other, the area of the annular opening between their outlet

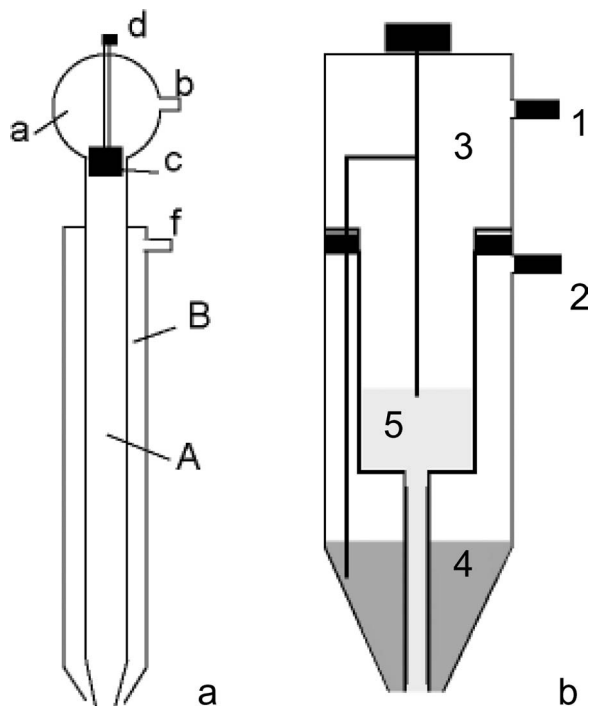


Figure 36. The critical component of a core–shell electrospinning set-up is a composite spinneret, already mentioned by Cooley [59]: (a) Cooley’s composite spinneret comprised of two separately fed chambers (A) and (B) that culminated in a co-axial capillary orifice, (b) Recent experimental set-up for core–shell electrospinning.

ends may be correspondingly adjusted or regulated. Into the space between two tubes, a supplementary fluid, preferably a solvent of the fluid, may be delivered through the tube A. The supplementary fluid or solvent may be conveniently supplied to its delivery tube B through the branch f from any convenient reservoir.

As said above, core–shell electrospinning is appropriate for processing materials, which are difficult or impossible to spin into nanofibres by conventional fibre-forming techniques or by electrospinning (Rutlege et al. [83]). Li et al. [84] demonstrated that the non-spinnable liquids can be stretched into thin filaments by co-axial electrospinning using a good fibre forming polymer used as a shell. This technique can also be employed to encapsulate nanoparticles like magnetic ones, as referred to by Song et al. [79], or to encapsulate bacteria, DNA, drugs and enzymes, vide Reznik et al. [85]. It is also possible to prepare biodegradable co-axial electrospun nanofibres for controlled release of bioactive agents (for more details, consult Jiang et al. [86]). A novel idea in developing electrospun scaffolds for tissue engineering, introduced by Gupta et al. [87], is to use core–shell structure with two different polymers that degrade at different rates.

The critical component of a core–shell electrospinning set-up is a composite spinneret, similar to Cooley invention, comprising two separately fed chambers that culminate into co-axial capillary orifice, i.e. small capillary tubes with one inside the other. The polymer solutions, or other liquid components, are fed at carefully determined flow rates, which are controlled by syringe pumps. A recent lab-scale set-up used for co-axial electrospinning of compound core–shell nanofibres is shown in Figure 36b.

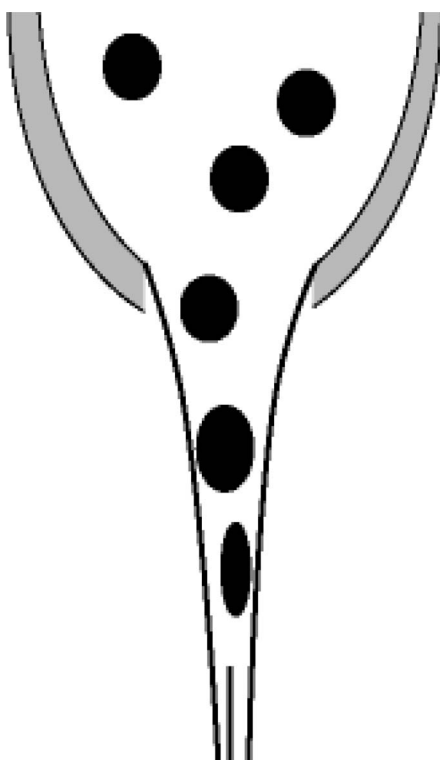


Figure 37. Schematic drawing of core–shell electrospinning of polymeric blend in case of a single nozzle technique.

Core–shell structured nanofibres can also be produced using a single nozzle technique (Figure 37). The single nozzle method was demonstrated by Bazilevsky et al. [80] using blends of immiscible polymers. Polymethylmethacrylate (PMMA) and polyacrylonitrile (PAN) were dissolved separately in DMF. It was proved that the outer shell flow is sufficiently strong to stretch the inner droplet into the Taylor cone, thus forming a core–shell jet. Schematic of core–shell electrospinning of PMMA/PAN blend is drawn in Figure 37. In the inset, the PMMA/DMF droplets are shown in black, while the PAN/DMF liquid is lighter. A theoretical analysis of the mechanism is quite complicated and can be found in details in Bazilevsky et al. [80].

It is not easy to demonstrate experimentally that a technology really provides with the core–shell configuration of electrospun fibres. Sun et al. [88] carried out two types of experiments to prove it. First, they produced core–shell electrospun nanofibres made of identical polymers, polyethylen oxide (PEO), but with different amounts of bromophenole in water–ethanol solvents in order to gain the contrast. The core–shell structure can then be clearly seen under transmission electron microscopy (TEM). In the last type of experiments, compound fibres were prepared from two different polymers, particularly from PEO and polysulphone (PSU) solutions. Core–shell fibres were also obtained from PEO in the shell and polydodecylthiophene (PDT) used as the core. In both cases, core–shell structure was recognisable under TEM. TEM investigations of the PEO–PDT co-axial fibres showed strong contrast between core and shell, since the TEM contrast of PDT is much stronger compared to PEO due to the presence of sulphur (Figure 38).

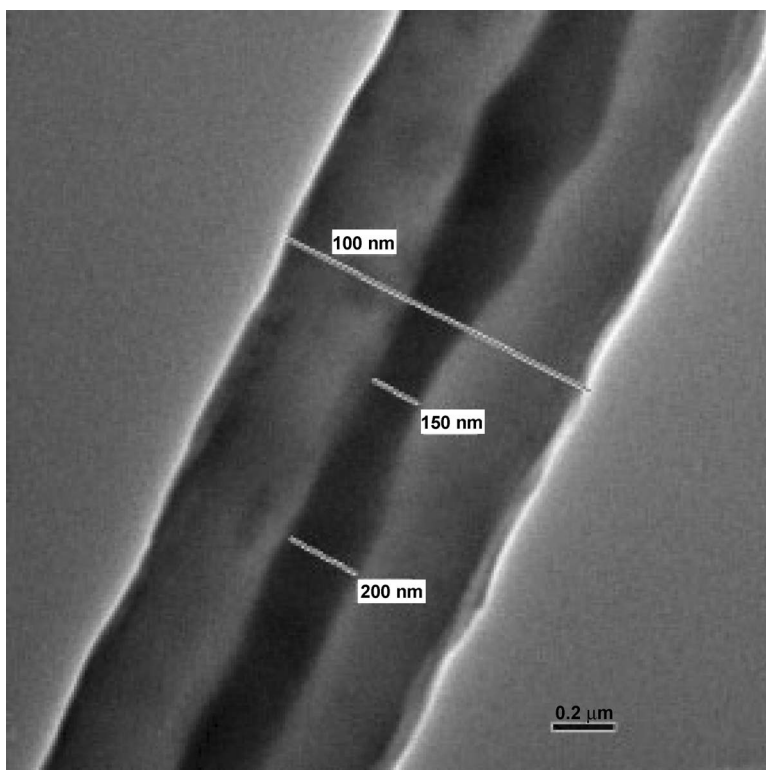


Figure 38. Transmission electron microscopy microphotographs of co-electrospun PEO (shell) and PDT (core) – reprinted with permission from Sun et al. [88]. Copyright © 2003. Advanced materials.

The core–shell electrospinning can also be adapted to prepare hollow tubular nanofibres. To obtain hollow fibres from core–shell fibres, the core part used as a template has to be selectively removed subsequently either by thermal decomposition or by choosing a selective solvent. The requirement is that the shell material is stable either against the annealing temperature or against the applied selective solvent. The hollow nanofibres made of polycaprolactone (PCL) as a core and PVA or PEO as a shell were made by Dror et al. [81]. Compositions of his core and shell solutions are given in Table 1. Core solution nos. 2 and 3 differ in their miscibility with the shell solution: the core solution no. 2 is immiscible, while the core solution no. 3 is miscible. Differences between the resulting hollow fibre morphologies are clearly seen in Figure 39.

Table 1. Compositions of the core and shell solutions used by Dror [81].

	Polymer	Solvent	Polymer content [% (w/w)]
Shell 1	PCL	Chloroform/DMF 80:20 (w/w)	10
Core 1	PEO	Ethanol/water 40:60 (w/w)	4
Core 2	PVA	Ethanol/water 50:50 (w/w)	9
Core 3	PEO	DMF	4
Core 4	PEO	Ethanol/water 40:60 (w/w)	4

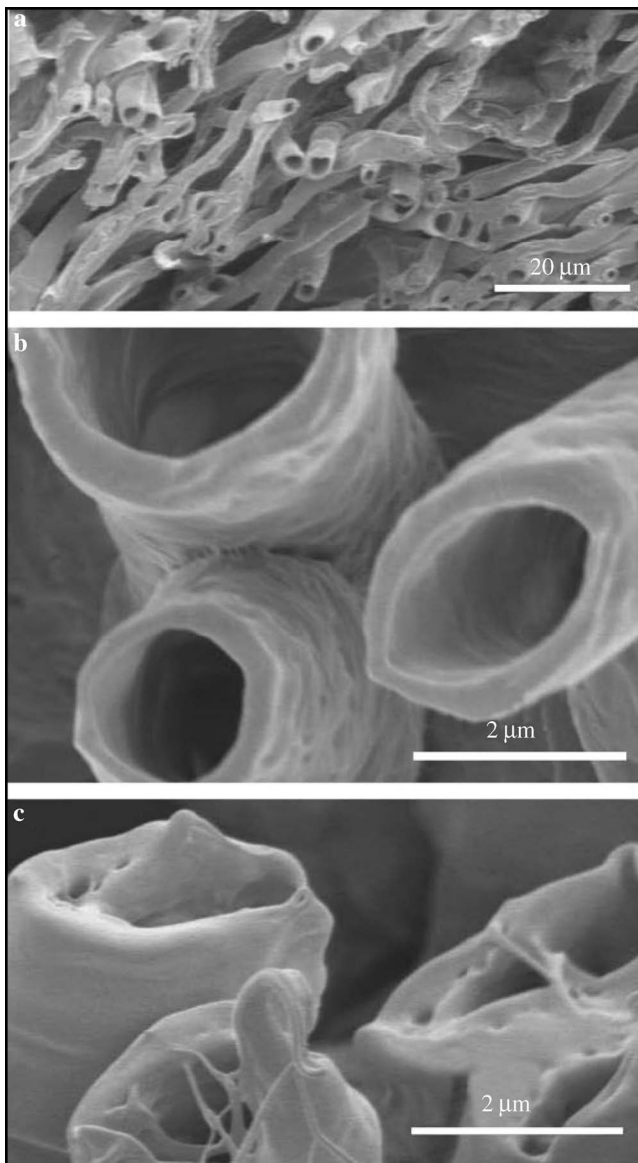


Figure 39. (a) HRSEM images of a co-electrospun fibre; (b) PCL shell, PVA core (shell solution 1, core solution 2, vide Table 1); (c) PCL in shell, PEO as core (shell solution 1, core solution 3, vide Table 1) – reprinted with permission from Dror et al. [81]. Copyright © 2007, John Wiley & Sons.

The core–shell electrospinning process is expected to be fast enough to prevent any mixing of the core and shell materials, as mentioned in Sun et al. [88]. The characteristic time  $\tau_1$  of a jet element passing the bending/whipping unstable zone of a jet must be shorter than a massive diffusion or mixing of two co-axially electrospun solutions. Under these conditions, a sharp boundary inside a fibre can be formed, as reported by Song et al. [82]. It was found that the characteristic time,  $\tau_1$ , of bending instability in electrospinning is of the order of milliseconds, as claimed by Sun et al. [88]. One supposes this time is nearly the same for the core–shell electrospinning too.

Characteristic time,  $\tau_1$ , of a jet passing through the bending instability has to be compared with characteristic times of two kinds of diffusions,  $\tau_2$  and  $\tau_3$ , to estimate sharpness of a wall between a core and a shell. Diffusive spreading in two identical polymers, doped by dyeing agents, can be described by a characteristic time  $\tau_2 = d^2/D_d$ , where  $d$  is a nanofibre cross-sectional diameter and  $D_d$  denotes the diffusion coefficient of the dopant. The last characteristic time  $\tau_3$  describes a spreading of a sharp boundary between two different polymers due to mutual diffusion of polymeric chains. For  $\tau_3$  holds:  $\tau_3 = d^2/D_p$ , where  $D_p$  is the polymer diffusion coefficient. More information about characteristic diffusion times can be referred to the work of Hiemenz and Lodge [89]. Characteristic diffusion times  $\tau_2$  and  $\tau_3$  are usually larger than  $\tau_1$ , and so all the boundaries survive in core–shell electrospun fibres as relatively sharp walls, which is in agreement with the experimental results of the Sun's [88] work.

In the case of a pair of various polymers both solved in the same solvent, mutual diffusion during jet formation can be essentially ruled out, since  $\tau_1 < \tau_2 < \tau_3$ . When core and shell polymers are dissolved in different solvents, these must be carefully selected to avoid any precipitation at the solution–solution interface. The use of immiscible solvents in the core and shell generally contributes towards the internal stability of the jet. Critical physical properties of solutions that determine the stability of co-axial jets are not well understood, as has been mentioned by Andradey [90]. Any instability of the jet may lead to the core being asymmetrically placed within the nanofibre, for more details about this effect, the work of Jiang et al. [86] may be consulted. A bimodal distribution or a mix of thin and thick fibres is sometimes observed in co-axial spinning, as was done by Andradey [90]. This suggests multiple jets from a two-layered cone rather than the branching or splitting of the main jet with the subsequent separation of its components during core–shell electrospinning.

## 7. Exceptional features of electrospinning

Two exceptional features of electrospinning are covered by this section. The first of them is an ion-driven electric wind that influences a jet path in a spinning zone that, undoubtedly, assists in solution evaporation and jet discharge. The last exceptional features are various kinds of radiations accompanying jet creation and nanofibre formation.

### 7.1 Electric wind in electrospinning

Electrospinning is an enormously versatile process in which dynamics of both polymeric jets and the ambient atmospheric gas/air are involved. Inside a spinning zone, i.e. in the space between a spinning electrode and a collector, a strong electrostatic field acts whose strength reaches its local maxima in the vicinity of tiny charged bodies, e.g. needle electrodes, tiny liquid jets or droplets. Ionisation of ambient gas/air and ion acceleration appearing in the zones of high field strength results in gas fluxes with the power of a wind. So, this effect will now be referred to as ‘electric wind’ [91]. Since electrospinning jets and their whipping parts culminate in nanofibres with enormously low mass but immense surface area, the flux of the ambient gas in the spinner can significantly affect the jet path. The electric wind partially sways the assembling process of nanofibres on a collector, and hence is an important factor from a technological point of view. Surprisingly, the electric wind has been overlooked in works on electrospinning.

A vivid idea about real electric wind power can be presented through Brown's patent [92] introducing his invention of an electro-kinetic apparatus generating a reactive draught aroused by an electric field in an asymmetric capacitor. This phenomenon is also known as the Bielefeld–Brown effect and the Brown's apparatus is frequently entitled ‘lifter’. The



Figure 40. Flying lifter.

lifter is in essence a reactive engine that works in the air of normal pressure and temperature and is strong enough to lift solid bodies against the Earth attraction, as shown in Figure 40. Lifters, as asymmetric condensers, are usually designed with one of two electrodes much more slender, compared to the last one, commonly made by a tiny wire, usually of a plate shape. The tiny wire electrode concentrates the electrostatic field that causes air ionisation in the vicinity of these slender bodies. Created ions depending on their charge sign are attracted either by the wire with which they immediately collide, or they drag along a long distance to the last plate-like electrode. During this long path, the ions are accelerated by the electric field, and hence they transmit their momentum to ambient gas molecules causing their organised wind-like motion. Electrospinners, particularly the needle ones, are also asymmetric capacitors with quite different surface areas of spinning electrodes and collectors, and hence the electric wind is generated by them too.

Unfortunately, the Bielefeld–Brown effect is only sparsely referred to. One of the exceptions is Canning et al.'s work [93] in which the formula is derived for a lifter drag force  $F$ :

$$F = \frac{2dnmI}{e}, \quad (7.1)$$

where  $F$  is a total reactive force caused by the lifter wind,  $d$  is the distance between asymmetric electrodes,  $n$  is a number of collisions of one particle in unit time under normal pressure and temperature. In air at atmospheric pressure, there are  $10^{10}$  collisions per second. Parameter  $m$  denotes an ion mass (the ions are mostly ionised nitrogen molecules, the most plentiful element in the air), commonly of the value  $4.7 \times 10^{-26}$  kg, and  $I$  represents electric current realised by the ionic flux. The ion charge  $e$  is supposed to be the

elementary one, i.e.  $1.6 \times 10^{-19}$  C. Canning et al. evaluated the reactive force  $F$  for a lifter with the distance between electrodes  $d = 7$  cm and the current  $I = 3.5$  mA as  $F = 1.44$  N.

Analogous relation to Equation (7.1) has been introduced by Primas [94]:

$$F = \frac{dI}{k}, \quad (7.2)$$

where parameter  $k$  is ion mobility. Ion mobility depends on a lot of parameters such as pressure, temperature, chemical nature of a gas, etc. For a positive ion, its mobility has the value  $k = 2.1 \times 10^{-4} \text{ m}^2 \text{ V}^{-1} \text{ s}^{-1}$ . Relation (7.2) provides an estimate of the lifter reactive force  $F$  slightly smaller than the Canning's formula for the same values of  $d$  and  $I$ ,  $F = 1.2$  N. Experimental measurements of the force value were carried out by Malik [95]. Undoubtedly, both estimates and also measurements give a sufficiently big force to significantly affect a path of an electrospinning jet in a spinning zone.

Using ion mobility,  $k$ , speed,  $v_d$ , of the electric wind can also be evaluated, since  $k$  is the proportionality constant between  $v_d$  and a field strength  $E$ . The field strength can be estimated from the rate of a voltage difference  $U$  between the electrodes and their mutual distance  $d$ . Hence, Equation (7.3) holds  $v_d$  introduced by Akopjan et al. [96]:

$$v_d = k \frac{U}{d}. \quad (7.3)$$

The drift ion velocity in a spinner with the voltage difference 10 kV and the distance 7 cm between the spinning electrode and the collector is estimated using Equation (7.3) as a value  $v_d = 2.1 \times 10^{-4} [\text{m}^2 \text{ V}^{-1} \text{ s}^{-1}] 10^4 [\text{V}] / 0.07 [\text{m}] = 30 [\text{m/s}]$ . More details about the average ion velocity in external electrostatic field can also be found in Lysenko [97]. The velocity of the electric wind is hence quite comparable with the velocity of a jet motion, vide Reneker and Yarin [4].

The ionisation inside lifters as well as inside spinning zones of electrospinners is caused predominantly by collisions of accelerated ions with neutral gas particles, see Petrzilka and Šafrata [98] and Grigor'ev and Sinkevich [99]. The gas/air at vicinities of charged slender bodies in a spinning zone may be considered to be in a stage just before a massive electric discharge accompanying avalanches of newly created ions. However, the field strength  $\vec{E}$  sizably decays in electrospinners with the increasing distance from sharp edges of needle tips or jets. Consequently, a self-employed discharge bridging the spinning electrode with the collector does not appear as a rule. Petrzilka claims that ionisation in air can be caused both by collisions of electrons and positive ions with electro-neutral gas molecules. Free electrons in the lower atmosphere are generated by natural Earths and cosmic radiations at a rate of 10 particles in cubic centimeter per second, see Stakhanov [100], and recombine in 10 ns with neutral air atoms and molecules to form negative ions. As a result, the natural voluminous particle density of negative ions near the Earth surface is from 500 to 800 particles per cubic centimeter, as introduced in Grigor'ev and Sinkevich [99]. This concentration is 7 to 12 times higher than that of the positive ions. Higher concentration of negative ions can be demonstrated using the following classic experiment.

Imagine an experimental apparatus that consists of sharp needles, each of which is connected with one of two poles of a high-voltage source. Massive air ionisation will appear in the needle tip vicinity due to high field strength in this area. The positive polarisation of the needle is assumed initially. Negative ions collide immediately with the positive needle as they are attracted by Coulombic forces. In this way, ions transmit most of their momentum

to the needle, and only a small percentage of it is transferred to air molecules. As has been described previously, the negative ions recombine with positive charges on the target. However, positive ions are repelled from the positively charged needle and accelerated on a relatively long distance to high velocity and momentum. This momentum is transmitted to the surrounding gas molecules via collisions, thus causing their flux. By analogy, similar events proceed in the vicinity of a negatively charged needle. So, this is the mechanism by which the electric wind is initialised. Since the initial concentration of negative ions in lower atmosphere of Earth is higher than the concentration of negative ones, the electric wind is stronger close to the negatively charged needle. The mechanism of this wind creation is graphically described in Figure 41. Details can be found in Kozlov and Solovyov's [101] work.

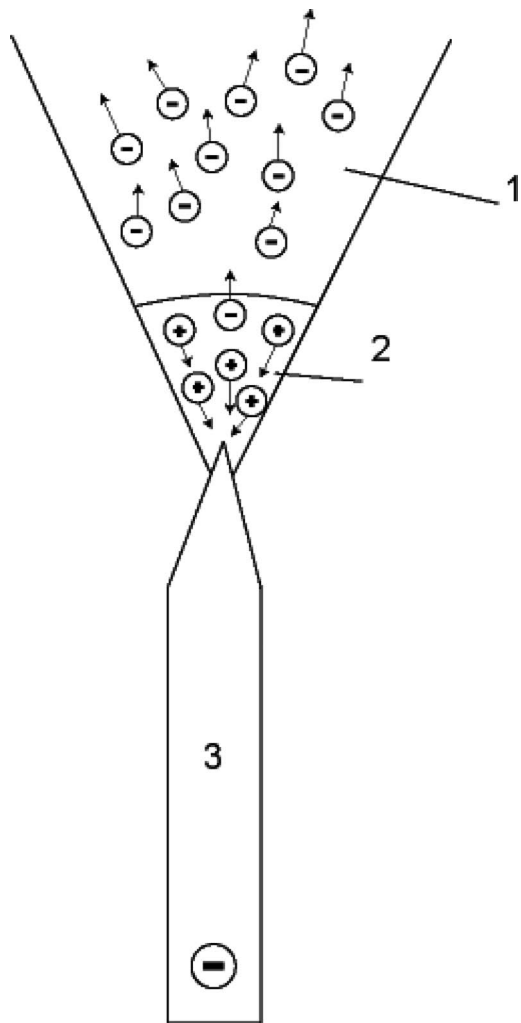


Figure 41. Emergence of the electric wind: in the vicinity of a point electrode (3), positive as well as negative ions are created inside the so-called bipolar area (2). The ions with charge of opposite nature to that of the point recombine with it. Remaining ions are repelled by the point and accelerated away, as shown by (1), called unipolar area.

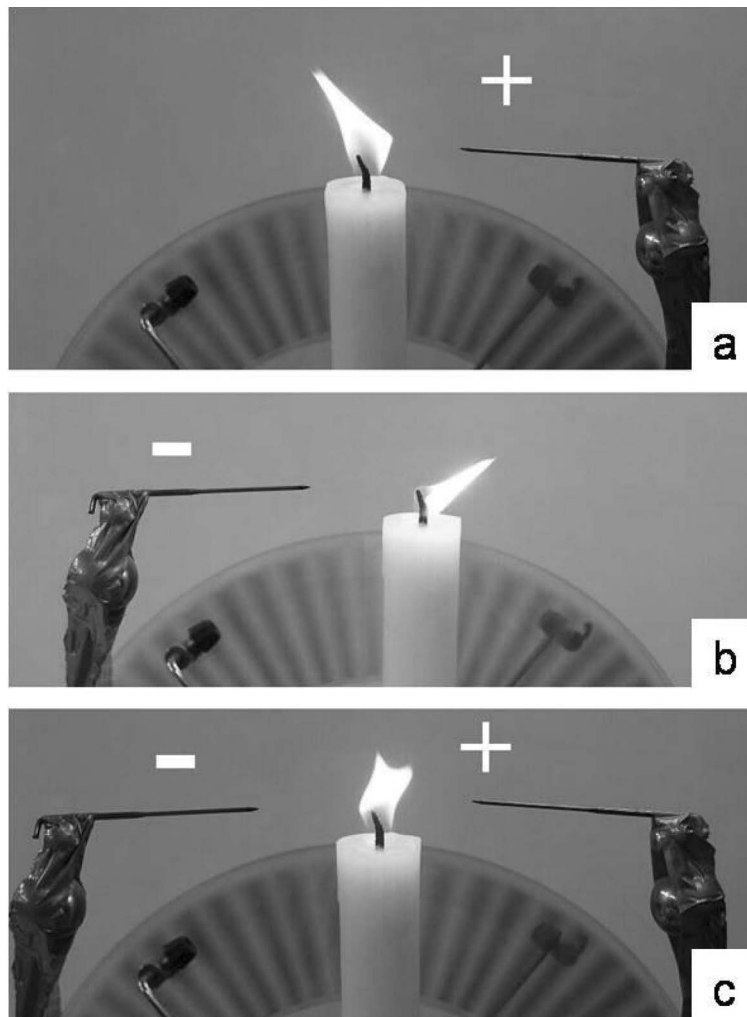


Figure 42. An inflection of a candle flame caused by electric wind: wind direction depends on its polarity: (a) Electric wind generated by a positively charged point electrode, (b) electric wind caused by a negatively charged point, and (c) the flame inflection proves that the negatively charged wind prevails the positive one at the same distance from point electrodes.

A classic experiment can demonstrate the power of the just-described electric winds caused by ions of different signs. As a high-voltage source for the experiment, the Wimshurst electrostatic machine [102] was used, ensuring nearly the same absolute potential values on both negatively and positively charged needles. A flame of a candle was employed as a detector of the electric wind strength. The experiment is shown in Figure 42 in three parts. The first of them, i.e. Figure 42a, depicts the flame inflection caused by the electric wind flowing from the negative needle electrode. The next figure, Figure 42b, depicts the effect of the wind from the positive needle, while Figure 42c depicts the simultaneous action of electric winds caused by both the needle electrodes. It is obvious from the last figure part that the negative wind prevails the same distance from both needles, as supposed to the previously introduced arguments.

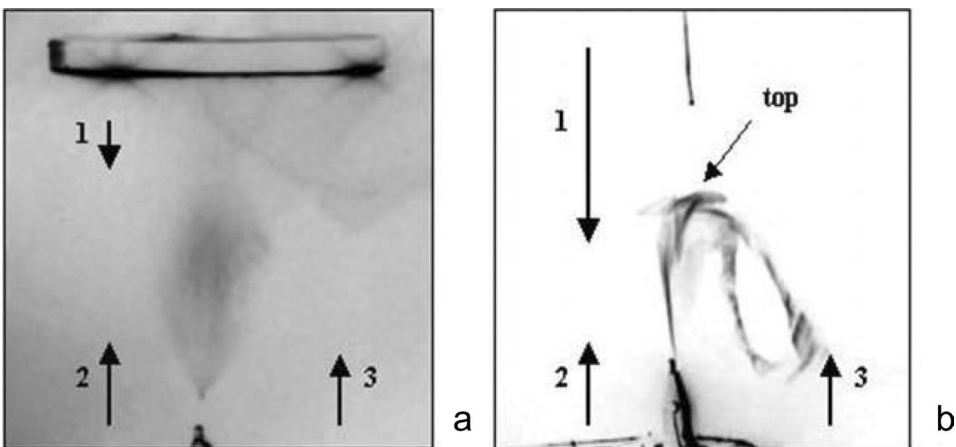


Figure 43. Comparison of jet path in two needle-spinners of various designs. (a) Electrosynthesizer with a plate collector, (b) electrosynthesizer with a needle-shaped collector. Spinning electrodes in both the cases are positively charged, while collectors are negative. The distance between the needle and collector are in both cases the same. Electric wind (1) caused by collectors is much stronger from the point collector than from the plate one. Electric winds (1) and (2) and electrostatic forces (3), in this case, compensate each other close to the middle of the spinning zone, where downward oriented wind (1) prevails and carries the jet back towards the spinning electrode.

Figure 43 illustrates electrospinning in two needle spinners that have collectors of different shapes. The first electrospinner, Figure 43a, is equipped with a plate collector, while the last one, Figure 43b, has a point/needle-shaped collector. In both the cases, the spinning needle electrodes are positively charged. The jet path is quite different inside the spinning zones of these two apparatuses. In the electrospinner with plate collector, the straight direction of the wind from the positive needle to the negative collector simply predominates. The negative wind does not prevail because the plate-like collector does not create sufficiently high field strength in its vicinity to create new ion pairs. The fibres are laid onto the collector since the wind does not have sufficient power to vanquish the Coulombic attraction between the jet and collector.

On the other hand, the jet in the spinner layout with needle-against-point collector shows a parabolic path during its flight. In the upward journey of the parabolic trajectory, the charge of the jet is high enough, and attractive Coulombic forces predominate over the electric wind. This is true for the first part of the jet in Figure 43b, where the jet is nearly mono-filamentous. The counter-current of the negative electric wind starts to balance electrostatic forces wherever the jet starts to whip/coil since its specific surface area increases accompanied by the appearance of the jet's discharge.

The jet discharge can be evaluated by several considerations and experimental evidences. The first of them is based on the observation of a solvent evaporation. Polymeric nanofibres, electrospun from polymeric solutions generally reach a collector in an almost perfectly dried state. More than 90% of a solvent evaporates from a jet during its path from a spinning electrode to a collector. One can assume the same fraction of an original net-charge, as the fraction of evaporated solvent, escapes from the jet too. The reason for the solvent evaporation due to the Kelvin law has been discussed in sub-section 4.2, while an experimental evidence of the charge decrease in the jet is introduced here.

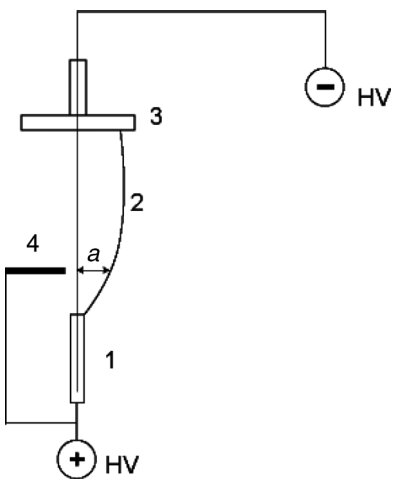


Figure 44. Diagram of the device with the auxiliary electrode, which measured the deflection of the jet path, as sketched in 45: (1) denotes a needle spinning electrode, (2) is a jet, (3) a collector, (4) auxiliary electrode, and parameter  $a$  is the deflection of the jet.

The discharge from the jet was also experimentally investigated using equipment designed by Chvojka [103] and depicted in Figure 44. The principle of the experiment consists in observation of the influence of the auxiliary electrode on the jet path. The auxiliary electrode has a shape of a small sphere movable along the jet path. As the spinning electrode was used, a hypodermic needle directly connected to a syringe. The jet path was recorded using the movie camera PANASONIC NV-CS120. The deviations of the jet from its straightforward path were evaluated from individual pictures of the record using the image analyses system LUCIA, see Figure 45. It is evident from the diagram that jet deviation varies along its path to the collector. It is obvious, therefore, that the repulsive force between the liquid jet and the ball-shaped auxiliary electrode are much stronger in the initial jet path than later in the area close to the collector.

Returning to the experiment with the spinner layout with needle-against-point, the equilibrium between electric wind and Coulombic forces sets in the summit of the parabolic jet trajectory (Figure 43b). During the subsequent part of the jet's journey, the electric charge in the jet is minimal since it escaped with evaporating solvent, and also neutralised by the oppositely charged ions of the electric wind. The strong attraction of oppositely charged particles by electrospinning jets will also be discussed in sub-section 7.2 while dealing with Radon daughter isotopes. The coiling jet creates a sort of 'sail' as a consequence of its elongation and the increment of its specific surface area. Accordingly, the jet creates sufficiently large surface area to which the electric wind can transfer its momentum. Therefore, the dry fibres in Figure 43b are carried down by the electric wind without any chance to be trapped by the point collector. From the given experiment, it is possible to enunciate an empirical rule for the design of any electrospinner: the ratio of minimum dimensions of spinning electrode to collector must not be lower than 1:7–1:12, see Chvojka [103], to avoid many difficulties affecting fibre collection onto a collector. On the other hand, this effect can be utilised in some efforts to extricate the electrospinning jets and nanofibres from a spinning zone and to manipulate them by forces that are not electrostatic in nature. This method can find some application, especially in medicine.

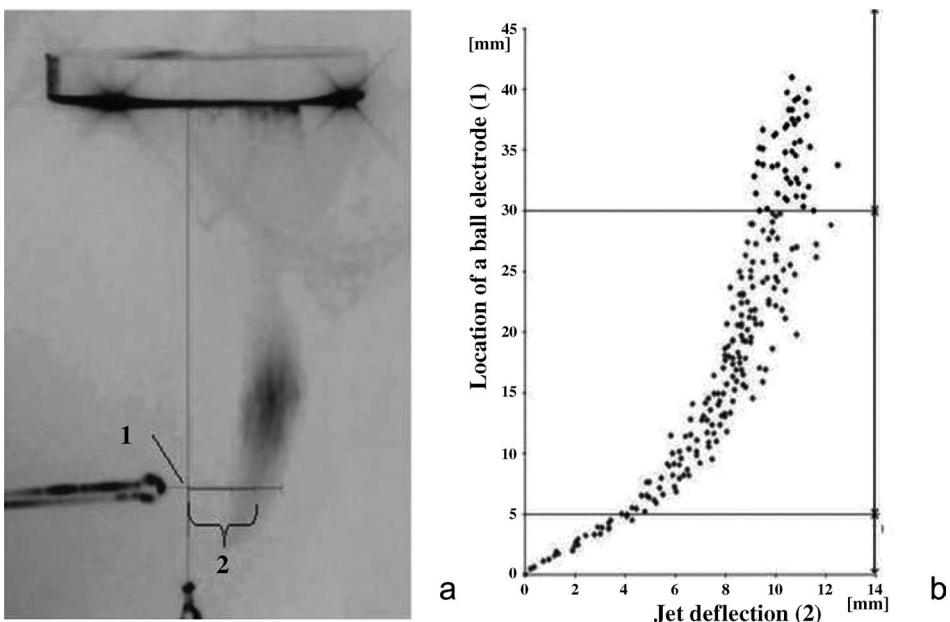


Figure 45. (a) Deflection of a jet path (2), caused by an auxiliary electrode (1). (b) The deflection depends on the position of the auxiliary electrode in the spinning zone.

In fact, it is both worthwhile and noteworthy to underline that the studies of electric wind strongly supported the idea of dielectric diffusion, as has been dealt with before in sub-section 3.7. The thorough and quite intriguing comprehensive study of electric wind does not only consolidate the concept of dielectric diffusion strongly, but also, remarkably, helps to reconcile and confirm the strong influence of influencing factors, like symmetry and relative orientation of the capacitor plates, as proposed by Sarkar [104] in his doctoral thesis on ‘Physical Principles of Electrospinning’. The change of the electrode geometry in electrospinners can heavily influence a local distribution of field strength,  $E$ , and consequently it affects the electric wind and the jet path. However, the experimental procedure to study the diffusion by observing electric wind and radiation, as presented below, could help in effective understanding of the phenomenon from the standpoint of quantum physics, thus enabling more efficient, accurate and sophisticated instrumentation to handle the technology.

## 7.2 Irradiation caused by electrospinning

The other exceptional features of electrospinning are various kinds of accompanying irradiations. The first report was by Zeleny [9], who referred about eradication, which was of very similar nature as St. Elmo’s fire. He observed and described a visible luminosity of a jet or spray inside a spinning zone of his apparatus described in Section 2. The other two kinds of radiation to be described and discussed further, are radioactive irradiation, caused by trapping of Radon decay daughter isotopes on negatively charged bodies in electrospinners, and soft Roentgen irradiation caused by freshly formed nanofibres.

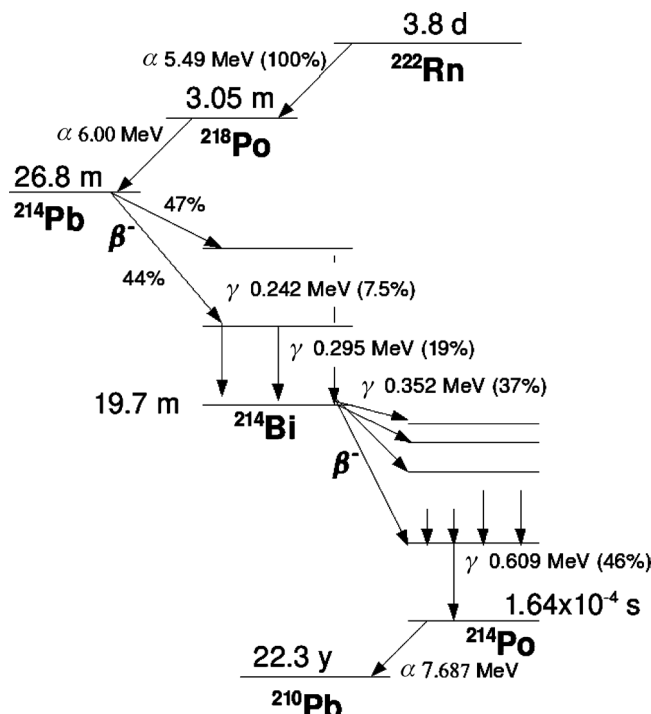


Figure 46. The decay scheme of  $^{222}\text{Rn}$ : all isotopes are assigned with atomic numbers, half-times in minutes [m] and types of emitted particles. For example,  $^{218}\text{Po}$  has an atomic number 218, half-time 3.05 min and disintegrates into  $^{214}\text{Pb}$  by emission of 6 MeV energetic alpha particle.

### 7.2.1 Radioactive radiation

The description of radiation starts here with nuclear decay caused by Radon,  $^{86}\text{Rn}$ , that is present in air. Radon is the chemical element with atomic number 86. It is the invisible, radioactive noble atomic gas that in nature results from radioactive decay of some forms of uranium,  $U$ , that is spread all over the world in igneous rock formations beneath buildings or in certain building materials. Uranium decay to Radium and Radon is being continuously produced by radioactive decay of Radium isotope  $^{226}\text{Ra}$ . Radon is one of the heaviest gases under the normal conditions. The most stable Radon isotope,  $^{222}\text{Rn}$ , has a half-life of 3.8 days, vide Remy [105]. Radon gas and its solid decay products are recognised and considered to be a serious health hazards since they are carcinogens. However, the Radon decay does not affect living tissues directly. The crucial effect occurs via a deposition mechanism of the radioactive Radon daughters, as introduced by Batkin et al. [106].

The deposition of Radon decay products on electrospun nanofibrous materials and electrodes of electrospinners was studied using various detection technologies ranging from etched-track detectors, proportional counters, gamma spectrometers, etc. Radon decay progeny are not gases (Po, Bb, Bi) but solids, see Figure 46. They can attach themselves to tiny particles in the air, and these particles may be trapped as contamination in the lungs of a human breathing the air, and cause lung damage from alpha and beta radiation.

The deposition of Radon during electrospinning is caused by an attraction between any negatively charged solid or liquid bodies and positively charged radon daughters. Radon daughters have the electric affinity to negatively charged surfaces since they are

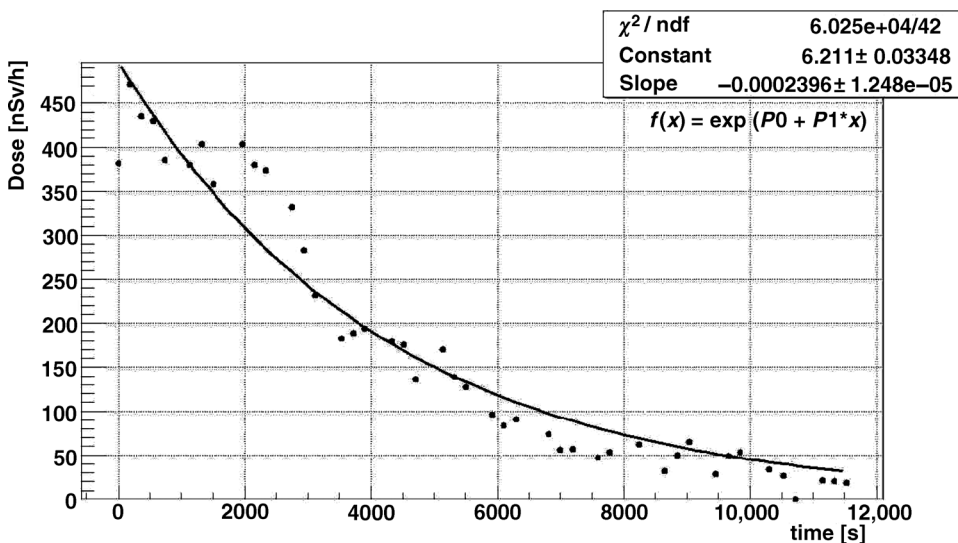


Figure 47. Deposits of electrospraying and electrospinning materials of a mass around tens of grams exhibit high-energy excitations that are four times higher than the laboratory background (gamma dose rate of  $123 \pm 8$  nSv/h). The activity was registered by twin Geiger-Müller Tubes of the Radiometer 'VOLTCRAFT HS-036'.

electrically positive as a result of stripping of electrons from the parent atom during their radioactive decays. The investigation of the deposition of aforementioned heavy metals should be critical for an application of nanofibrous materials in tissue engineering, since they may cause health hazards. Recent human health hazards have increased in the modern industrial age as a human body often carries a negative static charge caused by non-zero body potential, up to tens of kilovolts, that results from everyday activities such as walking across synthetic floors, working with plastic materials or from coming into contact with charged objects.

A series of electrospraying as well as electrospinning experiments have been carried out under special conditions to confirm that even scant mass of electrospun nanofibrous layer, not more than tens of grams, can exhibit high-energy excitations that should be more than four times higher than the natural background. The electrospun materials were prepared in the environment with the radioactive background having gamma dose rate of  $(123 \pm 8)$  nSv/h, where symbol Sv in SI system of units is the Sievert. The radioactivity was registered by twin Geiger-Müller Tubes of the Radiometer 'VOLTCRAFT HS-036'. Measurements of depositions on nanofibrous layers, see Figure 47, were made with negatively and positively charged collectors, for various temperatures, to exclude effects from an electron shell. For all samples, same half-time with various radiation intensities were measured. Irradiation intensities detected from nanofibres collected on positively charged collectors were about half than that of negatively charged ones under the same conditions. More complex measurements proved that Radon daughter deposits are more attracted by motionless negatively charged nanofibrous layers trapped on a collector than by a negative jet discharge attracted by a positively charged collector. The fundamental general theory explaining the process of Radon deposition in details was introduced by Batkin et al. [106]. Radon radioactive decay series leads to the Lead isotope  $^{210}\text{Pb}$  with half-time 22.3 years, as is obvious from Figure 46. Lead traces in electrospun samples were also analysed by

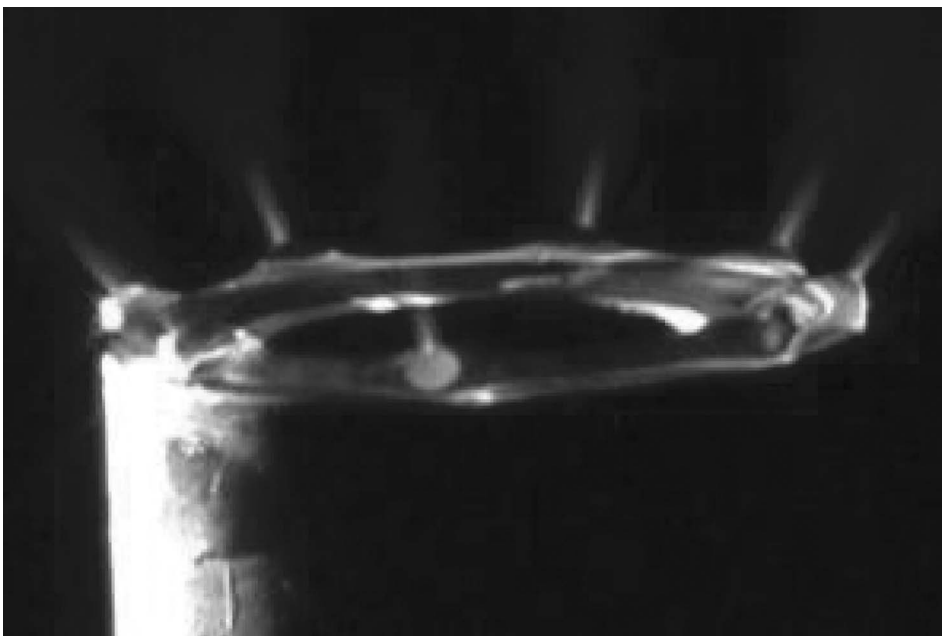


Figure 48. St. Elmo's fire created nearby Taylor cones during electrospraying of demineralised water.

scanning electron microscope JEOL JED-2300 with EDS (energy disperse X-ray analyser) but the presence of this isotope was immeasurable by this method.

Detected increased radioactivity of charged Radon daughters from electrospun materials is indirect evidence of discharge from jets during their path through spinning zones that has been mentioned in sub-section 7.1.

### 7.2.2 *St. Elmo's fire*

Another type of irradiation in electrospinning is St. Elmo's fire. Already, Zeleny [9] referred to the intensity and span of luminosity that depends on the prevailing type of a discharge realised by a spray in the vicinity of Taylor cones, vide Figure 48. Zeleny distinguished negative and positive discharges depending on the net charge involved in the spray. According to him, positive discharge is the one which transports positive net charge through a spinning zone and vice versa. Positive discharges provide fibrous brushes of light that reach out further away from the electrode towards the collector than those of the negative discharges.

A mechanism for St. Elmo's fire was described by Grigor'ev and Sinkevich [99]. Small charged droplets of residual solution are ejected from charged liquid bodies when a strong electric field is applied. From these mother droplets, smaller daughter droplets can be created due to their electric disintegration described in sub-section 3.4. The ratio of radii of small and big droplets  $r/R$  is, according to Grigor'ev, about 0.018. Daughter droplets can usually reach a diameter of units of micrometers and they extract almost all charge from its mother droplet, as described in Landau and Lifshitz [19]. Tiny daughter droplets emit high energy photons after impacts with external ions from ambient gas accelerated under strong electric fields of tiny daughter droplets. St. Elmo's fire is stronger around positively charged Taylor cones, since the concentration of negative ions is higher than the concentration of positive ones, as has been mentioned in sub-section 7.1.

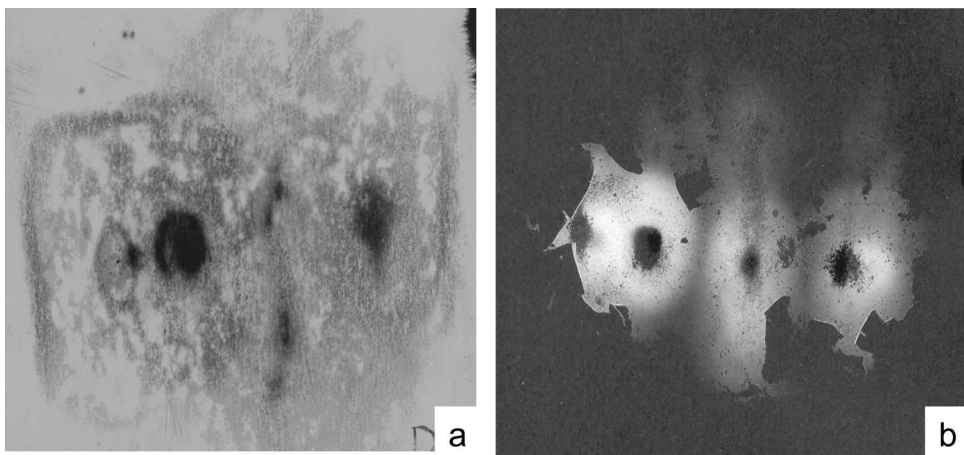


Figure 49. (a) Black traces detected by radiographic film. This radiation most probably arises from the end of the whipping zone. This hypothesis is indicated by geometrical similarity of tracks, recorded on a radiographic film, and heaps/spots of deposited nanofibres (b).

An energy produced by collisions of ions with other particles can simply be estimated by the following formula:

$$\lambda = \frac{hc}{q_e Es}, \quad (7.4)$$

where  $h$  is Plank's constant,  $c$  is speed of light,  $q_e$  is electron's charge,  $E$  is field strength and  $s$  is average free track length of an ion in the air before the collision, which is approximately 64 nm.

#### 7.2.3 Roentgen radiation

It was also observed that coiled electrospun jets of very complicated fractal structure, just before getting trapped by a collector, caused soft Roentgen irradiation. This radiation was detected using radiographic film INDUX R7 made by FOMA, Czech Republic, which was packed in 10  $\mu\text{m}$  thick aluminum film. This radiation most probably arose from the end of the whipping zone, which was proved by geometrical similarity of tracks recorded on a radiographic film and local heaps of deposited nanofibres (Figure 49). The wavelength of this radiation is in far UV or in low energetic X-ray area and it was not caused by Radon daughter deposition, because no radiation of this type was detected from electrospraying that could trap Radon decay products. One could easily eliminate the idea that the radiographic film became black due to accelerated electrons in high voltage electric field, because radiation was observed for both polarities of a collector. So, the most probable reasons behind the phenomenon are high energetic photons, emitted from electrospinning jets. It is surprising that this type of radiation can reach up to the frequency zone of X-ray.

## 8. Polymeric solutions for electrospinning

In order to carry initiate electrospinning, the polymer must be in a liquid form, either as molten or solute one. In this section, polymer solutions will be predominantly dealt with.

The properties of polymer solutions, like permittivity, conductivity, polarity, viscosity, surface tension, polymer solubility, etc., play a critical role in electrospinning, and significantly influence resultant fibre morphology. Moreover, according to experimental experience, a dominating factor affecting the process is the solvent quality. Solutions for electrospinning can be prepared by dissolving a polymer in its solvent(s) or in solvent mixtures. Primarily, two categories of solvents that recognised are ‘good’ solvents, in which polymeric chains/coils are expanded, and ‘bad’ solvents, which provide with more compact coils, as delineated by Hiemenz and Lodge [89]. Lowering of the solution temperature thermodynamically reduces the ‘goodness’ of a solvent. Changes in the polymer coil dimension affect physical properties of polymeric solutions, e.g. the intrinsic viscosity, as described by the Mark–Houwink Equation (8.12). There are two extreme shapes of polymeric chain: the sphere model and the rigid rod model, introduced by Hiemenz [107], and Lodge [89]. Certain types of solvents particularly impart productive spinnability of nanofibres of a polymer through electrospinning, while some other solvents do not, as discussed by Ramakrishna et al. [2].

Particularly, Jarusuwannapoom et al. [108] studied effects of solvent property on electro-spinnability and morphology of polystyrene (PS) fibres from it. Obtained results suggested that among important factors determining electro-spinnability of PS solutions are polar properties of the solvent and the conductivity of both the solvent and the solution. Other associated significant parameters are, boiling point of the solvent, solution viscosity and its surface tension.

### 8.1 Polymer solubility

Evaluation of certain thermodynamic potentials and related quantities allows prediction of a polymer’s solubility in a given solvent, i.e. if a polymer dissolves in the given solvent or not. Such thermodynamic potential is the ‘Gibbs free energy’ of mixing  $G_M$  and the assign thermodynamic quantities are solubility parameters  $\delta$ ’s. When a pure polymer is mixed with a pure solvent at a given temperature  $T$  and pressure, the change of Gibbs free energy of mixing is given by the following thermodynamic Equation (8.1):

$$\Delta G_M = \Delta H_M - T \Delta S_M, \quad (8.1)$$

where  $\Delta H_M$  is the enthalpy change of mixing and  $\Delta S_M$  is the entropy change of mixing. Changes of thermodynamic quantities are here considered as differences of their values in a mixture minus their values in a system, where polymer and solvent are separated. According to Equation (8.1), the polymer dissolution will take place only if the Gibbs free energy change of mixing  $\Delta G_M$  is negative, since systems in equilibrium minimise their free energy. Entropy change  $\Delta S_M$  is obviously positive, since in solutions the macromolecules, as well as the whole system, display more allowed conformations than in a solid polymer and solvent in a separated state. Therefore, generally, the term  $-T \Delta S_M$  in Equation (8.1) is negative and hence, drives the components of the system to mix. However, the enthalpy change of mixing,  $\Delta H_M$ , may be either positive or negative and, ultimately, governs the tendency of a polymer to be mixed with the solvent.

The entropy,  $S$ , is given by the Boltzmann Equation (8.2), where  $W$  is the number of allowed system configurations and  $k_B$  is the Boltzmann constant:

$$S = k_B \ln W. \quad (8.2)$$

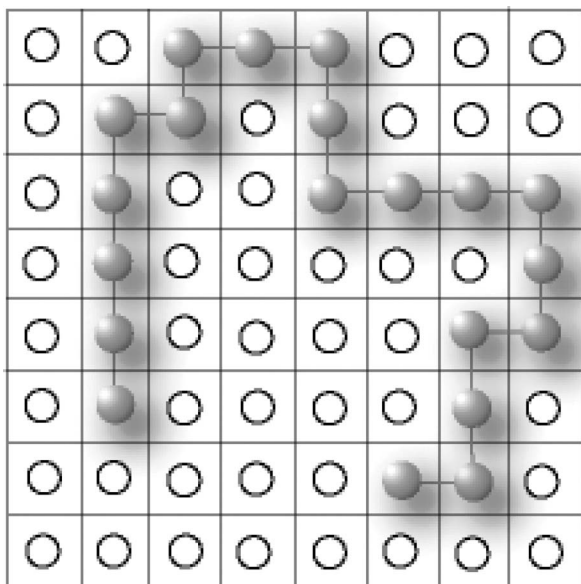


Figure 50. Two-dimensional lattice model of a mixture, consisting of a polymeric chain (grey circular segments) interconnected with bonds that mimic the polymer chain backbone, and solvent particle (depicted as white circles). The total site number  $N$  is here 64.

For low molecular weight solutes,  $W$  is considerably large; consequently, the value of entropy change of mixing  $\Delta S_M$  is high. A different situation arises when the solute molecules are polymers of high molecular weights. Simple lattice models are then introduced to investigate statistically and to understand theoretically the behaviour of polymers in solutions. Polymer chains are in these models considered as large segmented flexible necklace-like patterns, as shown in Figure 50. The entropy change of mixing  $\Delta S_M$  can be predicted using the Flory–Huggins lattice model, vide Flory [109], as

$$\Delta S_M = -k_B N \left( \varphi_1 \ln \varphi_1 + \frac{\varphi_2}{x} \ln \varphi_2 \right), \quad (8.3)$$

where  $N$  is the total number of sites in the model,  $N = N_1 + xN_2$ , with  $N_1$  being the number of solvent molecules and  $N_2$  denoting the number of polymer molecules, each of which has  $x$  segments, i.e.  $x$  is here the degree of polymerisation. Polymer volume fractions of a solvent,  $\varphi_1$ , and a polymer,  $\varphi_2$ , are given subsequently as  $\varphi_1 = N_1/N$  and  $\varphi_2 = xN_2/N$ .

The enthalpy change of mixing  $\Delta H_M$  is given by Equation (8.4):

$$\Delta H_M = N_1 \varphi_2 \Delta \varepsilon - T \Delta S_M, \quad (8.4)$$

where  $\Delta \varepsilon = (2\varepsilon_{PS} - \varepsilon_{SS} - \varepsilon_{PP})/2$  is the so-called energy change. The heterogeneous energy interactions  $\varepsilon_{PS}$ , coming along in  $\Delta \varepsilon$ , among polymer segments and solvent molecules, in connection with homogenous interaction  $\varepsilon_{SS}$  between pairs of solvent molecules and polymer segments  $\varepsilon_{PP}$  can be effectively described by the dimensionless polymer-solvent

interaction parameter  $\chi$ :

$$\chi = \frac{\Delta\epsilon}{k_B T}. \quad (8.5)$$

Substitution from Equations (8.3) and (8.4) into (8.1) gives the following relation for the Gibbs free energy change:

$$\Delta G_M = k_B T(N_1 \ln \varphi_1 + N_2 \ln \varphi_2 + N_1 \varphi_2 \chi). \quad (8.6)$$

### 8.1.1 Solubility parameters

Since the term  $\Delta S_M$  in Equation (8.1) is relatively small for polymeric solutions,  $\Delta H_M$  must be even smaller than  $T \Delta S_M$  in order to obtain a negative  $\Delta G_M$  to predict solubility. Enthalpy change of mixing  $\Delta H_M$  is given by an Equation (8.7) introduced by Hildebrand and Scott [110]:

$$\frac{\Delta H_M}{V_m} = \varphi_1 \varphi_2 (\delta_1 - \delta_2)^2, \quad (8.7)$$

where  $\delta_1$  and  $\delta_2$  are Hildebrand solubility parameters for a polymer and a solvent, while  $V_m$  denotes the molar volume. The solubility parameters determine the polymer solubility in the given solvent. Apart from solubility parameters, the related polymer structure heavily influences its solubility, as well described through previously mentioned sphere and rigid rod model of polymeric chains.

The Hildebrand solubility parameter method was conceptually extended by Hansen [111] aiming to estimate the relative miscibility of polar systems and system with hydrogen bonds. Hansen split up the square of the Hildebrand solubility parameter  $\delta^2$  into three components: a dispersion force component  $\delta_D^2$ , a polar interaction component  $\delta_p^2$ , and hydrogen bond component  $\delta_H^2$ . His approach, see Equation (8.8), is coined with the notion of ‘3-D solubility parameters’:

$$\delta^2 = \delta_p^2 + \delta_D^2 + \delta_H^2. \quad (8.8)$$

Charles Hansen used his three-dimensional geometrical model to interpret solubility of polymers graphically. This model introduces a ‘solubility volume’ of a polymer as a sphere in three-dimensional Cartesian coordination system, whose axes are represented by the three solubility components  $(\delta_D, \delta_p, \delta_H)$ . The centre of the solubility sphere is located in the point  $(^P\delta_D, ^P\delta_p, ^P\delta_H)$  with particular component values of the solubility parameters of the particular polymer. The radius of the solubility sphere is called the ‘interaction radius’  $R$ , vide Figure 51.

Solution viscosity, as well as configurations of polymer chains, depends on the position the triplet of three-dimensional solubility parameters  $(^S\delta_D, ^S\delta_p, ^S\delta_H)$  by virtue of Hansen solubility volume. Solvents with triplet solubility parameters located at the centre of the Hansen solubility volume dissolve the polymer so effectively that the individual polymer chains are free to uncoil and stretch out. On the other hand, if the polymer is dissolved in solvents localised off-centre of the Hansen solubility sphere, polymer chains remain coiled and grouped together into microscopic clumps that tend to create solutions of lower

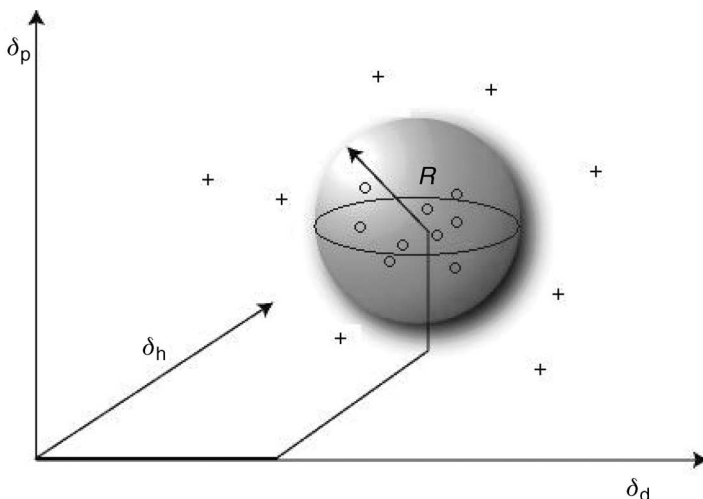


Figure 51. The Hansen volume of solubility for a polymer is depicted as a sphere in ( $\delta_D$ ,  $\delta_p$ ,  $\delta_H$ ) Cartesian coordinate system. At the centre of the solubility volume is a point with Hansen solubility parameters of the polymer, i.e. ( $^P\delta_D$ ,  $^P\delta_p$ ,  $^P\delta_H$ ). Solvent systems whose triplet solubility parameters ( $^S\delta_D$ ,  $^S\delta_p$ ,  $^S\delta_H$ ) are located within the Hansen volume, depicted as open circles, are active solvents for the polymer in question. Solvents out of the Hansen volume, sketched as crosses, are non-solvents for that polymer.

viscosity, as mentioned by Burke [112]. The variances in polymer chain configurations can significantly affect the electrospinning process.

Wannatong et al. [58] studied behaviour of PS solutions prepared from 18 various solvents. They observed that a significant difference between the solubility parameters of PS and its solvent is responsible for the bead-on-string morphology of electrospun fibres.

Liu and Hsieh [61] prepared polymer solutions of cellulose acetate (CA) dissolved in three solvents: acetone, acetic acid and dimethylacetamide (DMAc) with a range of solubility parameter, surface tension, viscosity and boiling temperature. They found that none of these solvents alone enables continuous formation of fibres; however, mixing DMAc with either acetone or acetic acid provides suitable solvent systems for electrospinning technology.

## 8.2 Volatility of a solvent

During electrospinning, the solvent evaporates as fibres are formed, vide sub-section 4.2. The solvent evaporation is another important parameter influencing the resultant morphology of nanofibres. When the rate of evaporation of the solvent is too low, then the process leads to formation of a thin film or flat ribbons that are deposited on a collector instead of smooth cylindrical nanofibres as has been reported by Reneker and Yarin [4]. On the other hand, if the rate of evaporation is too high, fibres are not formed since electrospinning is blocked by the creation of a tiny layer of gel formed on a polymeric solution surface. When a solvent has an optimal volatility, the presence of residual solvent in electrospun nanofibres facilitates the bonding between intersecting fibres grasped by a collector, creating a mechanically strong cohesive structure of nanofibre sheets. This is analogous to thermal or

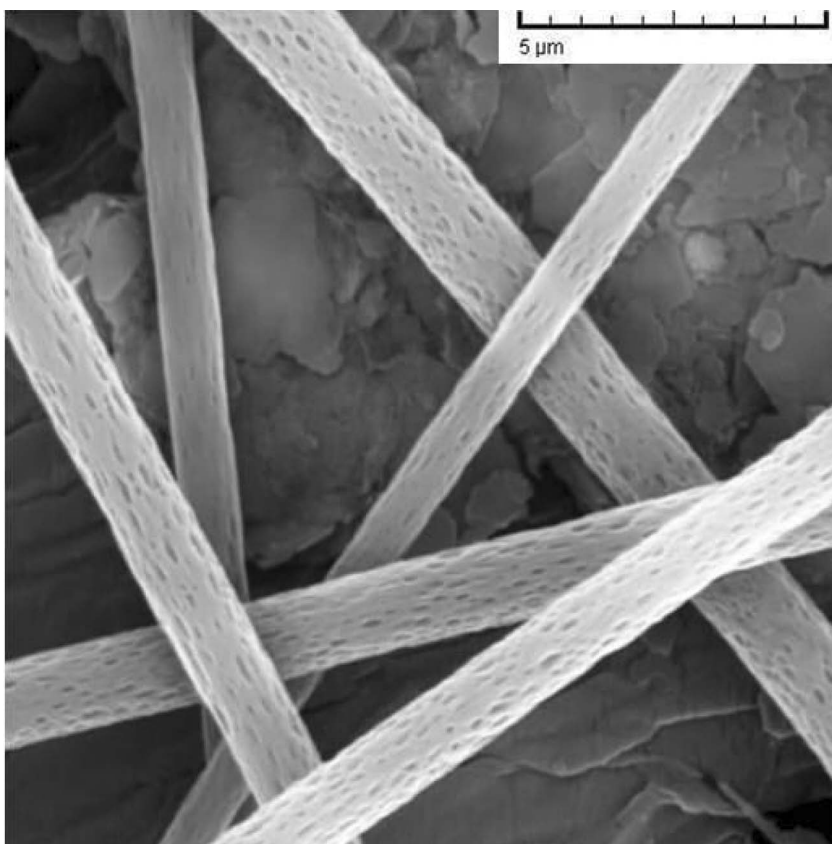


Figure 52. SEM micrographs of porous nanofibres, prepared from poly(2-hydroxyethyl methacrylate), i.e. poly(EOEMA), dissolved in dichlormethane/methanole.

chemical bonding of non-woven fabrics. For more details consult Jirsak and Wadsworth's [113] monograph.

An interesting finding is that the evaporation of solvents yields polymer fibres with a relatively regular porous structure as the one depicted in Figure 52. The regular phase morphology is induced by a rapid phase separation in electrospinning jet when a highly volatile solvent is used. The solvent rich regions in a jet are apparently transformed into pores after its intensive evaporation. The replacement of dichloromethane with solvents of lower vapor pressure, such as chloroform, reduces the tendency towards pore formation significantly, Bognitzki et al. [114]. The elongation of the pores along the fibre axis is most probably the result of a uniaxial jet extension that persists even after the solvent was evaporated.

Bognitzki et al. [114] prepared porous ultrafine fibres from PLA, polycarbonate and poly(vinyl carbazole) with dichlormethane used as the solvent. Khil et al. [115] prepared porous PCL filaments to study growth of cells on these non-woven fabrics. This work reviled the important role of scaffold porosity for proliferation of living animal cells. Han et al. [116] prepared ultrafine porous cellulose triacetate (CTA) fibres by electrospinning methylene-chloride (MC) and a mixed solvent of MC and ethanol (EtOH).

The evaporation rate of solvent depends on many factors, like vapor pressure, boiling point, specific heat, enthalpy, chemical potential difference and heat of vaporisation of the solvent, as referred by Ramakrishna et al. [2]. The vapor pressure of a solvent depends on its molecular weight, heat of vaporisation and temperature as expressed by the Clausius–Clapeyron Equation (8.9):

$$\frac{d(\ln p)}{dT} = \frac{M\Lambda}{RT^2}, \quad (8.9)$$

where  $p$  is the vapor pressure,  $T$  is temperature,  $M$  is the solvent molecular mass,  $\Lambda$  is the heat of vaporisation and  $R$  is the universal gas constant. The value of the vapor pressure in a spinning zone can heavily influence the solvent evaporation and hence it makes sense to electrospinning in various artificial atmospheres.

### 8.3 Concentration and viscosity of polymer solutions – Berry number

The quality of nanofibres, produced in electric field, depends on a solution viscosity. Specific viscosity  $\eta_{sp}$  of homogenous solutions of linear polymers is described by the well-known Huggins Equation:

$$\eta_{sp}(c) = [\eta] c + k_H([\eta] c)^2 + \dots, \quad (8.10)$$

where  $[\eta]$  is the intrinsic viscosity,  $c$  is the polymer concentration and  $k_H$  is a Huggins coefficient, vide Morawetz [117]. The dimensionless product of the intrinsic viscosity  $[\eta]$  and the concentration  $c$  is referred to as the Berry number, i.e.  $B_e \equiv [\eta]c$ , see Hager and Berry [118]. The significance of the Berry number  $B_e$  arises from the fact that it is related to the number of chain entanglements. In dilute polymer solutions, where polymer chains do not overlap each other, as sketched in Figure 53a,  $B_e$  can, at best, be unity,  $B_e \cong 1$ . The more subtle meaning of the Berry number is explained further and derived from the notion of intrinsic viscosity.

In Relation (8.10), the intrinsic viscosity  $[\eta]$  is the initial slope of the plot of specific viscosity on concentration for small  $B_e$ . Intrinsic viscosity  $[\eta]$  is also related to the root-mean squared end-to-end distance  $\langle R^2 \rangle^{1/2}$  of the linear polymer chain composed of  $x$

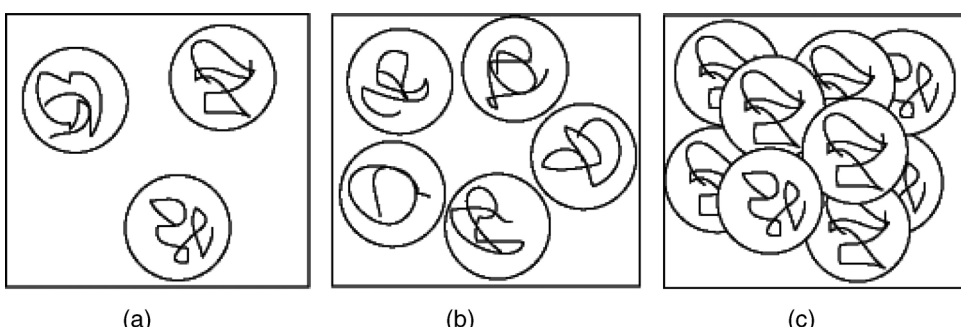


Figure 53. Graphical representation of the three solution regimes: (a) dilute,  $c < c^*$ , (b) semi-dilute unentangled,  $c^* < c < c_c$  and (c) semi-dilute entangled,  $c_c < c$ . The quantity  $c_c$  is critical concentration.

monomers by the Fox–Flory Equation (8.11) introduced in Flory [109]:

$$[\eta] \approx \frac{\langle R^2 \rangle^{3/2}}{x}. \quad (8.11)$$

In addition, the intrinsic viscosity  $[\eta]$  is related to the molecular weight  $M$  of a linear polymer by the Mark–Houwink–Sakurada Equitation (8.12), vide Tanford [119], where the constants  $K$  and exponent  $a$  depend on the polymer, solvent and temperature, as referred to by Rai and Rosen [120].

$$[\eta] = KM^a. \quad (8.12)$$

The number of elementary units/monomers/segments of a single molecule inside its pervaded volume  $\langle R^2 \rangle^{3/2}$  is called ‘overlap concentration’. Pervaded volume  $V$  is the volume of solution spanned by the polymer chain. Its bulk is as a rule estimated by the volume of the cube having the edge length equal to the root-mean squared end-to-end distance. The critical chain overlap concentration  $c^*$  means that just one macromolecule of the degree of polymerisation  $x$  is confined in each pervaded volume, i.e.  $c^* \equiv x/\langle R^2 \rangle^{3/2}$ . The critical chain overlap concentration  $c^*$  is the crossover concentration between the dilute and the semi-dilute concentration regimes, as graphically depicted in Figure 53. Using the Fox–Flory Equation, one can write  $c^*$  as

$$c^* \approx \frac{1}{[\eta]}. \quad (8.13)$$

Recall that the criterion  $c^*[\eta] \approx 1$  following from Equation (8.13) helps to interpret the meaning of the Berry number,  $B_e \equiv [\eta] c$ , as the quantity evaluating a number of macromolecules inside the pervaded volume.

The number of chain entanglements is one of many parameters that can significantly influence fibre formation during polymer electrospinning. While the importance of chain entanglements has been acknowledged, there is no clear understanding of how many entanglements are required to affect/stabilise fibres formation for particular polymer solution. Polymer solution rheology has been extended to formulate a semi-empirical analysis, as introduced by Shenoy et al. [23] to explain the transition from electrospraying to electrospinning from good solvents and non-specific polymer–polymer interaction limit. Fibre formation predicted by this theorem has at least one entanglement, belonging to each polymer chain. Complete, stable fibre formation occurs at a number of entanglements per chain greater than 2.5. This theoretical predictions are in good correlation with the work of Přádný et al. [121], where Berry numbers were obtained for many various polymer solutions, particularly for poly(2-hydroxyethyl methacrylate) abbreviated as poly(HEMA), and copolymer(2-hydroxyethyl methacrylate/2-ethoxyethyl methacrylate) denoted as poly(HEMA/EOEMA). The used polymers had molecular weights from  $5.8 \times 10^4$  to  $1.80 \times 10^6$  and concentrations of applied solutions, in this case were water/ethanol (66.3 %wt) or pure ethanol, spanned from 15.7 up to 22.9 wt%. When Berry numbers of these polymer solutions had higher values than 2.4, then electrospinning was realised through Nanospider™ technology provided with sub-micron fibres without any defects, as documented in Figure 54b.

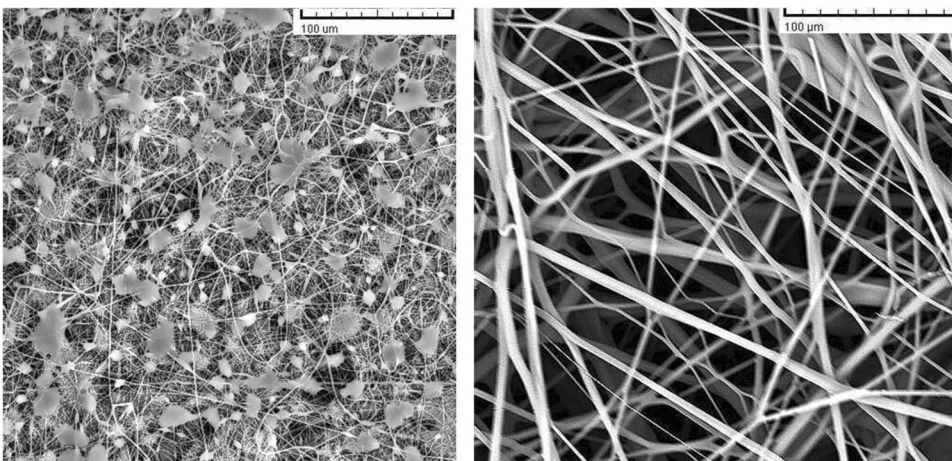


Figure 54. SEM micrographs of poly(HEMA) electrospun nanofibres from: (a) semi-dilute solution ( $B_e = 2$ ), (b) solution in semi-dilute entangled regime ( $B_e = 8.1$ ), where  $B_e$  denotes Berry number.

## 9. Conclusion and perspectives

In this paper, a review has been presented on electrospinning and electrospun nanofibres, focusing both on physical principles and technological aspects. Electrospinning has been introduced as an extraordinary self-organising phenomenon that enables to reform disordered polymeric solutions with high entropy into highly organised solid nanofibres, using various physical instabilities based on hydrodynamics, capillarity and electrostatics. While transforming the subject of electrospinning, having rich interdisciplinary nature to a successful productive technology of industrial interest, in a comparatively short span of time, it had to be approached in a well-planned and organised manner from the stand points of natural sciences, like chemistry and physics, and from instrumentation/mechanical engineering point of view as well too.

Electrospinning is considered as a novel method of spinning extremely fine fibres. However, more detailed insight unveils its surprisingly deep historical roots, leading even to the W. Gilbert's observations, performed in the earliest years of the seventeenth century. Eminent theoreticians, like Rayleigh, approached the topic of liquid droplet disintegration due to electric forces in the middle of the nineteenth century. Two outstanding inventions appeared at around the end of the nineteenth century, written in patents by Morton and Cooley. Through their prescient work one may track the whole journey that electrospinning took to develop to fully-fledged industrial technology, i.e. from needle to needleless variants, along with variants like, core-shell electrospinning, etc. A classic electrospinning set-up, based on needle spinning electrode, was designed by Zeleny, who was motivated to study thunderstorm clouds, just at the beginning of the First World War. His set-up is the most common one even in recent electrospinning labs. Also, the first industrial facility for producing nanofibrous materials by needle method is quite a lot older than one may suppose, since Russians constructed it already in 1939, to produce materials for their defense sector.

As has been shown, the theory about electrospinning is enormously rich and covers such disciplines as electrostatics, hydrodynamics, electro-hydrodynamics, capillarity, polymer chemistry and physics, thermodynamics and material engineering. It has been highlighted above that the phenomenon is formed as an instability of a tiny capillary wave on a

liquid surface, either on free liquid surface or on the one confined in a capillary, which is enhanced by external electrostatic field. The charged jet then undergoes other instabilities to whip/coil, and elongates up to diameters of tens or hundreds of nanometers. An extremely rapid decrease of its radius ousts solvent molecules from the jet due to thermodynamic reasons.

The jet path can be controlled by special collectors and spinning electrodes. It has been documented that this approach may lead to patterned nanofibrous layers, nanofibrous yarns and three-dimensional structures. A spinning electrode of cylindrical shape waded in a pool of polymeric solution is the most basic of NANOSPIDER™ technology that is now available in the market.

Two electrospinning variants, i.e. melt and core–shell electrospinning, have been discussed in detail. Melt-electrospinning is favoured since it provides cleaner processing, environmental safety, and does not need solvent recycling. On the other hand, melt-electrospinning devices are more complex as they require precise control of heating for polymer melting to prevent its thermal degradation. Melt-electrospinning is also limited by low flow indices of particular polymer melts. Core–shell electrospinning has been referred to as a unique sophisticated method to produce composite functionalised nanofibres with almost strictly organised core–shell structure. The shell consists of a spinnable polymeric material, while the core can consist of any other polymer or of another encapsulated mass, including liquids.

Two exceptional features of electrospinning, scarcely referred to have been introduced in much detail. The first is electric wind that influences a jet path in a spinning zone. It has been documented that the change of the electrode geometry in electrospinners can heavily influence the local distribution of field strength,  $E$ , and consequently affect the electric wind and the jet path. The last section of exceptional features of electrospinning reported about irradiations: St. Elmo's fire, radioactive irradiation caused by trapped Radon decay daughter isotopes by negatively charged bodies in electrospinners and, finally, soft Roentgen irradiation, caused by freshly formed nanofibres.

Lastly, it was shown that solvent quality has a dominant effect on the electrospinning process. The Hansen generalised approach for estimation of the relative miscibility of polymers with solvents was introduced. The interesting finding that the intensive solvent evaporation from solvent rich regions in a jet yielded polymer fibres with a relatively regular porous structure was described. The quality of produced nanofibres was influenced heavily by solution viscosity and a Berry number that was related to entanglements among neighbouring polymeric chains.

Given the breadth of the treated subject, drawing a simple conclusion is quite difficult, as is estimating the exact futuristic directions of the technology of electrospinning. In spite of that, there are some enlisting relevant points to convey its potentials, as understood to date:

- Needle electrospinning and core–shell electrospinning are unique technologies for production of highly functionalised nanofibrous materials, using simple devices at low production rates. This technology is enormously versatile and well suited for small- and middle-sized companies and firms. The lastly mentioned handicap, low productivity, can be overlooked in the area of medical application, particularly tissue engineering, where highly valued and precisely designed small nanofibrous samples are needed.
- In the industrial level, aimed at high productivity, the competition between electrospinning and enhanced melt blown technology that nowadays also provides us with fibres of sub-micron diameters, will thrive until the handicaps of electrospinning are

effectively overcome. On the other hand, solvent-based spinning of ultrafine nanofibres will probably remain in the realm of electrically charged jets.

- Promising, as well as attractive, electrospinning technology will arouse new interest in higher education studies in textile technology inside the community of students from all countries. The related onslaught on the existing knowledge of natural sciences, to understand deeply its subtle nature, will be quite an achievement and fruitful from an educational point of view.
- There is a high probability that the process of studying and engineering electrospinning, in itself, will open newer dimensions in restructuring society, reconcile ideas, and form newer concepts and more powerful technologies to solve critical hanging issues in various planes of development of human civilisation.

### Acknowledgements

D. Lukas and J. Chaloupek are thankful to The Ministry of Education of the Czech Republic, the project CEP1-1M0554, for their support in the frame of The Research Centre for Advanced Conservation Technologies. A. Sarkar, P. Mikes and J. Chvojka have been supported by GACR, grant no. 102/08/H081 ‘Nonstandard application of physical fields’. L. Martinova and K. Vodsedalkova have been granted by GAAV, grant no. IAA500390702 ‘Nanofibrous scaffolds for tissue engineering’. L. Martinova, D. Lukas and K. Vodsedalkova have been granted by GAAV, grant no. IAA500390702 ‘Nanofibrous scaffolds with liposomes for tissue engineering’. L. Martinova and D. Lubasova have been supported by GACR, grant no. 304/07/1129 ‘Polarised cultures of hepatocytes and mesenchymal cells on the nanofibre membranes in the experimental bioreactor’. Next co-author P. Pokorný is thankful for the support granted by MPO CR, grant no. FT-TA3/017. It would also not be out place to express our gratitude to the National Radiation Protection Institute, Czech Republic and FOMA Czech Republic for their valued advice and discussions in analysing various kinds of radiation. Authors also thank the companies ELMARCO and CUMMINS Filtration for their support and interest in this work.

### References

- [1] Y. Filatov, A. Budyka, and V. Kirichenko, *Electrospinning of Micro- and Nanofibres: Fundamentals in Separation and Filtration Processes*, Begell House Inc., Redding, CT, 2007.
- [2] S. Ramakrishna, K. Fujihara, W. Teo, T. Lim, and Z. Ma, *An Introduction to Electrospinning and Nanofibres*, World Scientific Publishing Co., Singapore, 2005.
- [3] D.H. Reneker and H. Fong, *Polymeric Nanofibres*, Oxford University Press, Washington, D.C., 2005.
- [4] D.H. Reneker and A.L. Yarin, *Polymer* 49 (2008), p. 2387.
- [5] A.I. Grigor'ev and S.O. Shir'aeva, *J. Phys. D Appl. Phys.* 23 (1990), p. 1361.
- [6] R.P. Gwinn, *The New Encyclopedia Britannica*, Vol. 5, Encyclopedia Britannica Inc., Chicago, 1991.
- [7] A. Nollet, *Recherches Sur les Causes Particulieres des Phenomenes Electrigues*, les Freres Guerin, Paris, 1749.
- [8] W.J. Morton, *Method of Dispersing Fluids*, U.S. Patent No. 705 691, 1902.
- [9] J. Zeleny, *Phys. Rev.* 3 (1914), p. 69.
- [10] J. Zeleny, *Phys. Rev.* 10 (1917), p. 1.
- [11] A. Formhals, *Process and Apparatus for Preparing Artificial Threads*, U.S. Patent No. 1 975 504, 1934.
- [12] C.L. Norton, *Method of and Apparatus for Producing Fibrous or Filamentary Material*, U.S. Patent No. 2 048 651, 1936.

- [13] Y.N. Filatov, *Electrospinning of Fibrous Materials [in Russian]*, Neft' i Gas Publishing House, Moscow, 1977.
- [14] O. Jirsak, F. Sanetnik, D. Lukas, V. Kotek, L. Martinova, and J. Chaloupek, *A Method of Nanofibres Production from a Polymer Solution Using Electrostatic Spinning and a Device for Carrying Out the Method*, U.S. Patent No. WO2005024101, 2005.
- [15] L. Rayleigh, Phil. Mag. 14 (1882), p. 184.
- [16] G.F. Taylor, Math. Phys. Sci. 280 (1964), p. 383.
- [17] G.F. Taylor and M.D. Van Dyke, Proc. R. Soc. Lond. A 313 (1969), p. 453.
- [18] J.B. Matthews, J. Geophys. Res. 72 (1967), p. 3007.
- [19] L.D. Landau and E.M. Lifshitz, *Electrodynamics of Continuous Media*, Butterworth-Heinemann, Oxford, 1984.
- [20] J. Doshi and D.H. Reneker, J. Electrostat. 35 (1995), p. 151.
- [21] G. Srinivasan and D.H. Reneker, Polym. Int. 36 (1995), p. 195.
- [22] D.H. Reneker and I. Chun, Nanotechnology 7 (1996), p. 216.
- [23] S.L. Shenoy, W.D. Bates, H.L. Frisch, and G.E. Wnek, Polymer, 46 (2005), p. 3372.
- [24] S.A. Theron, A.L. Yarin, and E. Zussman, Polymer, 46 (2005), p. 2889.
- [25] T.A. Bak and W.G. Kauman, Trans. Faraday Soc. 55 (1959), p. 1109.
- [26] D. Lukas, E. Kostakova, and A. Sarkar, *Computer simulation of moisture transport in fibrous materials*, in *Thermal and Moisture Transport in Fibrous Materials*, N. Pan and P. Gibson, eds., Woodhead Publishing Limited, Cambridge, UK, 2006, pp. 469–541.
- [27] A.W. Adamson and A.P. Gast, *Physical Chemistry of Surfaces*, John Wiley & Sons, New York, 1997.
- [28] E.D. Shchukin, A.V. Pertsov, E.A. Amelina, and A.S. Zelenev, *Colloid and Surface Chemistry*, Elsevier, Amsterdam, 2001.
- [29] C. Kittel and H. Kroemer, *Thermal Physics*, Freeman and Company, New York, 2000.
- [30] G. Gouy, Ann. Phys. 9 (1910), p. 455.
- [31] D.L. Chapman, Phil. Mag. 25 (1913), p. 475.
- [32] P. Debye and E. Huckel, Physikalische Zeitschrift 4 (1923), p. 185.
- [33] R.P. Feynman, R.B. Leighton, and M. Sands, *Feynman Lectures on Physics*, Vol. II, Addison-Wesley Publishing Company, Reading, MA, 1971.
- [34] F. Andrietti, A. Peres, and R. Pezzotta, Biophys. J. 16 (1976), p. 1121.
- [35] C.J. Smith, *A Degree Physics (Part V) – Electricity and Magnetism*, Radha Publishing House, London, 1992.
- [36] A. Doyle, D.R. Moffett, and B. Vonneguit, J. Colloid Interface Sci. 19 (1964), p. 136.
- [37] J.C. Berg and D.C. George, Monthly Weather Rev. 95 (1967), p. 884.
- [38] A.I. Grigor'ev, Sov. Phys. Tech. Phys. 30 (1985), p. 736.
- [39] J.H. Jeans, *The Mathematical Theory of Electricity and Magnetism*, Cambridge University Press, Cambridge, UK, 1908.
- [40] M.C. Gray, Q. Appl. Math. 11 (1953), p. 311.
- [41] D. Lukas, A. Sarkar, and P. Pokorny, J. Appl. Phys. 103 (2008), p. 084309.
- [42] A. Sarkar, D. Lukas, and M. Weng, *Electrospinning as an Application of the Physical Law of Dielectric Diffusion*, Poly-2008 Conference, New Delhi, India, 2008.
- [43] M.M. Breuer and D. Robinson, Nature 221 (1969), p. 1116.
- [44] L. da Vinci, *The Notebooks of Leonardo da Vinci*, E. MacCurdy, ed. and transl., Reynal and Hitchcock, New York, 1938.
- [45] *The Encyclopedia Americana: A Library of Universal Knowledge*. New York: Encyclopedia Americana Corp., 1918.
- [46] J. Eggers and E. Villermaux, Rep. Progr. Phys. 71 (2008), p. 1.
- [47] L. Rayleigh, Proc. Lond. Math. Soc. s1–10 (1878), p. 4.
- [48] J. Plateau, *Statique Experimentale et Theoretique des Liquids Soumis aux Seules Forces Moleculaires*, Gauthier-Villars, Paris, 1873.
- [49] R.J. Roe, J. Colloid Interface Sci. 50 (1957), p. 70.
- [50] S. Tomotika, Proc. R. Soc. Lond. A 150 (1935), p. 322.
- [51] B.J. Meister and G.F. Scheele, Am. Inst. Chem. Eng. J. 13 (1967), p. 682.
- [52] P.G. de Gennes, F. Wyart-Brochard, and D. Quere, *Capillarity and Wetting Phenomena: Drops, Bubbles, Pearls, Waves*, Springer-Verlag, New York, 2003.
- [53] S. Chandrasekhar, *Hydrodynamic and Hydromagnetic Instability*, Clarendon Press, Oxford, 1961.

- [54] X.H. Qin, Y.Q. Wan, J.H. He, J. Zhang, J.Y. Yu, and S.Y. Wang, *Polymer*, 45 (2004), p. 6409.
- [55] B.J. West, *Chaos, Soliton. Fract.* 20 (2004), p. 33.
- [56] J.T. Kuijka, *Int. J. Nonlinear Sci. Numer. Simul.* 4 (2003), p. 317.
- [57] Y.M. Shin, M.M. Hohman, M.P. Brenner, and G.C. Rutledge, *Polymer*, 42 (2001), p. 09955.
- [58] L. Wannatong, A. Sirivat, and P. Supaphol, *Polym. Int.* 53 (2004), p. 1851.
- [59] J.F. Cooley, *Apparatus for Electrically Dispersing Fluids*, U.S. Patent No. 692 631, 1902.
- [60] W.E. Teo and S. Ramakrishna, *Nanotechnology* 17 (2006), p. 89.
- [61] H. Liu and Y.L. Hsieh, *J. Polym. Sci. Part B Polym. Phys.* 40 (2002), p. 2119.
- [62] B. Sundaray, V. Subramaian, T.S. Natarajan, R.Z. Xiang, C.C. Chang, and W.S. Fann, *Appl. Phys. Lett.* 84 (2004), p. 1222.
- [63] I. Chun, *Fine Fibres Spun by Electrospinning Process from Polymer Solutions and Polymer Melts*, Ph.D. diss., University of Akron, OH, 1995.
- [64] L. Larrodo and R.S.J. Manley, *J. Polym. Sci.* 19 (1981), p. 909.
- [65] L. Larrodo and R.S.J. Manley, *J. Polym. Sci.* 19 (1981), p. 921.
- [66] L. Larrodo and R.S.J. Manley, *J. Polym. Sci.* 19 (1981), p. 933.
- [67] J. Lyons, *Melt-electrospinning of Thermoplastic Polymers: An Experimental and Theoretical Analysis*, Ph.D. diss., Drexel University, 2004.
- [68] J. Lyons, Ch. Li, and F. Ko, *Polymer*, 45 (2004), p. 7597.
- [69] M. Komarek and L. Martinova, *Melt-Electrospinning of Polypropylene Nanofibres*, Autex2006, Raleigh, NC, 2006.
- [70] N. Ogata, N. Shimada, S. Yamaguchi, K. Nakane, and T. Ogihara, *J. Appl. Polym. Sci.* 105 (2007), p. 1127.
- [71] H. Zhou, T.B. Green, and Y.L. Joo, *Polymer*, 47 (2006), p. 7497.
- [72] J. Tureckova, I. Prokopova, J. Nahlik, M. Komarek, V. Sasek, and C. Novotny, *Biodegradable Aromatic-aliphatic Co-polyesters Based on Poly(ethylenterephthalate) from Disposed PET Bottles Suitable for Melt Electrospinning*, Junior Euromat, Suisse, 2008.
- [73] E. Zhmayev, H. Zhou, and Y.L. Joo, *J. Non-Newtonian Fluid Mech.* 153 (2008), p. 95.
- [74] H. Giesekus, *J. Non-Newtonian Fluid Mech.* 11 (1982), p. 69.
- [75] C.P. Carroll and Y.L. Joo, *Phys. Fluids*. 18 (2006), p. 053102.
- [76] *McGraw-Hill Encyclopedia of Science and Technology*, 5th edition, The McGraw-Hill Companies, Inc., New York 2007.
- [77] J.H. Mason, *Proc. Inst. Electr. Eng. C* 102 (1955), p. 254.
- [78] H. Zhou and J.L. Yoo, *Apparatus and Method for Elevated Temperature Electrospinning*, U.S. Patent No. 7326043, 2008.
- [79] T. Song, Y. Zhang, T. Zhou, Ch. Lim, S. Ramakrishna, and B. Liu, *Chem. Phys. Lett.* 415 (2005), p. 317.
- [80] A. Bazilevsky, A.L. Yarin, and C.M. Megaridis, *Langmuir*, 23 (2007), p. 23114.
- [81] Y. Dror, W. Salalha, R. Avrahami, E. Zussmann, A.L. Yarin, R. Dersch, A. Greiner, and J.H. Wendorf, *Small* 6 (2007), p. 1064.
- [82] T. Song, Y.Z. Zhang, and T.J. Zhou, *J. Magnetism Magn. Mater.* 303 (2006), p. 286.
- [83] G. Rutledge, J.H. Yu, and S.V. Fridrikh, *Production of Submicron Diameter Fibres by Two-fluid Electrospinning Process*, World Intellectual Property Organization, Patent No. WO09568, 2005.
- [84] L.D. Li, Y. Wand, and Y. Xia, *Nano Lett.* 4 (2004), p. 933.
- [85] S. Reznik, A.L. Yarin, E. Zussman, and L. Berkovici, *Phys. Fluids* 18 (2006), p. 062101.
- [86] H. Jiang, Y. Hu, Y. Li, P. Zhao, K. Zhu, and W. Chen, *J. Control. Release* 108 (2005), p. 237.
- [87] B.S. Gupta, M.W. King, S. Hudson, R. Hufenus, J. Gluck, and A. Moghe, *Electrospun Core-sheath Fibres for Soft Tissue Engineering*, NTC Project, Project No. F05-NS04, 2007.
- [88] Z. Sun, E. Zussman, A.L. Yarin, J.H. Wendorf, and A. Greiner, *Adv. Mater.* 15 (2003), p. 1921.
- [89] P.C. Hiemenz and T.P. Lodge, *Polymer Chemistry*, Taylor & Francis Group, Boca Raton, FL, 2007.
- [90] A.L. Andrade, *Science and Technology of Polymer Nanofibres*, Wiley, Hoboken, NJ, 2008.
- [91] A. Ganot, *Traite elementaire de physique experimentale et appliquee et de meteorology*, 415 ed. Paris: Imprimerie, J. Claye, 1855.
- [92] T.T. Brown, *A Method of and an Apparatus or Machine for Producing Force or Motion*, British Patent No. 300311, 1927.
- [93] F.X. Canning, C. Melcher, and E. Wient, *Asymmetrical Capacitors for Propulsion*, Nasa/CR-2004-213312, Morgan town, West Virginia, 2004.

- [94] J. Primas, *Electrical Properties of High-voltage Capacitors with Asymmetrical Electrodes*, Diploma thesis, Technical University of Liberec, 2008.
- [95] M. Malik, *Mechanical Properties of High-voltage Capacitors with Asymmetrical Electrodes*, Diploma thesis, Technical University of Liberec, 2008.
- [96] A.A. Akopian, G.V. Butkevic, L.F. Dmochobskaja, E.S. Krucharkin, G.A. Lebedev, D.V. Razebig, A.S. Sergejev, and L.I. Sirotinskij, *Technika vysokich naprjazenij*, Gosenergoizdat, Moscow, 1951.
- [97] V. Lysenko, *VN zdroje*, BEN – technická literatura, Praha, 2008.
- [98] V. Petržílka and S. Šafrata, *Elektřina a magnetismus*, ĚS AV, Praha, 1956.
- [99] A.I. Grigor'ev and O.A. Sinkevich, Soviet Phys. Tech. Phys. 29 (1984), p. 735.
- [100] I.P. Stakhanov, *Physical Nature of Ball Lightning [in Russian]*, Atomizdat, Moscow, 1959.
- [101] B.A. Kozlov and V.I. Solovyov, Tech. Phys. 52 (2007), p. 892.
- [102] S. Ray, J. Sci. Instrum. 3 (1926), p. 126.
- [103] T. Chvojka, *Dependence Deflection Jet of Polymeric Solution on External Auxiliary Field at Electrostatic Electrospinning*, Diploma thesis, Technical University of Liberec, 2008.
- [104] A. Sarkar, *Physical principles of electrospinning*, Doctoral thesis, Department of Nonwovens, Textile Engineering, Technical University of Liberec, 2009.
- [105] H. Remy, *Lehrbuch der Anorganischen Chemie*, Akademische Verlagsgesellschaft Becker and Erler Kom. Ges, Leipzig, 1942.
- [106] I. Batkin, R.B. Del Re, J.G. Boutin, and J. Armitage, Phys. Med. Biol. 43 (1998), p. 487.
- [107] P.C. Hiemenz, *Principles of Colloid and Surface Chemistry*, CRC Press, New York, 1997.
- [108] T. Jarusuwannapoom, W. Hongrojanawiwat, S. Jitjaicham, L. Wannatong, M. Nithitanakul, C. Pattamaprom, P. Koombhongse, R. Rangkupan, and P. Supaphol, Eur. Polym. J. 41 (2000), p. 409.
- [109] P.J. Flory, *Principles of Polymer Chemistry*, Cornell University Press, Ithaca, NY, 1953.
- [110] J.H. Hildebrand and R.L. Scott, *The Solubility of Nonelectrolytes*, Dover Publications, New York, 1964.
- [111] Ch. Hansen, *Hansen Solubility Parameters: A User's Handbook*, CRC Press, New York, 2007.
- [112] J. Burke, The Book and Paper Group Annual 3 (1984), p. 13.
- [113] O. Jirsak and L.C. Wadsworth, *Nonwoven Textiles*, Carolina Academic Press, Durham, 1999.
- [114] M. Bognitzki, W. Czado, T. Frese, A. Schaper, M. Hellwig, M. Steinhart, A. Greiner, and J.H. Wendorff, Adv. Mater. 13 (2001), p. 70.
- [115] M.S. Khil, S.R. Bhattachari, H.Y. Kim, S.Z. Kim, and K.H. Lee, J. Biomed. Mater. Res. 72B (2004), p. 117.
- [116] S.O. Han, W.K. Son, J.H. Youk, T.S. Lee, and W.H. Park, Mater. Lett. 59 (2005), p. 2998.
- [117] H. Morawetz, *Macromolecules in Solution*, Wiley, New York, 1975.
- [118] B.L. Hager and G.C. Berry, J. Polym. Sci. Polym. Phys. Ed. 20 (2003), p. 911.
- [119] C. Tanford, *Physical Chemistry of Macromolecules*, Wiley, New York, 1961.
- [120] P. Rai and S.L. Rosen, J. Polym. Sci. Part B Polym. Phys. 35 (1997), p. 1985.
- [121] M. Přádný, L. Martinová, J. Michálek, T. Fenclová, and E. Krumbholcová, Cent. Eur. J. Chem. 5 (2007), p. 779.